ASSESSING THE EFFECT OF PRETREATMENT ON CELLULOSE ACCESSIBILITY FOR CELLULOSIC BIOFUELS PRODUCTION

A Dissertation
Presented to
The Academic Faculty

by

Xianzhi Meng

In Partial Fulfillment
of the Requirements for the Degree
Doctor of Philosophy in the
School of Chemistry and Biochemistry

Georgia Institute of Technology
December 2015

ASSESSING THE EFFECT OF PRETREATMENT ON CELLULOSE ACCESSIBILITY FOR CELLULOSIC BIOFUELS PRODUCTION

Approved by:

Dr. Arthur J. Ragauskas, Advisor
School of Chemistry and Biochemistry
Georgia Institute of Technology

Dr. Pamela Peralta-Yahya
School of Chemical and Biomolecular Engineering
Georgia Institute of Technology

Dr. Charles L. Liotta
School of Chemistry and Biochemistry
Georgia Institute of Technology

Dr. Preet Singh
School of Molecular Science and Engineering
Georgia Institute of Technology

Dr. Loren Williams
School of Chemistry and Biochemistry
Georgia Institute of Technology

Date Approved: August 10, 2015

ACKNOWLEDGEMENTS

This dissertation would be impossible to complete without help from many individuals. First and foremost, I'd like to express my appreciation to my advisor Professor Dr. Art Ragauskas, who has been a tremendous mentor for me. His encouragement, guidance, enthusiasm, patience was tremendous throughout my doctoral study, and it has been an honor to be one of his graduate students. I would also like to appreciate my former college research advisor, Dr. Hellen and Dr. Morgan for training me the fundamental experimental skills which are the groundwork of my Ph.D. project. Their love for teaching is contagious and motivational for me during those tough times in the Ph.D. pursuit. In addition, I would also like to thank my thesis committee, Dr. Charles Liotta, Dr. Loren Williams, Dr. Pamela Peralta-Yahya, and Dr. Preet Singh, for their priceless comments and help from the very beginning (literature exam, second year seminar, oral qualify example, etc.) to the final stage of my research.

I would like to thank the co-workers from the Ragauskas group at Georgia Tech for their friendship, helpful discussions, and collaborations. My special sincere thanks go to Dr. Yunqiao Pu, Dr. Fang Huang, Dr. Marcus Foston, Dr. Haoxi Ben, Dr. Matyas Kosa, Dr. Reichel Samuel, Dr. Seokwon Jung, Dr. Garima Bali, Dr. Fan Hu, Dr. Qining Sun, Dr. Zhoujian Hu, Dr. Yang Li, Allison Tolbert, Hannah Akinosho, and Mark Cannatelli. I am also thankful to Dr. Cam Tyson and Michele Yager for their guidance and supports. My time at Georgia Tech was made enjoyable in large part due to their help and support.

I also would like to thank my family for their never-ended love and complete understanding all the way. I cannot express how lucky and grateful I am to my father, mother, uncle for all the sacrifices they have made on my behalf.

Finally, I would like to acknowledge the financial support from the Bioenergy Science Center (BESC). BESC, established by U.S. Department of Energy in 2007, is a multi-institutional (18 partners), multidisciplinary research (biological, chemical, physical, and computational sciences; mathematics; and engineering) organization focused on the fundamental understanding and elimination of biomass recalcitrance.

TABLE OF CONTENTS

Page

LIST OF TABLES

Page

LIST OF FIGURES

Page

LIST OF ABBREVIATIONS

AFEX	Ammonia fiber explosion
AFM	Atomic force microscopy
AIL	Acid insoluble lignin
ASA	Accessible surface area
ASL	Acid soluble lignin
ATR-FTIR	Attenuated total reflectance fourier transform infrared spectroscopy
BET	Brunauer-Emmett-Teller
BSA	Bovine serum albumin
CAD	*Cinnamyl-alcohol dehydrogenase*
CBH	Cellobiohydrolase
CBM	Carbohydrate-binding module
COMT	Caffeic acid O-methyltransferase
CP/MAS	Cross polarization/magic angle spinning
CPMG	Carr-Purcell-Meiboom-Gill
CrI	Crystallinity index
DAP	Dilute acid pretreatment
DB	Direct blue
DI	Deionized
DO	Direct orange
DP	Degree of polymerization
DP_n	Number-average degree of polymerization
DP_w	Weight-average degree of polymerization
FTIR	Fourier transform infrared
G	Guaiacyl lignin unit
GPC	Gel permeation chromatography
H	*p*-Hydroxyphenyl lignin unit
HW	Hot water

HPAEC-PAD	High-performance anion-exchange chromatography with pulsed amperometric detection
HPLC	High-performance liquid chromatography
HW	Hardwood
IL	Ionic liquid
ILT	Inverse Laplace transforms
LCCs	Lignin-carbohydrate complexes
LHW	Liquid hot water
MPa	Mega pascal pressure unit
M_n	Number average molecular weight
M_w	Weight average molecular weight
NMR	Nuclear magnetic resonance
PAA	Peracetic acid
PBS	Phosphate buffered saline
PDI	Polydispersity index
PFG	Pulse field gradient
PGSE	Pulsed gradient spin echo
PMO	Polysaccharide monooxygenases
PSD	Pore size distribution
RFS	Renewable Fuel Standard
S	Syringyl unit lignin
SS	Simons' stain
SEM	Scanning electron microscopy
SW	Softwood
TEM	Transmission electron microscopy
TGC	Fluoresce protein
UA	Uronic acid
UV	Ultraviolet
WAXD	Wide-angle x-ray diffraction
WRV	Water retention value
XRD	X-ray diffraction

SUMMARY

Bioethanol has become one of the most promising biofuels as an alternative renewable energy source largely in response to limited fuel supply and efforts to reduce greenhouse gas emission. To address the traditional "food vs. fuel" issue caused by first generation biofuels, lignocellulosic biomass (e.g., woody biomass, waste residues from agriculture and forestry) has been recognized and promoted as a potential low-cost, renewable source of mixed sugars for fermentation to bioethanol throughout world. Numbers of steps must be applied in order to convert biomass to ethanol, including an essential process known as biomass pretreatment to alter physical and chemical structure of plant cell wall, increase cellulose accessibility and therefore overcome natural biomass recalcitrance which is the major technical barriers to the cost-effective transformation of lignocellulosic biomass to fermentable sugars. Therefore, a fundamental understanding of biomass recalcitrance, particularly how different biomass characteristics influence biomass recalcitrance and how different pretreatment alter these factors therefore increase cellulose accessibility is extremely important from the perspective of bioethanol commercialization. Obviously, it requires enhanced characterization methodology to measure the chemistry, structure, and interactions of individual biomass components.

The first objective of this thesis focuses on the determination of biomass porosity before and after dilute acid and steam explosion pretreatment. Several recent developed analytical techniques including a modified Simons' stain method along with various NMR techniques (e.g., NMR cryoporometry, relaxometry, diffusometry) were applied to

characterize surface area/pore size information, thus assess cellulose accessibility on untreated and pretreated biomass. The development and combination of different techniques generate a much more accurate description of cellulose accessibility change upon different chemical and physical biomass pretreatment. The appropriate determination of cellulose accessibility before and after pretreatment can assist to understand the effectiveness of a particular pretreatment in overcoming lignocellulosic recalcitrance.

The second part of thesis is focused on investigating the effect of alkaline pretreatment methods on cellulose structure and accessibility using Simons' stain developed earlier. Various alkaline pretreatments including sodium hydroxide, calcium hydroxide, and soaking in ammonia solution were applied on milled hybrid *Populus* (*Populus trichocarpa x deltoids)*. The pretreatment conditions were chosen according to literature and were optimized for enzymatic release of sugars. Cellulose structural features such as degree of polymerization, crystallinity, accessibility were then measured using various analytical tools such as GPC, NMR and Simons' stain. This study reveals the changes in cellulose structure and accessibility upon a variety of low-cost and mild alkaline pretreatments, subsequently identifies important relevant parameters responsible for reduction of biomass recalcitrance via alkaline pretreatment.

The third part of the thesis provides insights into the effect of hemicellulose and lignin removal on cellulose accessibility increase and the role of cellulose accessibility in biomass recalcitrance. Previous two studies revealed that acid and alkaline pretreatment

increase cellulose accessibility through removing hemicellulose and lignin, respectively. However, the relative importance of the removal of one of these two components over the other is still quite limited. *Populus* (*Populus trichocarpa x deltoids)* was pretreated by dilute acid, hot water and dilute alkaline at different severities, producing substrates differing substantially in the chemical composition and structure. Simons' stain and mercury porosimetry were used to measure accessible surface area of cellulose and different scales of biomass porosity as related to cellulose accessibility of these different pretreated substrates. With compositional, accessibility and digestibility data available for these pretreated substrates, a comprehensive investigation of the effect of removal of each individual cell wall component by different pretreatment on cellulose accessibility as well as the relation between cellulose accessibility and substrate digestibility were then performed.

The last part of this thesis focuses on understanding the limitations occurring during enzymatic hydrolysis of lignocellulosic substrates that might be responsible for the gradual slowing down of the reaction. *Populus* and switchgrass were pretreated by dilute acid and alkaline and subjected to enzymatic hydrolysis for 72 h. The reducing sugar yield was measured by high performance liquid chromatography at different hydrolysis time points. Hydrolyzed biomass samples were isolated from the hydrolysis system and the cellulose accessible surface area and degree of polymerization were characterized by Simons' stain and GPC. Long enzymatic hydrolysis time and high enzyme loading add significant operating costs to the overall biomass to ethanol bioconversion process, and analyzing how the biomass structural relevant factors change during enzymatic

hydrolysis is essential for strengthening the understanding of intrinsic hydrolysis reaction mechanisms and interactions between cellulase enzymes and plant cell wall components, therefore ultimately reducing the costs associated with enzymatic hydrolysis.

CHAPTER 1

INTRODUCTION

The demand for renewable fuel sources continues to grow, due to the diminishing supply of fossil fuel resources, increasing global energy demand, growing concerns about energy security, rural development and environmental stewardship [1]. Advances in biochemistry, biotechnology, genetic, and chemical engineering are leading to a promising new concept for producing of biofuels such as bioethanol. At present, the commercialized bioethanol production largely represents the 1st generation biofuel, also known as simply ethanol which is produced by fermentation of sugar or starch-based raw materials such as corn and sugar cane, with almost 50 billion liters produced annually in United States [2]. However, the most contentious issue associated with the first generation biofuel is the "food vs. fuel" debate, which indicates one of the reasons for the global increase in food prices over the past few years is due to the rising production of biofuels directly from food crops [3]. To address the limitations of the first generation biofuels, second generation biofuels produced from lignocellulosic substrates such as woody biomass, agricultural and forest residues have been developed throughout the world, which offers large-scale availability with low cost and limited conflict with food crops [4].

The Renewable Fuel Standard (RFS), a federal program that requires transportation fuel sold in the U.S. to contain a minimum volume of renewable fuels, originated with the Energy Policy Act of 2005 and was expanded and extended by the Energy Independence

and Security Act of 2007 [5]. It requires increasing amounts of renewable fuel to be blended into transportation fuel each year, reaching approximately 36 billion gallons by 2022 with at least 16 billion gallons from cellulosic biofuels (Figure 1.1), which obviously indicates the need to research and develop technologies to boost cellulosic biofuel production while the conventional starch ethanol production requirement is almost achieved. However, the real volumes for cellulosic ethanol and other advanced fuels have slipped substantially from the projected volumes due to the slow development of biofuels production capacity. Environmental Protection Agency has the authority to reduce the volume requirements based on considerations such as the limitations in the ability of the industry to produce sufficient volumes of qualifying renewable fuel.

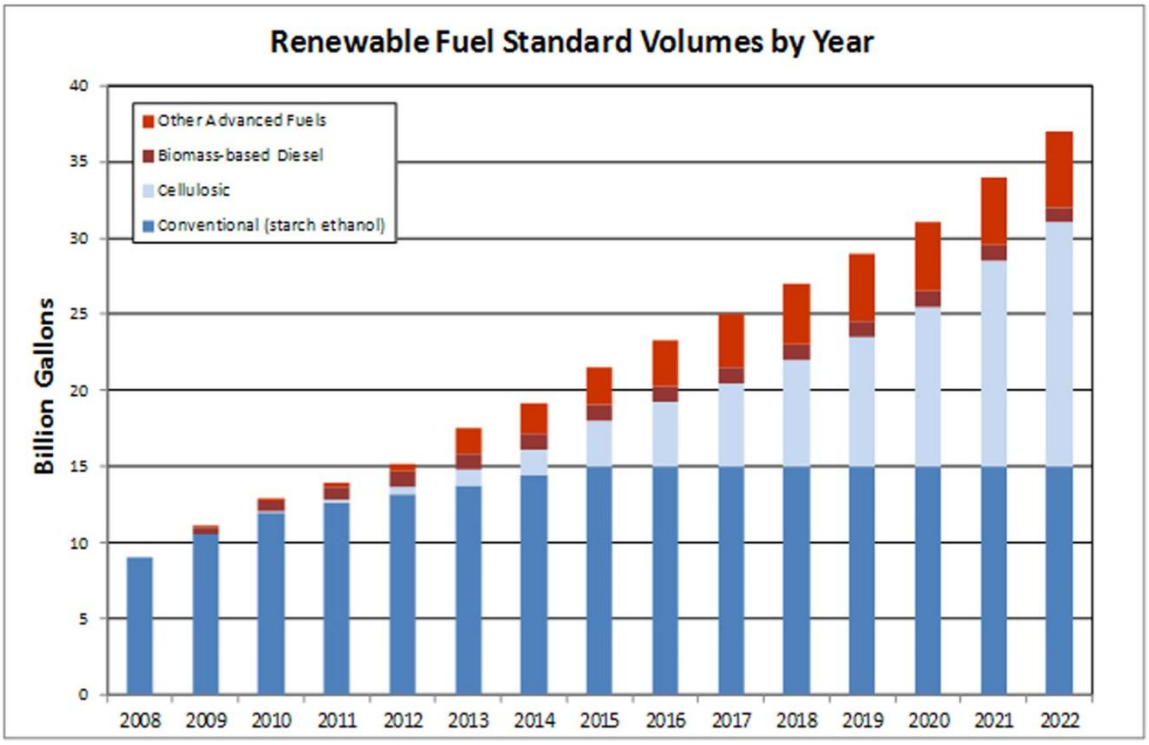

Figure 1.1 The Energy Independence and Security Act of 2007 set yearly RFS volume requirements for each renewable fuel category. Source: Alternative Fuels Data Center, U.S. Department of Energy.

Currently the bioconversion of biomass to biofuels is significantly hindered by the innate biomass recalcitrance, which refers to the complex characteristics of lignocellulose to protect its carbohydrates from degradation by cellulase enzymes [6,7]. As a result, achieving reasonable conversion rate and yield of bioethanol requires a critical step known as biomass pretreatment to remove or redistribute cell wall components, disrupt the plant cell wall matrix encapsulating cellulose, ultimately increasing the proportion of cellulose accessible surface area [8]. Although the mechanisms of different biomass pretreatment and the fundamentals of biomass recalcitrance are still not completely clear, it has been proposed that cellulose accessible surface area and biomass porosity could be one of the most important factors governing the enzymatic hydrolysis [9,10].

Understanding the exact role of cellulose accessibility in biomass recalcitrance calls for fundamental measurement of biomass substrate surface area and porosity, and it is believed that using a signal analytical technique will probably provide incomplete information because different techniques are based on different principles of measurement and their results reflect different physical measurement associated with accessibility [11]. Chapter 4 introduced several promising analytical techniques that were successfully applied on untreated and pretreated lignocellulosic substrate (*Populus*). In addition, the advantages and limitations of these analytical techniques were also discussed. The study in this chapter showed that acid-based pretreatment increased cellulose accessibility via removing of hemicellulose, generating new pores and expanding the size of existing pores. To further investigate the effect of other types of

pretreatments on cellulose accessibility and highlight the important role of cellulose accessibility in biomass recalcitrance, Chapter 5 examines the effects of various alkaline pretreatment methods on cellulose structure and its accessibility in milled hybrid *Populus*. This part of study not only reveals the changes that occur in cellulose structure (e.g., cellulose degree of polymerization, crystallinity) and accessibility upon a variety of low-cost and mild alkaline treatments, but also determines some of the key factors responsible for the reduction of biomass recalcitrance by comparing and correlating these structural changes with the enzymatic hydrolysis.

It has been hypothesized that increasing cellulose accessibility depends on not only how much total biomass components was removed but also what components with a specific structure and from where it was removed [12]. Studies reported in chapter 4 and 5 suggested acid and alkaline pretreatment increased cellulose accessibility by mainly removing hemicellulose and lignin, respectively. The study in Chapter 6 was conducted to determine the relative importance of the removal of one of these two components over the other. In addition, the most fundamental barrier in terms of biomass porosity scale for efficient enzymatic hydrolysis is also investigated. Chapter 7 studied the effect of enzymatic hydrolysis on the structure and accessibility of cellulose with a purpose to find insights into the limiting characteristics that might be responsible for the gradual slowing down of the enzymatic hydrolysis.

Understanding how to increase accessibility of biomass substrates so that appreciable amount of cellulose enzymes could have access to cellulose plays a critical role in the

development of large scale commercialization of bioethanol production. This thesis provides information about changes in cellulose accessibility upon different pretreatments and during enzymatic hydrolysis, along with the changes in chemical compositions, physical and chemical structures, will be extremely helpful to understand the fundamental mechanisms involved in biomass recalcitrance therefore to further optimize the current pretreatment technologies.

CHAPTER 2

LITERATURE REVIEW

2.1 Lignocellulosic ethanol

In contrast to first generation bioethanol which is derived from sugar or starch-based raw materials such as corn and sugar cane, lignocellulosic ethanol could be produced directly from biomass, representing the second generation of biofuel. Biomass is one of the most abundant, renewable and sustainable resource on the plant [1]. Because of its carbon neutrality and non-food competition, the greenhouse gas emissions from cellulosic ethanol are expected much less than petroleum based resources and using it does not create the food vs. fuel scenario [13]. As part of this public policy effort to expanding the role of biomass as an energy source, the U.S. Department of Energy envisioned a 30% replacement of the current U.S. petroleum consumption with biofuels by 2030 which will require more than approximately one billion dry tons of biomass feedstock annually [14]. Compared to first generation bioethanol production, in which the sugar extracted from sugar rich crops can be directly fermented to ethanol, conversion of biomass to cellulosic ethanol requires a much more complicated processes (Figure 2.1). Currently this bioconversion of biomass to biofuels generally includes five main steps: biomass collection and size reduction, pretreatment, enzymatic hydrolysis, fermentation, and distillation/rectification/dehydration to meet fuel specifications [15]. Pretreatment step is usually required before enzymatic hydrolysis to remove or redistribute plant cell wall component, and reduce natural biomass recalcitrance. Free sugars can be then produced

by applying cellulolytic enzymes on pretreated materials to depolymerize the carbohydrate polymers. Finally, the hexose sugars such as glucose are fermented to ethanol subsequently followed by a purification process including distillation, rectification and dehydration to meet fuel specifications [16].

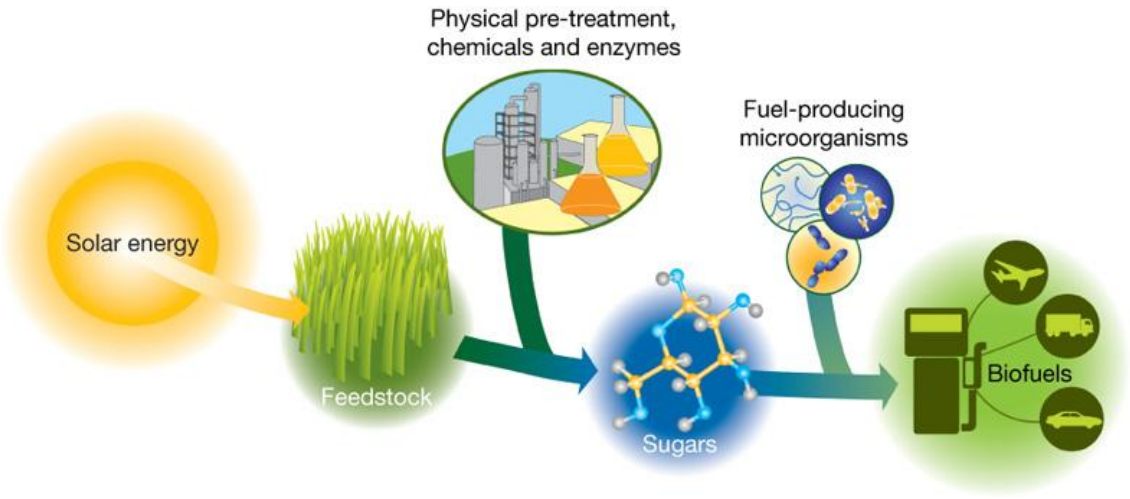

Figure 2.1 Bioconversion of biomass feedstock to biofuels via biological platform [15].

2.2 Lignocellulosic biomass

Biomass is one of the most abundant potential sustainable sources for renewable fuel production. Various biomass feedstocks are used all over the word to generate electricity, produce heat and liquid transportation fuels. Figure 2.2 summarizes the primary energy consumption by major fuel source from 1980 to 2008. As shown in the figure, biomass surpassed hydroelectric, ranked well below petroleum, natural gas, coal, and nuclear. Since early 2000s, there has been a gradual increase in biomass consumption likely due to the lignocellulosic ethanol production [17]. Forest lands, and in particular timberlands

have the potential to produce approximately 370 million dry tons of biomass annually in United States, while agricultural lands can provide nearly 1 billion dry tons of sustainably collectable biomass and continue to meet food, feed and export demands [14]. The annual biomass supply is more than enough to scale up to a large-scale biorefinery industry to meet the Renewable Fuels Standard by 2030.

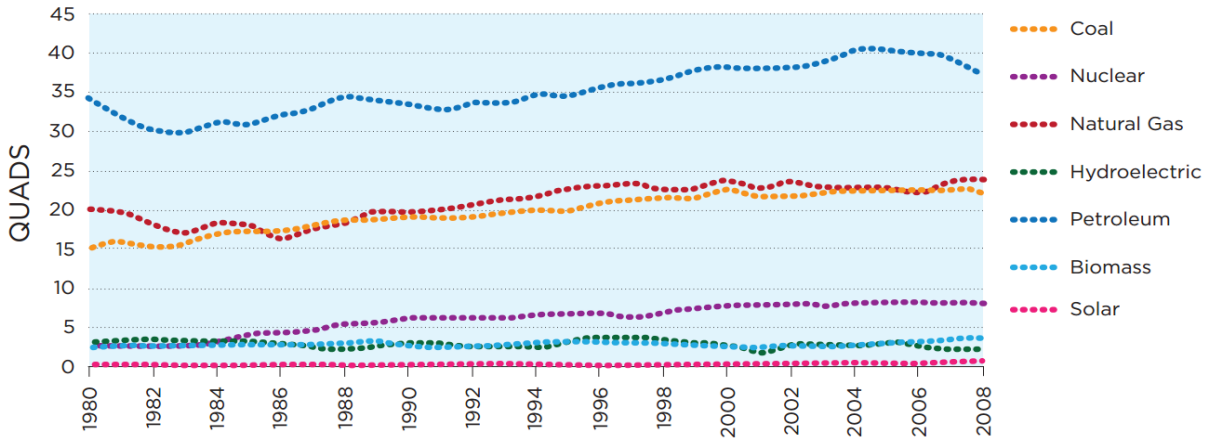

Figure 2.2 Primary energy consumption by major fuel source from 1980 to 2008 [17].

The general classification of biomass varieties as fuel resources can be divided preliminary into several groups and sub-groups according to their distinct biological diversity and similar source and origin (Table 2.1) [18]. The word "lignocellulosic biomass" is used to refer to higher plants, such as grasses, hardwoods and softwoods, and understanding the structure and chemical composition of lignocellulosic biomass is a prerequisite for developing effective conversion technologies to deconstruct its rigid structure, release glucose from recalcitrant plant, and engineering microorganisms to convert sugars into ethanol [19].

Table 2.1 General classification of biomass as solid fuel resources according to their biological diversity, source and origin [18].

Biomass groups	Biomass sub-groups, varieties and species
Woody biomass	Coniferous or deciduous; angiospermous or gymnospermous; soft or hard; stems, bark, chips, lumps, pellets, sawdust, sawmill
Aquatic biomass	Marine or freshwater algae; macroalgae or microalgae; seaweed, lake weed, water hyacinth
Herbaceous and agricultural biomass	Annual or perennial and field-based or processed-based such as: ➢ Grasses and flowers (alfalfa, bamboo, brassica, cane, cynara, Miscanthus, switchgrass, timothy) ➢ Straws (barley, bean, flax, corn, oat, rape, rice, sesame, sunflower, wheat) ➢ Other residues (fruits, shells, pits, pips, stalks, kernels, bagasse, pulps, grains)
Animal and human biomass wastes	Meat-bone meal, chicken litter, various manures
Contaminated biomass and industrial biomass wastes	Municipal solid waste, demolition wood, refuse-derived fuel, sewage sludge, hospital waste, paper-pulp sludge, waste papers, paperboard waste, chipboard, fibreboard, plywood, wood pallets and boxes, railway sleepers, tannery waste

2.2.1 Structure and composition of lignocellulose

Lignocellulosic biomass contains three major constituents; cellulose, hemicellulose and lignin (Figure 2.3). Cellulose unit, known as elementary fibril which is believed to contain ~36 β-D-glucan chains, coated with other non-cellulosic polysaccharides to form microfibrils, which are then cross-linked by hemicellulose/pectin matrixes to form macrofibrils that mediate structural stability in the plant cell wall [20]. Lignin fills the spaces in the cell wall between cellulose, hemicellulos, and pectin matrixes, covalently links to hemicellulose therefore conferring mechanical strength to the plant cell wall [21].There is significant variation of cellulose, hemicellulose, and lignin content in lignocellulosic biomass depending on its biological species, growth stage, and natural cell

type. Table 2.2 summarizes the distributions of major biomass components in the most common sources of biofuel crops. Cellulose and hemicellulose typically make up two-thirds of cell wall dry matter, other compounds present in lignocellulosic biomass, also known as extractives, include fats, fatty acids, phenolics, resins, phytosterols, salts, and minerals.

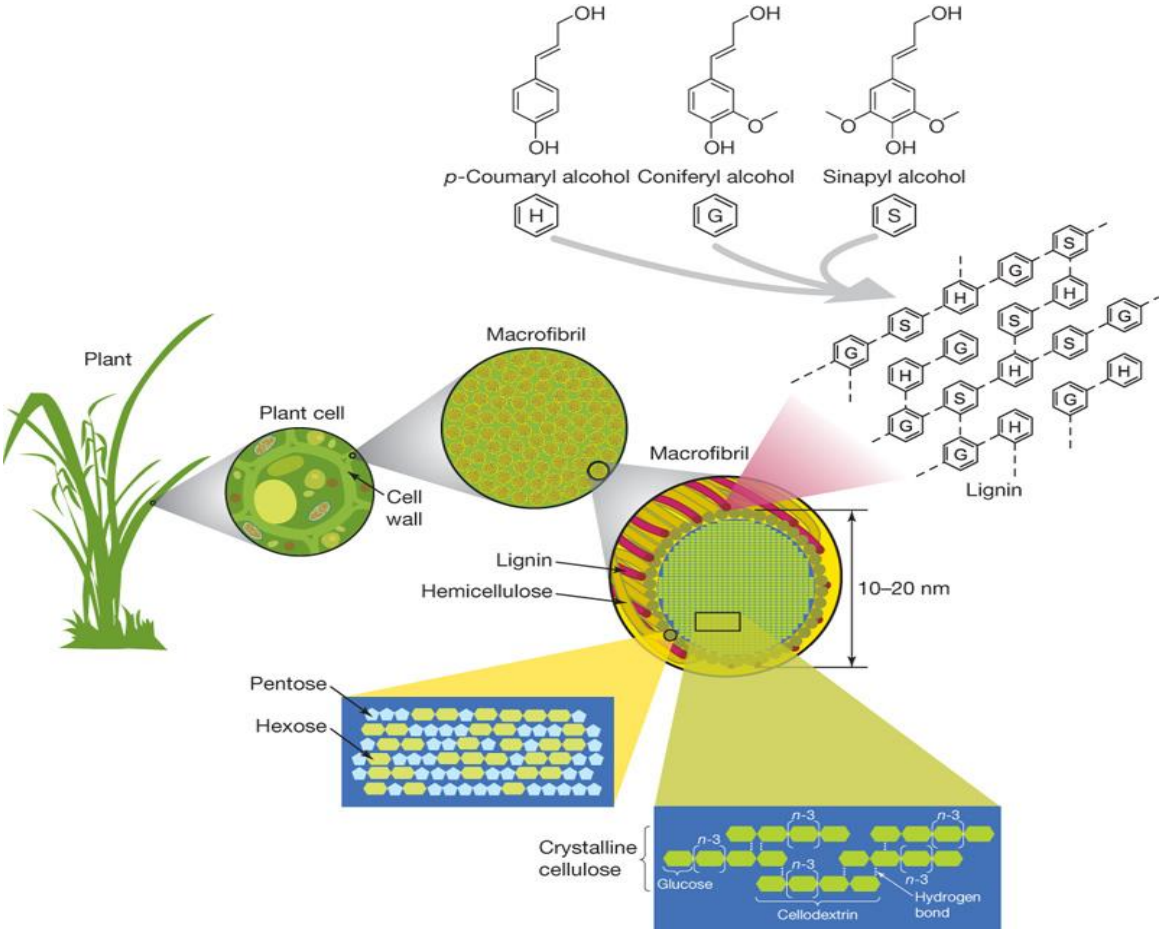

Figure 2.3 Structure of lignocellulose [15].

Table 2.2 Composition of typical lignocellulosic biomass (% dry basis).

Biomass	Cellulose	Hemicellulose	Lignin	Reference
Agave	33.7	8.8	11.9	[22]
Bagasse	38.0	27.0	20.0	[23]
Bemuda grass	25.0	36.0	6.0	[23]
Corn stover	40.0	25.0	17.0	[24]
Cotton stalk	31.0	11.0	28.0	[25]
Miscanthus	39.3	24.8	22.7	[26]
Poplar	44.7	18.6	26.4	[27]
Pine	44.6	21.9	27.7	[27]
Rice straw	37.0	34.0	12.0	[28]
Switchgrass	32.0	25.2	18.1	[27]
Spruce	45.0	6.6	27.9	[29]
Wheat straw	37.8	27.2	19.7	[30]

2.2.2 Cellulose

Cellulose is a linear glucose polymer linked by β-1,4 glycosidic bonds with cellobiose as its repeating unit, consisted of approximately 40-50% of total feedstock dry matter (Figure 2.4). Cellulose chain has a strong tendency to form inter and intra-molecular hydrogen bonds by the hydroxyl groups on these linear cellulose chains, which stiffens the chains and promotes aggregation into a crystalline structure (Figure 2.5) [31]. Cellulose contains highly ordered regions (crystalline) and less ordered regions (amorphous). Four different crystalline allomorphs of cellulose have been identified by X-ray diffraction (XRD) patterns and solid-state 13C NMR spectra: Cellulose I, II, III, and IV [32]. Cellulose I is the most abundant form found in nature, and its crystalline structure is mixture of two distinct crystalline forms, cellulose Iα (triclinic) and Iβ (monoclinic) [33]. The relative amounts of cellulose Iα and Iβ vary with the source of the cellulose, with I_α form being rich in cell wall of primitive microorganisms such as bacterial and I_β form being dominant in higher plants such as cotton, wood and ramie fibers [34]. Para-crystalline cellulose is loosely described as chain segments having less

ordered and more mobile than crystalline domain, but more ordered than amorphous chains segments [35]. Amorphous cellulose can be divided into accessible fibril surface portion and inaccessible fibril surface portion (Figure 2.6). Accessible fibril surfaces are those in contact with water, while the inaccessible fibril surfaces are fibril-to-fibril contact surfaces and surfaces due to distortions in the fibril interior [36].

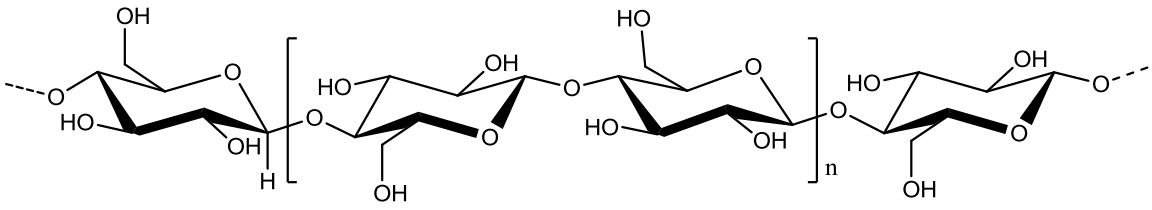

Figure 2.4 The structure of cellulose.

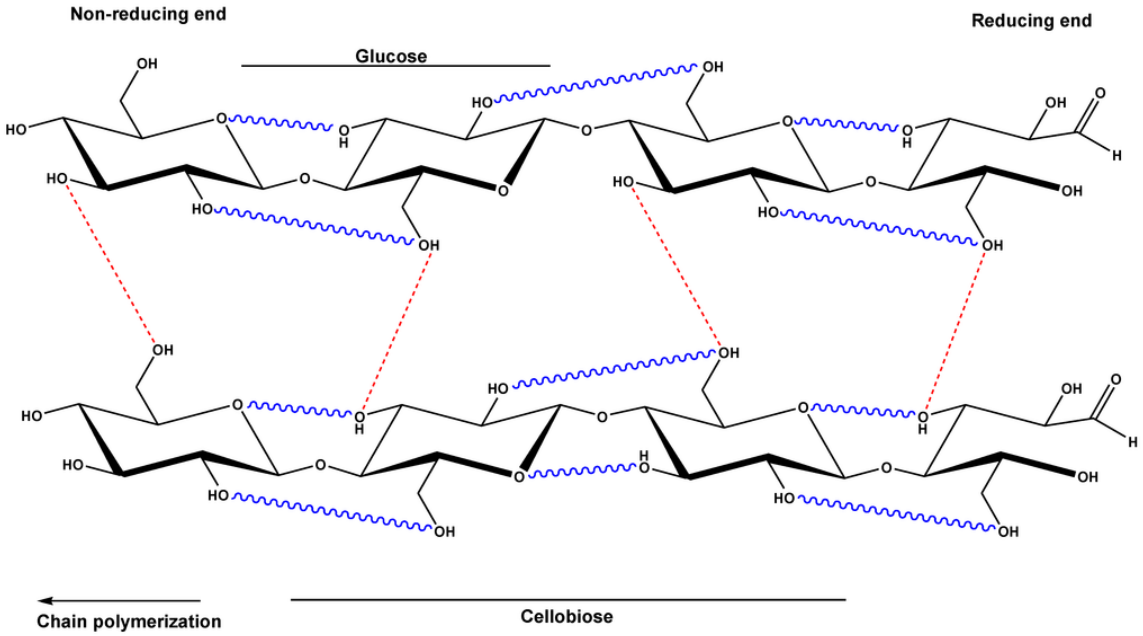

Figure 2.5 Structure of cellulose with inter- and intra-molecular hydrogen bonds [37]. Red and blue lines represent intra-molecular and inter-molecular hydrogen bonds, respectively.

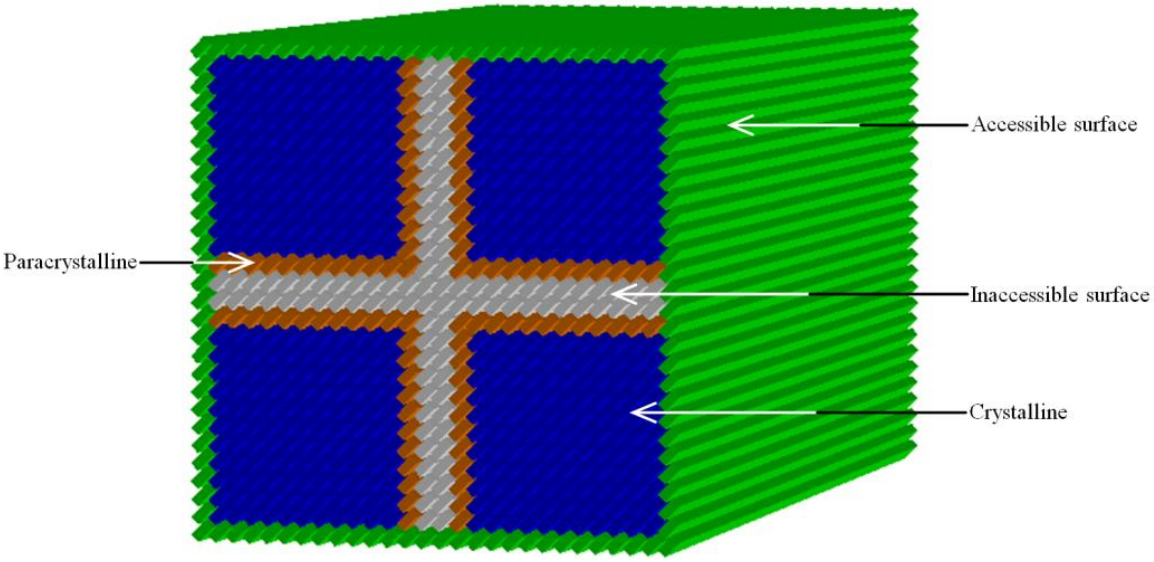

Figure 2.6 Schematic model of four aggregated cellulose I fibrils [38].

2.2.2.1 Cellulose crystallinity

Crystallinity index (*CrI*) is typically used to describe the relative amount of crystalline portion in cellulose, and can be measured using several analytical techniques including X-ray diffraction (XRD), solid-state ^{13}C nuclear magnetic resonance (NMR), and infrared (IR) spectroscopy. XRD can provide strong signals from the crystalline fraction of the cellulose, and the *CrI* is usually defined as [39]:

$$\text{CrI} = [(I_{002} - I_{amorphous})/I_{002}] \times 100$$

where I_{002} is the diffraction intensity at 002 peak position at $2\theta = 22.5^{o}$ and $I_{amorphous}$ is the scattering intensity of amorphous region at $2\theta = 18.7^{o}$. The non-crystalline part of cellulose is represented by broader and less clearly refined features in the XRD pattern, leading to challenges in the evaluation of the signals for a quantitative crystallinity measurement [40]. It has been showed that ^{13}C high-resolution cross-polarization magic angle spinning (CP/MAS) solid state NMR could also be used to determine the CrI values.

In CP/MAS ^{13}C NMR, CrI could be calculated from the area of the crystalline and amorphous C4 signals by using the following equation [19]:

$$CrI = [A_{86\text{-}92ppm}/(A_{79\text{-}86ppm} + A_{86\text{-}92ppm})] \times 100$$

where $A_{86\text{-}92ppm}$ represents the area of the crystalline C4 signal, $A_{79\text{-}86ppm}$ is the area of the amorphous C4 signal. Similar to other biological materials, the NMR spectra of cellulose contains multiple broad and overlapping peaks. To addressing this problem, a least-squared model and spectra fitting method was established to quantitatively estimate the relative fraction of ultrastructural components, including crystalline cellulose (i.e. cellulose I_α and I_β), para-crystalline cellulose, and amorphous domain of accessible or inaccessible fibril surfaces [36]. Figure 2.7 shows a non-linear least-squared line fitting of the C_4 region for a ^{13}C CP/MAS spectrum of isolated cellulose, with the peak assignments of the signals presented in Table 2.3. Lorentzian line shapes were applied to the carbon signals attributed to the domain of cellulose I_α, I_β, $I_{\alpha+\beta}$, while Gaussian lines were used to describe the signals from inaccessible and accessible fibril surfaces comprising the amorphous domains [41].

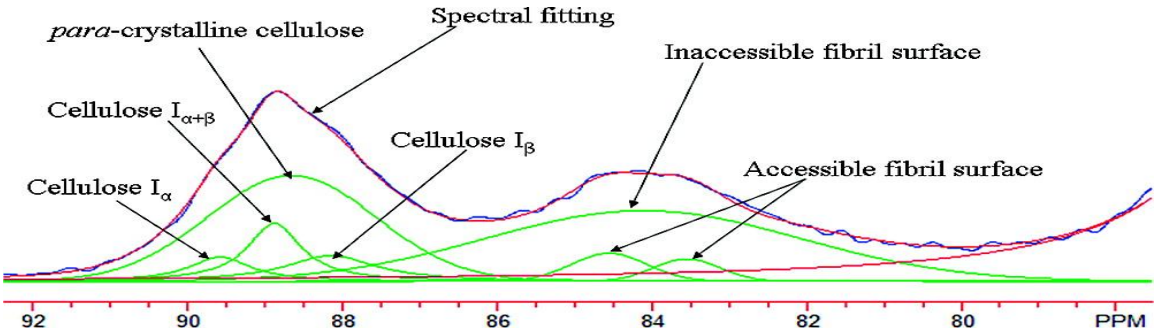

Figure 2.7 Spectra fitting for the C-4 region of the CP/MAS ^{13}C NMR spectrum of cellulose [42].

Table 2.3 Assignments of signals in the C-4 region of the CP/MAS ^{13}C NMR spectrum [42].

Assignment	Chemical shift (ppm)	Intensity (%)	Line type
Cellulose I_α	89.6	4.2	Lorentz
Cellulose $I_{\alpha+\beta}$	88.9	8.7	Lorentz
Para-crystalline cellulose	88.7	32.9	Gauss
Cellulose I_β	88.2	6.5	Lorentz
Accessible fibril surface	84.6	3.9	Gauss
Inaccessible fibril surface	84.1	41.1	Gauss
Accessible fibril surface	83.6	2.7	Gauss

Table 2.4 listed the relative contents of amorphous, para-crystalline, and crystalline portion of cellulose isolated from *Populus*, *Buddleja Davidii*, and switchgrass. Para-crystalline cellulose is the largest fraction observed for *Populus*, while inaccessible fibril surface of cellulose is the largest fraction observed for *Buddleja Davidii* and switchgrass. *Populus* is composed of relatively higher crystallinity (~63%) and accessible fibril surface (~10.2%) compared switchgrass and *Buddleja Davidii*. Information about cellulose crystallinity can be also obtained by other methods such as Fourier transform-infrared (FTIR) spectroscopy, which gives only relative values of crystallinity. The ratio of amorphous to crystalline cellulose associates with the ratio of intensities of the bands at 900 cm^{-1} and 1098 cm^{-1} [19].

Table 2.4 Cellulose crystallinity, relative content (%) of crystalline, para-crystalline and amorphous portion of cellulose from *Populus*, *Buddleja Davidii*, and Switchgrass determined by CP/MAS ^{13}C NMR.

Biomass feedstock	CrI	I_α	$I_{\alpha+\beta}$	I_β	Para-crystalline	Accessible fibril surface	Inaccessible fibril surface	Reference
Populus	63	5.0	14.2	19.8	31.1	10.2	18.3	[43]
Buddleja Davidii	55	4.2	8.7	6.5	32.9	6.6	41.1	[42]
Switchgrass	44	2.3	8.0	4.8	27.3	6.2	51.3	[44]

2.2.2.2 Cellulose degree of polymerization

Besides cellulose crystallinity, the size of cellulose molecule defined by the average number of monomer units, also referred as the degree of polymerization (DP) is another important property of cellulose. It can be measured by various analytical techniques including viscometry, and gel permeation chromatography (GPC) [45]. The determination of cellulose DP starts with the isolation of cellulose, including several steps: Soxhlet extraction to remove extractives, delignification to generate holocellulose (i.e. mixture of cellulose and hemicellulose) by oxidative degradation of lignin, concentrated alkaline extraction to remove hemicellulose. The conventional delignification method selectively removes lignin from biomass with only trace solubilization of glucan and xylan by applying glacial acetic acid and sodium chlorite [46]. However, there has been a concern about this method that the addition of acetic acid increases the likelihood of chain degradation due to the acid hydrolysis. Kumar et al. reported a reduction of nearly 75% in the average degree of polymerization of filter paper after delignification using acid-chlorite method [47]. Instead of removing lignin completely, it has been showed that the introduction of even a small portion of lignin to the system greatly reduced the negative DP effect [46]. A recent study compared several laboratory delignification methods for their selectivity, and impacts on physiochemical characteristics of cellulosic biomass, indicating that delignification using peracetic acid (PAA) is more selective than chlorite-acetic acid and has less severe impacts on cellulose degree of polymerization [48]. Cellulose DP varies from 5000 in native wood to 1000 in bleached wood pulp, and 500 to 1000 in the herbaceous cellulose as shown in Table 2.5.

Understanding and accurate characterization of cellulose DP is critical to the study of cellulase-cellulose interaction, particularly in the case of ex-cellulases [49].

Table 2.5 DP of native wood and non-woody cellulose using the viscometric method [45].

Biomass species	DP*
Trembling aspen	5000
Beech	4050
Red maple	4450
Eastern white cedar	4250
Eastern hemlock	3900
Jack pine	5000
Tamarack	4350
White spruce	4000
Balsam fir	4000
White birch	5500
Eucalyptus regnans	1510
Pinus radiate	3063
Bagasse	925
Wheatstraw	1045

* DP value is determined using glucose as the repeating unit

2.2.3 Hemicellulose

Hemicellulose is a heterogeneous class of polymers representing a family of polysaccharides that are found in the plant cell wall which may contain arabinose (Ara), xylose (Xyl), mannose (Man), glucose (Glu), and galactose (Gal), uronic acids (UA), and/or other sugars such as rhamnose and fucose. The most relevant hemicelluloses are xylans and glucomannans, with xylans being the most abundant hemicellulose components of secondary cell walls constituting 20-30% of biomass of hardwoods and herbaceous plants [50]. Mannan-type of hemicelluloses like galactoglucomannans and arabinoglucuronoxylan are the major hemicellulosic components of the secondary wall of

softwood whereas in hardwood glucuronoxylan is the major hemicellulose (Figure 2.8) [8].

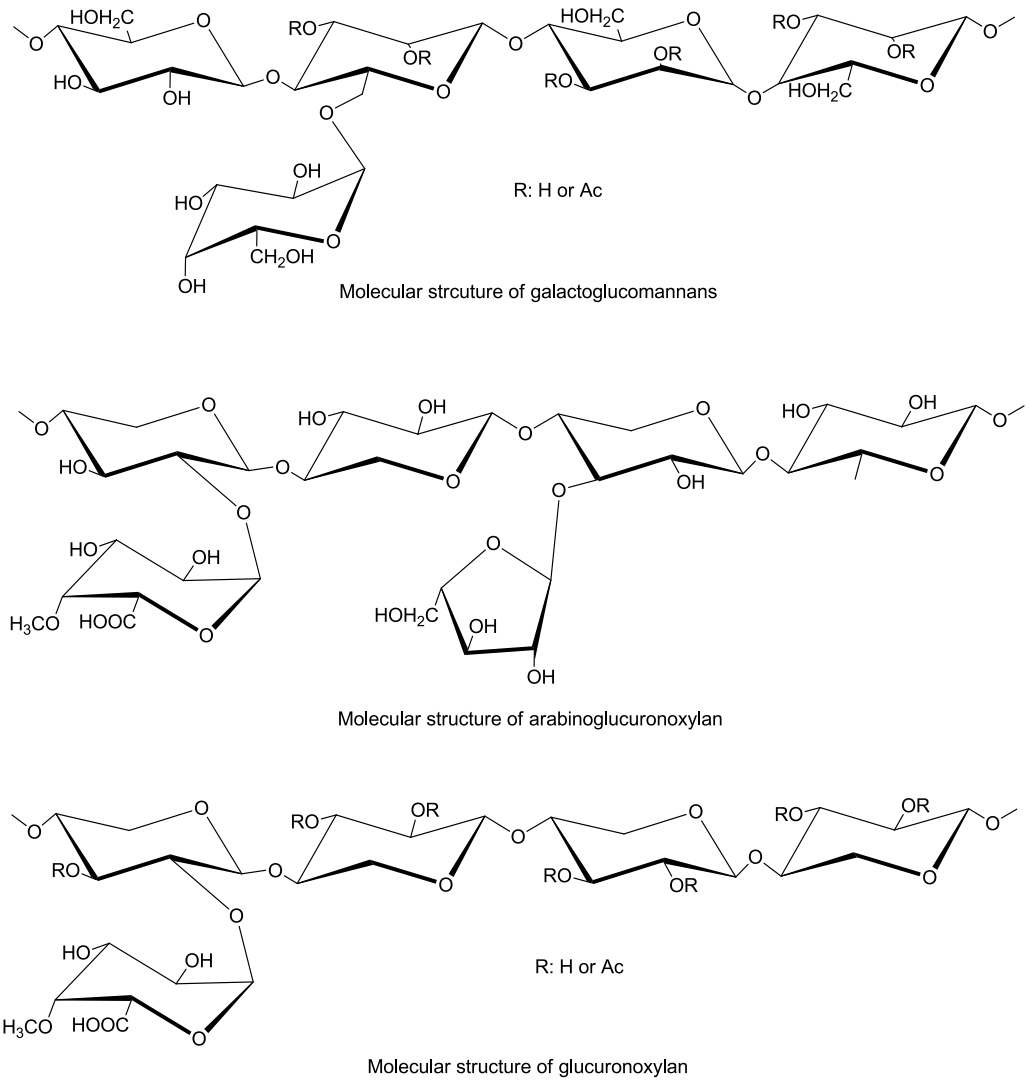

Figure 2.8 Principal structures of polysaccharides in hemicellulose of softwood and hardwood [8]

Table 2.6 summarizes the main structural features of hemicellulose appearing in grass, cereal, softwood and hardwood resources. Upon hydrolysis, the hemicelluloses can be breakdown into their monomers (Table 2.7). In addition, sugar components could take

part in the formation of lignin-carbohydrate complexes (LCC) by covalent linkages between lignin and carbohydrates [51].

Table 2.6 Structural features of main types of polysaccharides present in hemicelluloses [50].

Hemicellulose type	Biological origin	Amount (% dry)	Backbone	Side chains	linkage	DP
Arabinogalactan	Softwood	1-3	β-D-Gal*p*	β-D-Gal*p* α-L-Ara*f* β-L-Ara*p*	β-(1→4) α-(1→3) β-(1→3)	100-600
Arbinoglucuronoxylan	Grasses, softwood	5-10	β-D-Xyl*p*	4-O-Me-α-D-Glcp*A*β-L-Araf	α-(1→2) α-(1→3)	50-185
Arabinoxylan	Cereals	0.15-30	β-D-Xyl*p*	α-L-Ara*f*Feruloy	α-(1→2) α-(1→3)	N/A
Xyloglucan	Hardwood, grasses	2-25	β-D-Glc*p*	β-D-Xyl*p* β-D-Gal*p* α-L-Ara*f* α-L-Fuc*p* Acetyl	β-(1→4) α-(1→3) β-(1→2) α-(1→2) α-(1→2)	N/A
Galactoglucomannan	Softwood	10-25	β-D-Man*p* β-D-Glc*p*	β-D-Gal*p* Acety	α-(1→6)	40-100
Glucomannan	Hardwood, softwood	2-5	β-D-Man*p* β-D-Glc*p*	N/A	N/A	40-70
Glucuronoxylan	Hardwood	15-30	β-D-Xyl*p*	4-O-Me-α-D-Glcp*A* Acety	α-(1→2)	100-200
Glucuronoarabinoxylan	Grasses, cereals	15-30	β-D-Xyl*p*	α-L-Ara*f* 4-O-Me-α-D-Glcp*A* Acetyl	α-(1→2) α-(1→3)	N/A

Table 2.7 Hemicelluloses composition (g/100g of dry biomass) of various lignocellulosic substrates [50].

Biomass	Xyl	Ara	Man	Gal	UA
Poplar	17.7-21.2	0.9-1.4	3.3-3.5	1.1	2.3-3.7
Maple	18.1-19.4	0.8-1.0	1.3-3.3	1.0	4.9
Oak	21.7	1.0	2.3	1.9	3.0
Sweet gum	19.9	0.5	0.4	0.3	2.6
Pine	5.3-10.6	2.0-4.2	5.6-13.3	1.9-3.8	2.5-6.0
Spruce	5.3-10.2	1.0-1.2	9.4-15.0	1.9-4.3	1.8-5.8
Corn stover	14.8-25.2	2.0-3.6	0.3-0.4	0.8-2.2	1.7-1.9
Rice straw	14.8-23.0	2.7-4.5	1.8	0.4	N/A
Wheat straw	19.2-21.0	2.4-3.8	0-0.8	1.7-2.4	N/A

2.2.4 Lignin

Lignin is an amorphous, cross-linked, and three dimensional polyphenolic polymer. The biosynthesis of lignin is generally considered to stem from the polymerization of three types of phenylpropane units as monolignols; coniferyl, sinapyl, and p-coumaryl alcohol, which can then form the so-called guaiacyl (G), syringyl (S), and p-hydroxyphenyl (H) lignin units, respectively (Figure 2.9). Table 2.8 summarizes the typical G/S/H ratio from several sources of biomass. The polymerization process is typical initiated by an enzyme-catalyzed oxidation of the monolignols phenolic hydroxyl groups to yield free radicals, which can then generate a dilignol by coupling with another free radical (Figure 2.10). Subsequent nucleophilic attack by water, alcohols, or phenolic hydroxyl groups on the benzyl carbon of the quinone methide intermediate will restore the aromaticity of the benzene ring [8]. The generated dilignols will then undergo further polymerization to form aryl ether bonds (β-*O*-4) being the most common and important inter-unit linkage.

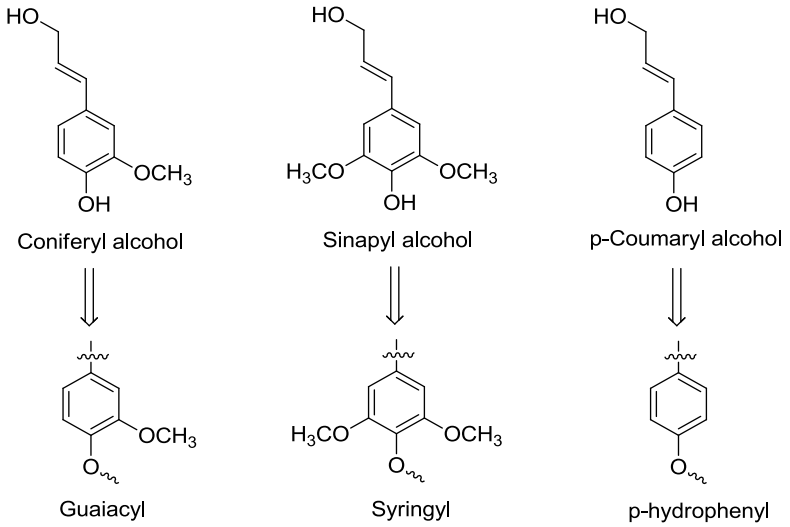

Figure 2.9 Typical phenylpropanoid precursors employed in the biosynthesis of lignin.

Table 2.8 Lignin G/S/H ratio for selected biomass resources.

Biomass substrates	G lignin (%)	S lignin (%)	H lignin (%)	Reference
Poplar	29	61	10 (as *p*-hydroxybenzoate)	[52]
Miscanthus	52	44	4	[53]
Wheat straw	45	46	9	[54]
Rice straw	45	40	15	[55]
Corn stover	51	3.6	46	[56]
Loblolly pine	86	2	12	[57]
Spruce	94	1	5	[58]
Beech	56	40	4	[59]

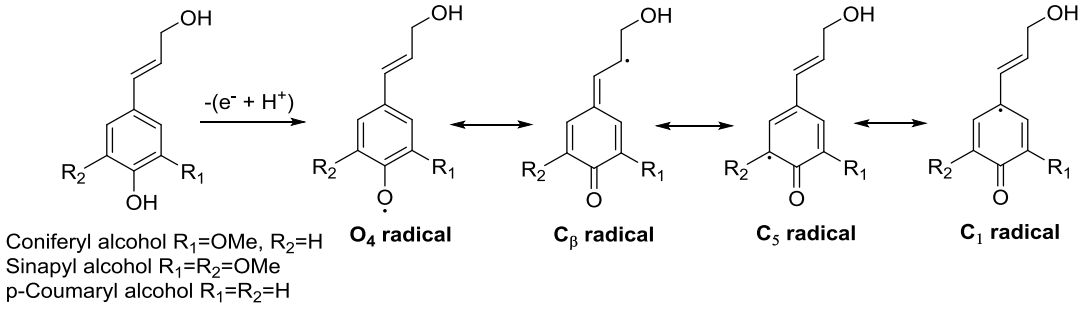

Figure 2.10 Resonance stabilized phenoxy radical during lignin biosynthesis.

Despite the fact that the exact structure of protolignin is still unclear, the dominant structures in lignin have been elucidated as the methods for identification of the degradation products and for the synthesis of model compounds have improved. Examples of the elucidated structural features of lignin include the dominant linkages between the phenylpropane units and their abundance as well as the frequency of some functional groups. Figure 2.11 shows some of the common linkages found in both softwood and hardwood. Softwood lignin is composed mainly of coniferyl alcohol units, while hardwood lignin is composed mainly of coniferyl and sinapyl alcohol units. Lignin in grasses typically contains all three types of monolignols units, with peripheral groups such as hydroxycinnamic acids incorporating into its core structure [60].The distribution of these types of linkages and functional groups are shown in Table 2.9.

Table 2.9 Proportions of different types of linkages connecting the phenylpropane units in lignin [8].

Linkage type	Dimer structure	Percentage
β-O-4	Phenylpropane β-aryl ether	50
β-5	Phenylcoumaran	9-12
5-5	Biphenyl	15-25
5-5/α-O-4	Dibenzodioxicin	10-15
4-O-5	Diaryl ether	4
β-1	1,2-Diaryl propane	7
β-β	β-β-linked structures	2

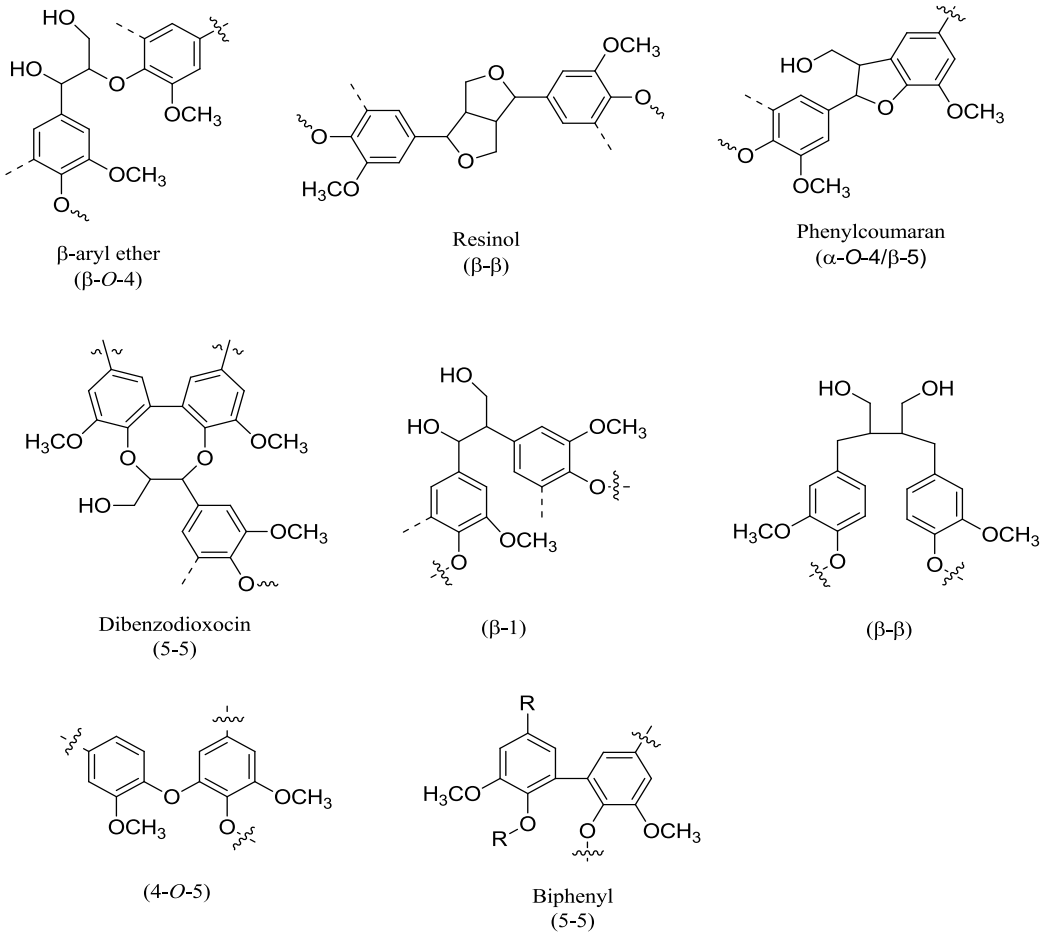

Figure 2.11 Some common inter-unit linkages found in lignin [8].

2.2.5 Lignin-carbohydrate complex

Lignin and carbohydrate molecules can be physically or chemically bonded with each other mainly through covalent bonds forming lignin-carbohydrate complexes (LCCs). Different models for the type and origin of native lignin-carbohydrate bonding has been proposed. Glycosidic bonds between the wood polysaccharides and the lignin have been proposed [61], but the most favored models are probably those involving the nucleophilic addition of carbohydrate units to quinone methide intermediates to give benzyl ether or benzyl ester type bonds (Figure 2.12) [62]. The quinone methide intermediates could

either be those formed intermediately during the lignin biosynthesis or compounds formed by elimination of water from the lignin present in mature wood [63]. With benzyl ethers, the α-hydroxyl group of lignin is connected to the hydroxyl group of carbohydrates. In the case of benzyl esters, the α-hydroxyl group is linked to the carboxyl group of a glucuronic residue in xylan. For phenylglycosides, the alcoholic or phenolic hydroxyl group of lignin is linked to a mono- or a polysaccharide. Finally, the acetal bond involves two hydroxyl groups of a polysaccharide linked to lignin, and the reaction of an acetal group with acid will produce hydroxyl and carbonyl groups [64].

Hardwood and grass LCCs are exclusively composed of 4-*O*-methylglucuronoxylan and arabino-4-*O*-methylglucuronoxylan [65], while in softwood LCCs, the carbohydrate portions are mainly composed of galactomannan, arabino-4-*O*-methylglucuronoxylan, and arabinogalactan, which are linked to lignin at benzyl positions [66]. The mechanism associated with the formation of ester and ether LCCs linkages could be related to the biosynthesis of lignin. Tanaka et al. reported that glucuronic acid reacted with a lignin model to form an ester linkage between the carboxyl group of glucuronic acid and the α-position of phenylpropane unit [67]. Iversen et al. investigated the nature of the lignin-carbohydrate bonding in materials isolated from thoroughly milled spruce wood, suggesting the formation of lignin-carbohydrate bonds present could be explained by the formation of p-alkoxybenzyl ether bonds to the polysaccharides during the biosynthesis of the lignin [63]. In order to convert the carbohydrates or lignin into valuable chemicals or fuels, these covalent LCCs bonds must be broken to separate the carbohydrates from the lignin.

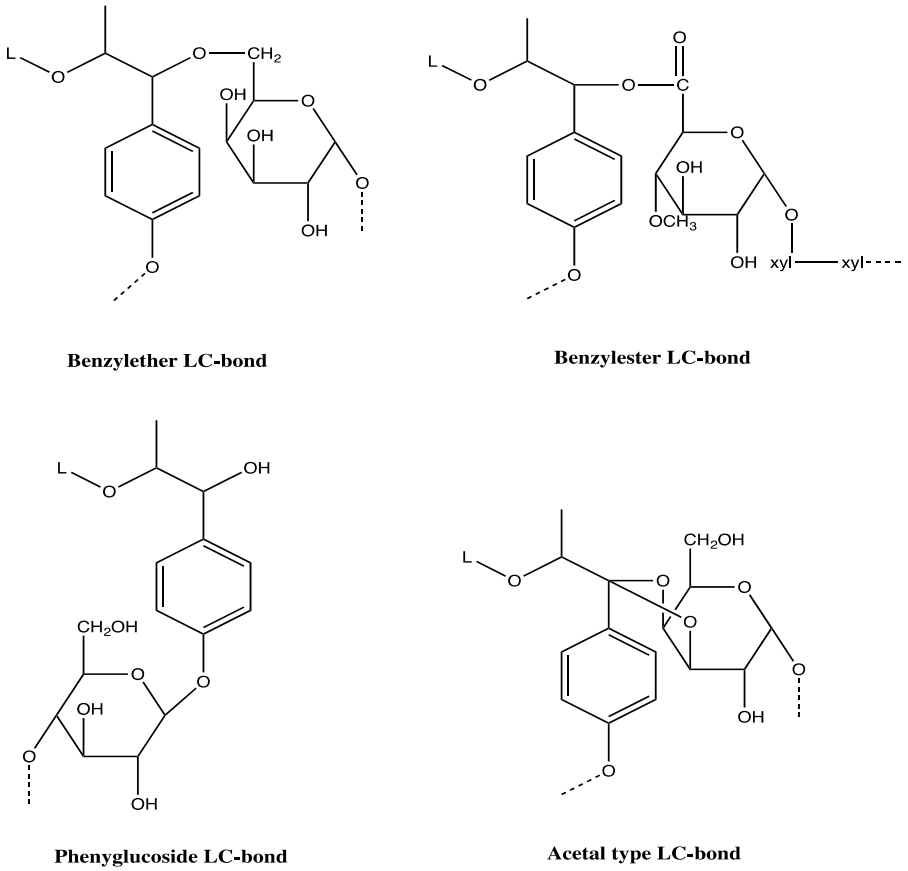

Figure 2.12 Proposed types of lignin carbohydrate linkages [64].

2.3 Reduction of biomass recalcitrance via pretreatment

2.3.1 Biomass recalcitrance

Plant biomass has evolved complex structural and chemical mechanisms for resisting assault on its structural sugars from the microbial attack. Natural factors believed to contribute to recalcitrance of lignocellulosic biomass to enzymes include epidermal tissue, arrangement and density of vascular bundles, amount of sclerenchymatous tissue, degree of lignification, the structural complexity of cell wall constituents (i.e. crystalline nature of cellulose, hemicellulose coating on the cellulose-containing microfibrils of cell wall),

the challenges for enzymes acting on an insoluble substrate (Figure 2.13) [68]. In an effort to assess directly the effects of these cell wall substrate characteristics, years of research have tried on modifying substrate factors and correlating these alteration to changes in biomass recalcitrance, however, much of the literature has reported conflicting trends on the individual effects of many substrate characteristics considered important to biological deconstruction [9]. Lignin is an important factor limiting the rate and extent of enzymatic hydrolysis of biomass, with majority of literature indicated that cellulose digestibility is increased with lignin removal [69,70]. Lignin can not only physically block the access of cellulases to cellulose, but also could adsorb cellulase irreversibly thus decrease the effectiveness of enzymes [71,72]. Conversely, it has also been reported that there was no obvious correlation between lignin content and sugar release of a large natural population of poplar [73]. It has been reported that softwood is usually more resistant to enzymatic hydrolysis than that of hardwood at the same level of delignification, likely due to the S/G ratio [74]. Studer et al. reported that a strong negative correlation between sugar release and lignin content was only found for samples with an S/G less than 2.0, and for higher S/G ratio, sugar release was generally higher indicating the negative influence of lignin was less pronounced [75]. A few reasons have been proposed to explain the higher reactivity of S-rich lignin. First of all, S-rich lignin features predominantly linear chains with less cross-linking than G-rich lignin because of the fact that C-5 position is occupied by a methoxyl group, resulting in fewer highly stable 5-5 and β-5 linkages [76]. The higher occurrence of β-β units is S-rich lignin can lead to shorter chain lengths and subsequently lower molecular weights [77]. The more branched guaiacyl units are likely to have a more spreadable distribution which could act

as a surface barrier restricting the swelling of the cellulosic substrate and reducing the accessible surface area available to the enzymes [78].

Besides lignin, extensive hemicellulose branching and substitutions are also believed to sterically hinder enzyme attack of cellulose. The degree of acetylation on the xylan backbone has been shown to play an important role in the mechanism of plant cell wall resistance to enzyme hydrolysis [79,80]. Grohmann et al. reported as the xylan fraction becomes deacetylated, it becomes 5-7 times more digestible [79]. Chang et al. showed that deacetylation had more significant effects on hemicellulose digestibility than on cellulose digestibility of poplar [69]. Lignin-carbohydrate complexes are also believed to influence the recalcitrance of lignocellulosic plant material, and removal of hemicellulose is typically associated with the breakdown of the cross-linked polysaccharides [81].

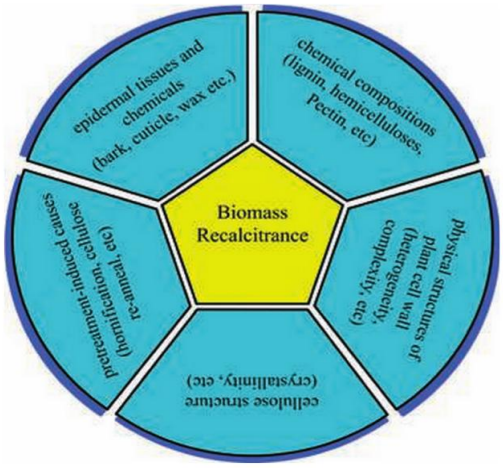

Figure 2.13 Factors constructing biomass recalcitrance [6]

It is generally believed that amorphous cellulose should be hydrolyzed at a much faster rate than *para*-crystalline and crystalline cellulose, indicating the initial degree of

crystallinity of cellulose plays a major role as a rate determinant in the hydrolysis reaction [82]. On the other hand, several reviews reported that it is difficult to conclude that crystallinity is a key determinant of the rate of enzymatic hydrolysis [83,84]. This is because different types of cellulose with different degrees of crystallinity are employed in these studies, therefore it is of prime importance to study samples that have the same basic composition and provenance in order to relate the CrI with hydrolysis rate correctly [85]. In addition, cellulose crystallinity is also believed to affect the ability of cellulase enzyme modules including cellulose binding modules (CBM) and catalytic domains to adsorb or to function on cellulose. The degree of crystallinity of cellulose influences adsorption at a given protein loading and the maximum adsorption constant was shown to be greatly enhanced at low crystallinity indices [86].

Similarly to cellulose crystallinity, the effect of cellulose DP on enzymatic hydrolysis is still under debate. Nahzad et al. reported that initial DP of the pulps did not significantly affect the final extent of hydrolysis [87]. Although it is quite challenging to assess the effect of any individual factors on enzymatic hydrolysis because biomass recalcitrance does not originate from a single structure factor and interactive effects naturally exist between these factors, cellulose accessibility has been consistently reported as probably one of the most important factors.

2.3.2 Cellulase enzyme system

Cellulase is any of several enzymes produced by fungi, bacterial, and protozoans that catalyze cellulolysis – the decomposition of cellulose and of some related

polysaccharides. There are three main types of enzymes involved in hydrolyzing cellulose microfibrils: endoglucanase, exoglucanase, and β-glucosidase. Endoglucanases, e.g., 1,4-β-D-glucan-4-glucanhydrolase (EC 3.2.1.4), can randomly cleave internal bonds at amorphous sites that create new chain ends that can be attacked by exoglucanase. It is generally active against acid-swollen amorphous cellulose and soluble derivatives of cellulose [88]. During hydrolysis of cellulose via endoglucanase, rapid DP decrease of cellulose and dissolution of cello-oligomers are normally observed [89]. Exoglucanase, e.g., 1,4-β-D-glucan-cellobiohydrolases (EC 3.2.1.91), act in a possessive manner on the reducing or non-reducing ends of cellulose polysaccharide chains, generating glucose or cellubiose as major products. This type of enzymes is usually used to active against crystalline substrate such as avicel, amorphous celluloses and cello-oligosaccharides [88]. Finally, β-glucosidase, e.g., β-glucoside-glucohydrolases (EC 3.2.1.21), hydrolyze cellubiose to glucose from non-reducing ends. It is inactive against crystalline or amorphous cellulose. Figure 2.14 illustrates a proposed mechanism for cellulose depolymerization by cellulases. Most reported source of cellulases are derived from *Trichoderma reesei*, which has a size of 5.1 nm in diameter [90].

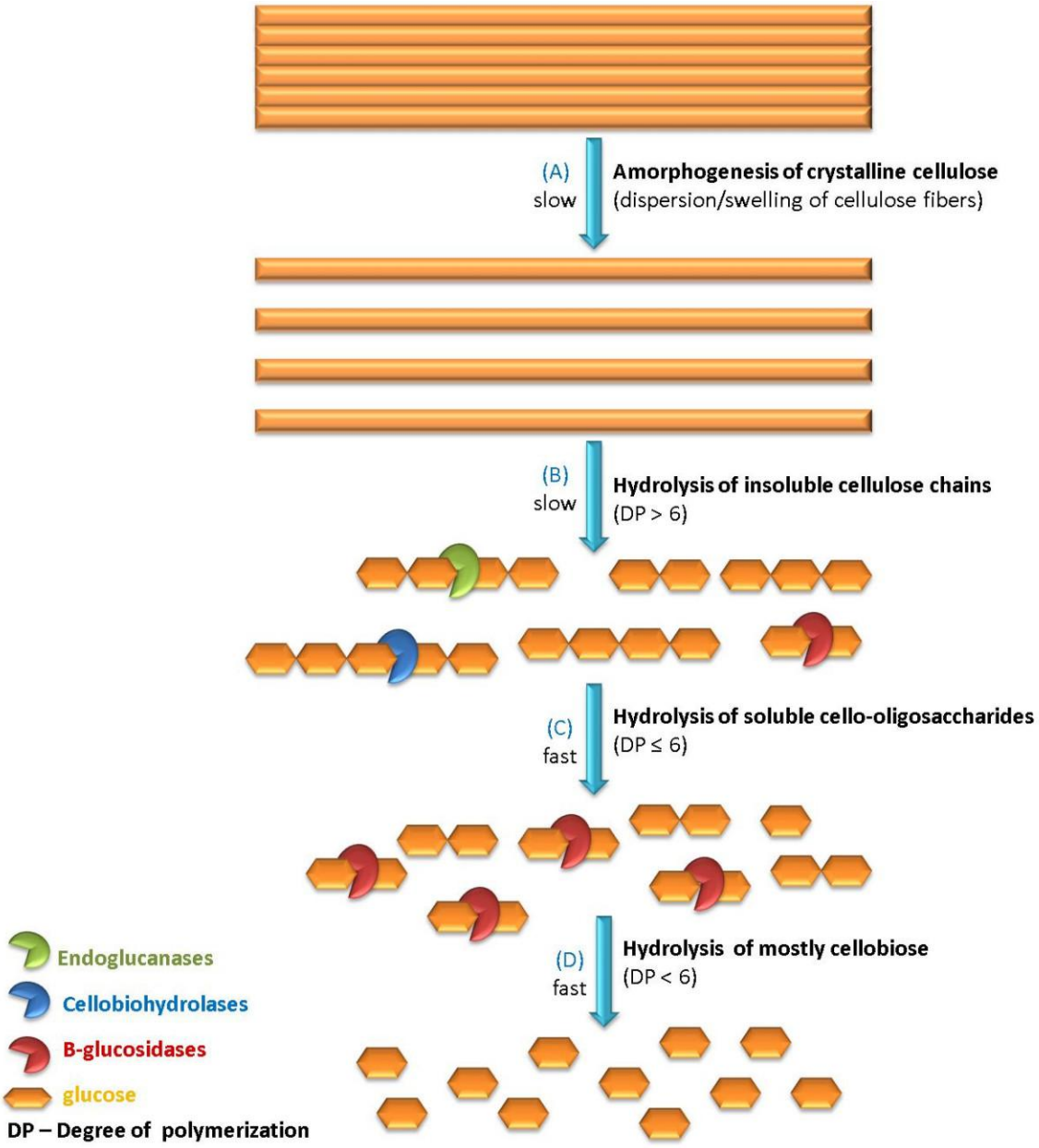

Figure 2.14 Proposed mechanism for cellulose depolymerization by cellulases [91]. (A) Amorphogenesis of crystalline cellulose. (B) Hydrolysis of insoluble cellulose chains. (C) Hydrolysis of soluble cello-oligosaccharides. (D) Hydrolysis of mostly cellubiose.

2.3.3 Cellulose accessibility in biomass recalcitrance[*]

The intimate contact between the cellulose and cellulase, such as *Trichoderma reesei* cellobiohydrolase (CBH), is the prerequisite step for enzymatic hydrolysis to occur, thus the surface area of cellulose should be a critical factor for enzymatic hydrolysis yield and rate [91,92]. Surface area of substrate can be divided into interior surface area which is governed by the size and number of fiber pores, and exterior surface area which is largely determined by the individual fiber dimension [93]. Particle size of lignocellulosic substrate is generally believed to reflect the available exterior specific surface area and it has been found that the decrease of particle size normally leads to an increase of exterior specific surface area [94]. The relationship between particle size/exterior surface area and sugar yields is summarized in a recent review [95]. As shown in Table 2.10, negative relationship between particle size and sugar yield have been reported in a majority of literature. However, a few researches found the average size of cellulose particles did not influence the efficiency of hydrolysis to any noticeable extent [96]. All these controversial findings may be due to cellulase accessibility to cellulose is probably mainly through the pores in the cell wall rather than substrate external surface, and more specifically, approximately over 90% of the substrate enzymatic digestibility is contributed by the accessible pore surfaces [92].

[*] This part of literature review was accepted by Current Opinion in Biotechnology, 2014. It is entitled as "Recent advances in understanding the role of cellulose accessibility in enzymatic hydrolysis of lignocellulosic substrates". The other authors are Arthur J. Ragauskas from School of Chemistry and Biochemistry ate Georgia Institute of Technology. The copyright permissions will be submitted to the thesis office of Gatech.

Table 2.10 Reported relationship between particle size and sugar yield for two categories of cellulosic biomass.

Biomass category	Particle/Mill screen size (μm)	Glucose yield	Relationship	Reference
Pure cellulose	25.52	40.3%	Negative	[97]
	5.54	55.4%		
	0.85	75.7%		
	74-105	~12.5 μmol/ml	Neutral	[98]
	46-63	~12.5 μmol/ml		
	38-46	~11.5 μmol/ml		
Lignocellulosic biomass	1000-2000	72.6%	Negative	[91,99,100,101,102]
	3000-4000	69.1%		
	5000-6000	70.8%		
	32	2.0 g/L	Neutral	[96]
	19	6.6 g/L		
	17	6.2 g/L		
	3200	81.3%	Positive	[103,104]
	6500	84.1%		

The interior surface area is essentially reflected by biomass porosity (Figure 2.15). There are several scales of porosity exist in biomass from the cell lumen to the nano-pores between coated microfibrils [105]. The cell lumen, represents the largest scale of porosity, can trap air that could impede the bulk flow of pretreatment chemistry throughout a biomass particle, but it is not a critical barrier for cellulolytic enzymes because its size is normally in the range of tens of micrometers. Pits are regions in the cell wall where the secondary cell wall is absent and an open pore is maintained between adjacent cell lumen. They are only 20-100 nm and can be considered as part of the nano-scale porosity. However, pits still do not represent a fundamental barrier to cellulolytic enzymes. Clearly, a fundamental barrier to effective enzymatic hydrolysis is the accessibility of a reactive cellulose surface. Carpita et al. estimated the architecture of

plant cell wall pores to be approximately ~5-10 nm in diameter which is nearly sufficient to allow some diffusion of proteins but is too small to allow significant accessibility to cellulolytic enzymes [106]. Transport phenomena suggest that pore size should be at least in the range of 50-100 nm to allow sufficient penetration of enzymes into cell walls [105]. Unlike the exterior surface area, many researches have indicated a positive relationship between interior surface area and enzymatic hydrolysis rate [107,108,109]. Earlier work by Grethlein [110] reported a linear correlation between the initial hydrolysis rate of steam pretreated hardwood and the pore volume of the substrate accessible to a nominal diameter of 5.1 nm representative of the diameter of cellulase.

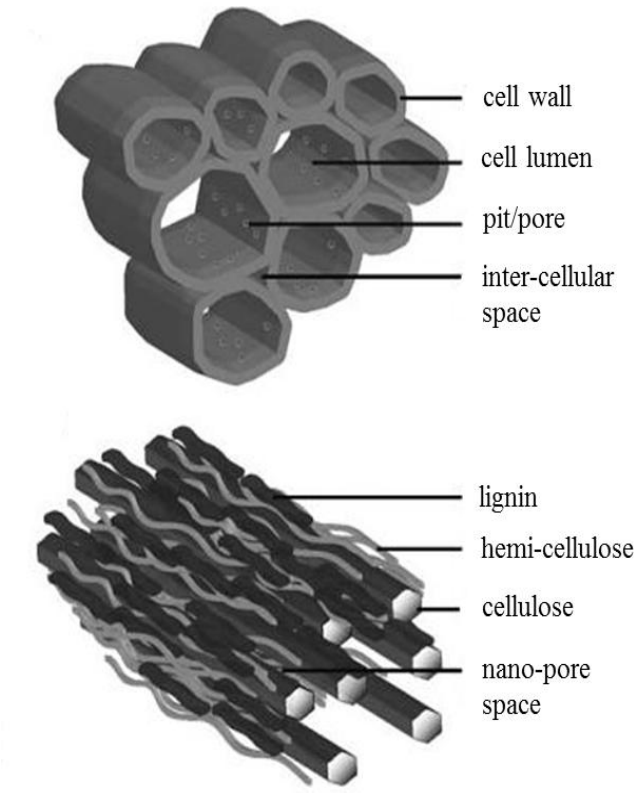

Figure 2.15 Cartoon depiction of several scales of porosity from the cell lumen to the nano-pores between coated microfibrils [111]

2.3.3.1 Analytical techniques used to measure cellulose accessibility

Accurate measurement of cellulose accessibility is the prerequisite step for understanding the role of cellulose accessibility in biomass recalcitrance. One of the classic techniques to measure the specific surface area is the Brunauer-Emmett-Teller (BET) method using nitrogen adsorption [112]. However, it requires prior drying of the substrate which makes it typically less effective due to water removal from nonrigid porous materials could produce partial irreversible collapse of pores. Measurement of porosity has been frequently used as an alternative to represent the amount of accessible surface area of substrate, but it is not straightforward and most of the time very difficult to define by a single number because properties such as dimension, geometry, topology, and connectivity should be all considered. For example, the "ink-bottle" effect which refers to a large pore connected to a small opening, can limit the accessible surface area of the substrate, therefore should be considered during a pore size measurement. However, this is obviously not easily measured and therefore pore size analysis are usually based on the assumption that biomass pores are cylindrical in shape [113]. Solute exclusion, a widely used method to investigate the pore characteristics of the lignocellulosic substrates, is based on the measured accessibility of pores to various sizes of non-interacting probe molecules such as dextran. Wang et al. evaluated the cellulose accessibility of a set of hornified pretreated lodgepole pine using solute exclusion, and reported that 24 h air drying in a humidity controlled environment at 25 ^{o}C can decrease the surface area that available to solute of 5.1 nm diameter from ~22 m^2/g to ~17 m^2/g [92]. Although it can measure the substrate in its wet state, it is time consuming, unspecific to cellulose, and only measures the interior surface areas. Another promising approach for quantitative

determination of total substrate accessibility to cellulases relies on the adsorption of a non-hydrolytic fusion protein containing cellulose-binding module (CBM) and fluoresce protein (TGC) which have very similar molecular size to that of cellulase enzymes [92]. However, these proteins also bind unspecifically to lignin and therefore require a step using bovine serum albumin (BSA) to block the lignin prior the adsorption of cellulase enzymes. An alternative approach to examining pore size employs direct dyes such as Simons' stain as a potentially useful semi-quantitative method for estimating the total available surface area of lignocellulosic substrates [114]. It evaluates the large-to-small ratio of a substrate by applying two different dyes: Direct Blue 1 and Direct Orange 15 (Figure 2.16). Direct Blue 1 has a well-defined chemical formula $C_{34}H_{24}N_6Na_4O_{16}S_4$ with a molecular diameter of ~1 nm. Direct Orange 15 is a condensation product of 5-nitro-*o*-toluenesulfonic acid in aqueous alkali solution with a diameter in the range of ~5-36 nm, and it also has much higher binding affinity for the hydroxyl groups on a cellulosic surface compared Direct Blue 1. Therefore, the ratio between the Direct Orange 15 and Direct Blue 1 adsorption capacities can be calculated as a measure of large-to-small pore ratio of a substrate. In addition, techniques involved using NMR are also valuable diagnostic tools in terms of porosity measurement, including NMR cryoporometry, relaxometry and diffusometry, but they are expensive and most of time require special training, complicated setup and long experiment time [11,115,116,117].

A summary of these analytical methods for characterization of cellulose accessibility for lignocellulose substrates , including their advantages and disadvantages is presented in Table 2.11. Different techniques can give considerably different results, due to the

differences in the principles of measurement between the techniques. The mean pore diameter of pine kraft fibers was determined to be around 3 nm using solute exclusion, while it is significantly higher when measured by a NMR technique, about 13 nm [118].

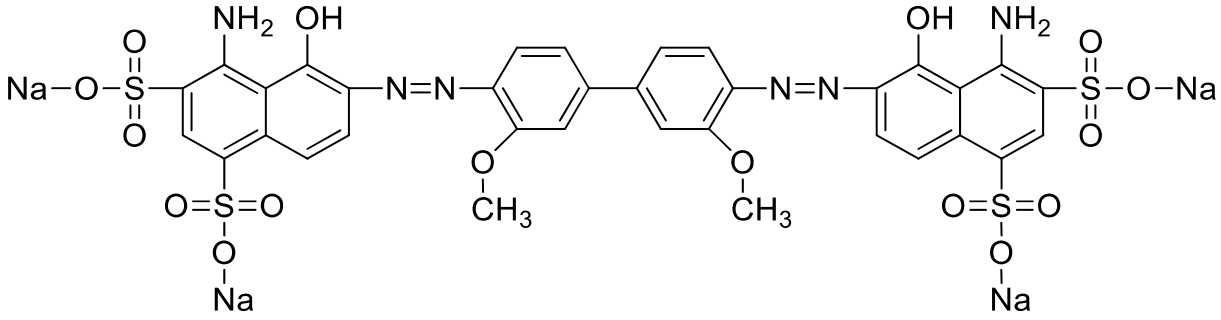

Direct Blue 1

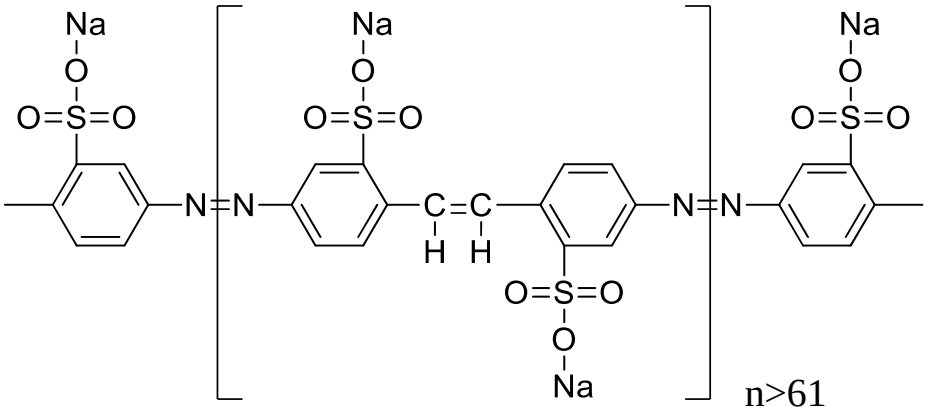

Direct Orange 15

Figure 2.16 Molecular structures of the direct dyes for Simons' stain.

Table 2.11 Summary of analytical methods for characterization of cellulose accessibility for lignocellulose substrates [119]

Techniques	Analytical background and procedure	Advantages & Disadvantages	References
Nitrogen adsorption	Nitrogen passes readily though cell walls and its uptake provide a good general measure of total surface area. Samples were dried, degassed, and then cooled in the presence of nitrogen gas, allowing nitrogen as to condense on the surfaces and within the pores. The quantity of gas that condensed was determined from the pressure decrease after the sample was exposed to gas, and the surface area was calculated using Brunauer-Emmett-Teller (BET) model that relates the gas pressure to the volume of gas adsorbed	Advantages: ◆ Accurate, quick and robust method for determining the surface area accessible to nitrogen Disadvantages: ◆ Measurement requires a prior drying of the substrate which makes it typically less effective due to the partial irreversible collapse of pores ◆ Small size of nitrogen cause over-estimation of cellulose accessibility	[120,121]
Mercury porosimetry	Similar to nitrogen adsorption, dried and degassed sample s were introduced into a chamber surrounded by mercury with pressure on the mercury gradually increased to force mercury into the pores. Relationship between pore diameter and applied pressure was given by the Washburn equation. The volume of mercury entering the pore was measured as the pressure increased, indicating the cumulative volume of all available pores of radius equal to, or greater than a corresponding pore diameter.	Advantages: ◆ Allows the pore size analysis to be undertaken over a wide range of mesopore-macropore widths ◆ Provides a wide range of information, e.g. pore size distribution, total pore volume, specific surface area, tortuosity, permeability, fractal dimension. No other porosity characterization technique can achieve this Disadvantages: ◆ Measurement requires a prior drying of the substrate ◆ Measures the largest entrance towards a pore, but not the actual inner size of a pore	[122,123]
Solute exclusion	Solute exclusion technique is based on the accessibility of probe molecules to the substrate pores of different sizes. A known concentration of a solute molecule solution is added into the swollen substrate. The probe molecule solution was then diluted by water contained in the initial substrate. The water presented in the pores that was not accessible to the probe molecules will not contribute to the dilution. As a result, the substrate pore size and volume distribution can be determined using the concentration of a set of different solute solutions with various molecule sizes.	Advantages: ◆ Measurement can be done in wet state quantitatively Disadvantages: ◆ Laborious, unspecific to cellulose, does not account for the external surface area ◆ Not an acceptable tool for determination of absolute pore size and volume distribution; Effected by pore shape and osmotic pressure	[110,124]

Simons' stain	Simons' stain evaluates the large-to-small ratio of a substrate by applying two dyes with different color, molecular size and cellulose binding affinity. Samples were treated using a serious of mixed solution of orange and blue dye with increasing concentrations. The maximum amount of dye adsorbed to the lignocellulosic substrates was calculated using the Langmuir adsorption equations. The ratio of adsorbed orange and blue dye, a value used to estimate the relative porosity and assess the overall accessible surface area, can be then calculated.	Advantages: ◆ Measurement can be done in wet state ◆ Relatively fast, simple and sensitive ◆ Measure both interior and exterior surface area Disadvantages: ◆ Effected by pore shape and tortuosity ◆ Not fully quantitative	[93,125]
Protein adsorption	Quantitative determination of cellulose accessibility to cellulase based on the Langmuir adsorption of a fusion protein containing a cellulose-binding module and a green fluorescent protein. Protein adsorption on cellulose usually conducted in a typical enzymatic hydrolysis buffer solution, and the protein adsorption on the solid surface can be calculated by the Langmuir equation	Advantages: ◆ Perfectly applied in enzymatic hydrolysis process due to the exist of a cellulose-binding module as cellulase has ◆ Probing molecule have a very similar molecular size to that of cellulase enzymes Disadvantages: ◆ Total exposed surface to the probe molecules include some non-cellulosic surface, for example, lignin.	[92]
NMR cryoporometry	Cryoporometry is a technique for determining pore size distribution that takes advantage of the fact that small crystals formed from liquid within pores melt at a lower temperature than bulk liquid known as melting point depression caused by enthalpic interaction with the pore surface. Hydrated samples were cooled to negative temperature to completely freeze all the adsorbed water, and the intensity of the NMR signal which represents the amount of unfrozen water at a specific temperature was measured by a Carr-Purcell-Meiboom-Gill sequence (CPMG) as temperature increases to generate the melting curves. The melting point depression of the liquid can be related to the pore size through the Gibbs-Thompson equation	Advantages: ◆ Non-destructively and quantitatively determination of pore size distribution ◆ Measurement can be done in wet state Disadvantages: ◆ Pore size determination range is limited by the temperature control ◆ Expensive, requires complicated setup and long experiment time	[11,115]

NMR Relaxometry	NMR relaxation experiment can provide information pertaining to the molecular mobility within a porous system. The spin-spin (T_2) relaxation curve can be obtained via a CPMG sequence to investigate the changes in the nature of biomass-water interactions and subsequent accessibility. Basically, as the T_2 relaxation time increases, the degrees of freedom of water in the pores also increases, causing a decrease in the proportion of amount of water located at pore surface versus the pore interior. Therefore, in systems of increasing average pore size, the pore surface area to volume ratio will decrease and is therefore detected by an increase in the T_2 relaxation time. It is also well known that liquid molecules near a solid surface will have different spin-lattice (T_1) relaxation profiles from that of the bulk liquid because of the interactions at the solid-liquid interface. As a result, the observed average T_1 time of the adsorbed water could also reflect the surface area to volume ratio of the pores	Advantages: ◆ Non-destructively measurement, not affected by pore inlet size or shape Disadvantages: ◆ Expensive, requires complicated experiment setup	[11,117]

2.3.3.2 Effect of lignin and hemicellulose on cellulose accessibility

It has been suggested that increasing cellulose accessibility depends on not only how much total biomass was removed but also what component with a specific structure and from where it was removed [12]. Hemicellulose, which is generally found on the outer surface of cellulose fibers but is also diffused into the inter-fibrillar space through fiber pores, has been proposed to act as a physical barrier that limits the cellulose accessibility. Therefore, the addition of accessory enzymes such as xylanase during enzymatic hydrolysis can increase the cellulose accessibility as a result of xylan solubilization. A recent study reported that this significant improvement in cellulose accessibility indicated by Simons' stain is due to the increase in fiber swelling and fiber porosity caused by synergistic interaction of the xylanase and cellulase [126]. Besides xylan removal, the effect of side-chain components such as acetyl groups on cellulose accessibility has been also investigated recently, indicating that acetyl groups may restrict cellulose accessibility by inhibiting productive binding through increasing the diameter of cellulose chain or changing its hydrophobicity [80,127]. Although removing lignin has been shown to increase yield of enzymatic hydrolysis in most current studies, the direct effect of lignin removal on cellulose accessibility is not fully clear because lignin reduces the effectiveness of enzymatic hydrolysis by limiting the cellulose accessibility as well as by binding cellulase unproductively, and the relative contribution of these two roles of lignin is not yet fully understood. A recent study reported that the presence of lignin may not directly occlude cellulose present in lignocelluloses but rather impact cellulase action indirectly by its association with xylan [128]. Kumar and Wyman also reported that delignification of corn stover greatly enhanced enzyme effectiveness but had a very

limited effect on cellulose accessibility, indicating that lignin did not directly control cellulose accessibility but restricted xylan accessibility which in turn controlled the access of cellulase to cellulose [127].

2.3.3.3 Increase of cellulose accessibility via non-hydrolytic proteins

In very recent years, several cellulolytic organisms have been shown to produce non-hydrolytic proteins that could be used as cellulase activity enhancement factors due to its ability to deagglomerate the cellulose manifested as dispersion of the microfibrils, loosening of the macrofibrils, swelling and roughening of lignocellulosic substrates, thereby increasing the cellulose accessibility. These non-hydrolytic disruptive proteins could be categorized into two distinct groups based on their catalytic mechanisms [91]. For example, proteins with uncharacterized catalytic function including Expansins, Swollenin, and Loosenin are thought to increase cellulose accessibility mainly through disruption of the hydrogen bonding network of the substrate. Recently, fungal-derived, copper-dependent polysaccharide monooxygenases (PMOs), formally known as GH61 proteins, have been shown to catalyze the oxidative cleavage of glycosidic bonds on the surface of cellulose without requiring separation of a glucan chain, increase the substrate accessibility for hydrolytic enzymes [129].

2.3.3.4 Increase of cellulose accessibility via biomass pretreatment

To date, numerous physical or chemical pretreatment methods have been developed to overcome biomass recalcitrance, including dilute acid (DAP), hot water, steam explosion, lime, organic solvent, ionic liquid (IL) and ammonia fiber expansion (AFEX). The

changes in lignocellulosic structure during these commonly applied pretreatment technologies have been recently reviewed by Hu and Ragauskas [130]. Although the mechanism of each pretreatment is different, the final objective is always the same – increasing cellulose accessibility. The major mode of action to increase the cellulose accessibility by different pretreatments is summarized in Table 2.12.

The increase of cellulose accessibility by hot water pretreatment, steam explosion and DAP is mainly due to the removal of hemicellulose [11,121,131,132], while organosolv pretreatment increases cellulose accessibility mainly by removal of lignin as well as hemicellulose [133,134]. Lignocellulosic structure of biomass simultaneously underwent fragmentation and swelling during DAP with fragmentation releasing small components, thereby enlarging the specific surface area. However, with the pretreatment time extended, the swelling behavior of biomass became more drastic, resulting in a much lower specific surface area. Chen et al. reported that the specific surface area of DAP sugarcane bagasse decreased from 2.38 m^2/g to 0.98 m^2/g as the pretreatment time increased from 5 min to 10 min [112]. A decrease in molecular weight of lignin during DAP, its hydrophobicity, and the surface tension effects of water can cause the deposition of spherical lignin droplets on the fiber surface, which increases the pore size for the enzymes to diffuse into and out of the cell-wall matrix, but at the same time it also significantly reduces the surface area upon which enzymes can productively bind [135,136]. However, this limitation in cellulose accessibility could be overcome by high enzyme loadings, delignification or treatments such as neutral sulfonation that increase lignin's hydrophilicity by incorporating sulfonic acid groups onto lignin [137]. It was

also found that the near complete removal of xylan and lignin by DAP could result in decreased cellulose accessibility possibly due to the aggregation of adjacent cellulose microfibrils [138]. In contrast, AFEX pretreatment improved cellulose accessibility via cleaving lignin-carbohydrate ester linkages, partially solubilizing cell wall extractables and relocating these extractables to cell wall surfaces, thereby creating interconnected tunnel-like networks of nanoporous structures with sizes from 10 to 1000 nm, as visualized by transmission electron microscopy (TEM) and 3D-electron tomography [139]. Alkaline pretreatment increases the cellulose accessibility via removing lignin as well as some acetyl groups and various uronic acid substitutions on hemicellulose that lower the accessibility of enzyme to the cellulose [140]. IL effectively dissolves the highly-ordered hydrogen bond in cellulose fibers causing the increase in accessibility much more effective than traditional pretreatments [141,142]. Li et al. reported a significant increase in the BET surface area from 0.7 to 15.1 m^2/g, which is 21.6 times greater after IL pretreatment using 1-ethyl-3-methylimidazolium acetate for corn stover at room temperature [120]. Table 2.13 summarizes the cellulose accessibility change after different biomass pretreatment reported in literature using different techniques.

In conclusion, all the pretreatment significantly increases the accessible surface area of cellulose via various mechanisms such as lignin and hemicellulose removal/redistribute, particle size reduction, and pore expansion. DAP is probably one of the most effective pretreatment techniques among the traditional pretreatments due to its ability to redistribute the lignin and significant pore expansion besides nearly complete removal of hemicellulose. The relatively new IL pretreatment is probably the most effective

pretreatment techniques to increase cellulose accessibility, though facing significant challenges, has receiving growing interest from the biofuels community. In our opinion, the ideal pretreatments should minimize the recalcitrance and at the same time maintaining the integrity of fermentable sugars.

Table 2.12 Summary of major mode of action for different pretreatments in terms of cellulose accessibility increase.

Pretreatment	Major mode of action*	References
Hot water	● Preserving most of the cellulose ● Significant removal of hemicellulose ● Partially depolymerization of lignin ● Increase of plant cell wall pore size/volume	[10,131,143]
DAP	● Nearly complete removal of hemicellulose ● Significant disruption and redistribution of lignin ● Increase of plant cell wall pore size/volume	[10,11,117,143]
Steam Explosion	● Reduction of particle size associated with increase of specific surface area ● Significant removal of hemicellulose ● Partial transformation of lignin ● Significant expansion of pore size and increase of pore volume caused by explosive decompression	[117,132,143]
Alkali	● Significant removal of lignin ● Significant removal of acetyl groups and uronic acid substitutions on hemicellulose ● Swelling of cellulose leading to an increase of internal surface area	[130,143,144]
AFEX	● Ammonolysis of lignin-carbohydrate complex ester linkages, solubilization and relocation of cell wall extractables leading to the formation of nanoporous, interconnected tunnel-like networks ● Rapid pressure release leading to the formation of large pores at the middle lamella cell wall	[139,143]
Organosolv	● Significant removal of lignin and hemicellulose ● Increase of accessible surface area and pore volume	[133,134]
Ionic liquid	● Regeneration of nearly complete amorphous cellulose ● Disruption of inter- and intro-molecular hydrogen bonds resulting in the increase of accessible binding sites of cellulose for cellulase	[120,145]

* This section only focuses on the major mode of action of each pretreatment to increase cellulose accessibility.

Table 2.13 Characterization of cellulose accessibility before and after pretreatment by different techniques.

Biomass substrates	Analytical techniques	Cellulose accessibility		Reference
Untreated poplar	NMR	Average spin-lattice T_1 times of D_2O (ms)	23.9	[117]
5 min DAP poplar at 160 ^oC	relaxometry		27.8	
10 min DAP poplar at 160 ^oC			32.0	
60 min DAP poplar at 160 ^oC			36.3	
Untreated switchgrass	Simons' Stain	Orange:Blue ratio	0.08	[125]
10 min microwave-based $Ca(OH)_2$ pretreated switchgrass			0.26	
10 min microwave-based NaOH pretreated switchgrass			0.39	
10 min microwave-based Na_2CO_3 pretreated switchgrass			0.14	
Untreated mixed hardwood	Solute exclusion	Specific surface area available to solute of 5.1 nm diameter (m^2/g)	14.8	[124]
30 min H_2O_2 pretreated mixed hardwood at 25 ^oC			24.5	
30 min Organosolv pretreated mixed hardwood at 90 ^oC			30.7	
Untreated spruce	Nitrogen adsorption	Burnauer-Emmett-Teller (BET) surface area (m^2/g)	0.4	[121]
7 min SO_2 pretreated spruce at 194 ^oC			1.3	
7 min SO_2 pretreated spruce at 207 ^oC			2.7	
7 min SO_2 pretreated spruce at 220 ^oC			8.2	
Never dried pulp	NMR Cryoporometry	Cumulated pore volume from 2 to 10 nm (cm^3/g)	0.064	[115]
Bench dried pulp			0.062	
Oven dried pulp			0.044	

One of the most critical challenges that must be addressed in order for lignocellulosic biofuels to become commercially available is to develop cost-effective pretreatments. Steam explosion and hot water pretreatment makes use of water and therefore has the lowest recycling and environment cost. The reactor system for DAP is significantly more costly than hot water pretreatment reactor, and the acid neutralization and recovery after pretreatment also increases the costs. As an alkaline pretreatment, lime pretreatment can be performed at low temperature which significantly reduces huge energy and cost demand required to maintain high thermal steady conditions as well as the use of pressured vessels [146]. The relative high cost of organic solvents used in organosolv pretreatment makes it much more expensive than other leading pretreatment processes, however, it also potentially lowering the enzyme costs by separation of lignin before the enzymatic hydrolysis. As the most effective pretreatment in terms of cellulose accessibility increase, ionic liquid currently suffers significant challenges that stand in the way including high cost associated with the use of ionic liquid as well the subsequent requirement of ionic liquid recovery and recycling [147]. Table 2.14 highlights some typical pretreatment conditions and their features reported in literature.

Table 2.14 Selected pretreatment methods and typical conditions [148].

Pretreatment methods	Pretreatment conditions	Remarks
Mechanical comminution	Chipping, grinding, milling	Milling: vibratory ball mill, knife or hammer mill
Steam explosion	Saturated steam at 160-290 ^{o}C with pressure (*P*) 0.69-4.85 MPa for several sec or min, then decompression until atm. pressure	It can handle high solids loads; lower energy input; 80-100% hemicellulose hydrolysis, and 45-65% xylose recovery
Hot water	Pressurized hot water at 170-230 ^{o}C with pressure > 5 MPa for 1-46 min; solids load < 20%	Addition of H_2SO_4 or SO_2 improves efficiency; Lignin is not solubilized but redistributed; 80-100% hemicellulose hydrolysis; 88-98% xylose recovery; low formation of inhibitors;
Ammonia fiber explosion	1-2 kg ammonia/kg dry biomass, 90 ^{o}C, 30 min, p = 1.12-1.36 MPa	Ammonia recovery is required; 0-60% hemicellulose hydrolysis; No inhibitors formation; ~10-20% lignin solubilization
Dilute acid pretreatment	0.74-5% H_2SO_4, HCl, or HNO_3, P ~ 1 MPa; 5-10 wt% dry substrate loading; T = 160-200 ^{o}C	pH neutralization is required; 80-100% hemicellulose hydrolysis; Lignin is not solubilized but redistributed; Acid recovery is required
Alkaline hydrolysis	Dilute NaOH, 24 h, 60 ^{o}C; $Ca(OH)_2$, 4 h, 120 ^{o}C; it can be complemented by adding H_2O_2 at lower temperature (35 ^{o}C)	Reactor costs are lower compared to acid pretreatment; > 50% hemicellulose hydrolysis; 60-75% xylose recovery; low inhibitors formation; 24-55% lignin removal for hardwood, and lower for softwood
Organosolv process	Organic solvents (methanol, ethanol, acetone, ethylene glycol) or their mixture with 1% of H_2SO_4 or HCl; 185-198 ^{o}C; 30-60 min, pH = 2.0-3.4	Solvent recovery required; Almost total hydrolysis of hemicellulose, and total lignin solubilization and breakdown of internal lignin and hemicellulose bonds

2.4 Genetic modification of biomass feedstock with low recalcitrance

Recently, genetic manipulation of biomass feedstock has been mainly focused on changing the cell wall components and structures to improve cellulose accessibility. One of the strategies is to develop low-lignin transgenic plant. Research on the molecular mechanisms regulating lignin biosynthesis in biomass feedstock, such as switchgrass has just started in recent years. Transgenic switchgrass with a down-regulated caffeic acid O-methyltransferase (COMT) gene in the lignin pathway revealed a normal growth phenotype, reduced lignin content, showed significantly improved saccharification efficiency by 29-38% without pretreatment [149]. Another switchgrass lignin biosynthesis gene, *cinnamyl-alcohol dehydrogenase* (CAD) was also recently identified, and the down-regulation resulted in a decreased lignin content of switchgrass that potentially enhances the biofuel production [150]. Furthermore, a very recent study demonstrated that overexpression of PvMYB4 gene, a general transcriptional repressor of the phenylpropanoid/lignin biosynthesis pathway, could lead to high yield ethanol production through dramatic reduction of recalcitrance [151]. Altering hemicellulose levels and their side chain is another main approach to genetically modify the plants to increasing cellulose accessibility. Silencing of the *PoGT47C* gene in poplar, a glycosyltransferase homologous to *Arabidopsis FRA8* involved in hemicellulose biosynthesis, has been reported to reduce the xylan content and increase the glucose yield [152].

CHAPTER 3

EXPERIMENTAL MATERIALS AND PROCEDURES

3.1 Chemical and Materials

3.1.1 Chemicals and materials

Chemicals and materials were purchased from Sigma-Aldrich (St. Louis, MO) or VWR (West Chester, PA), and used as received unless otherwise specified. All gases were purchased from Airgas (Radnor Township, PA). G8 glass fiber filter for carbohydrate analysis were purchased from Thermo Fisher Scientific (Madison, WI). Direct Blue 1 (Pontamine Fast Sky Blue 6BX) and Direct Orange 15 (Pontamine Fast Orange 6RN) dyes were obtained from Pylam Products Co. Inc. (Garden City, NY). Ultrafiltration apparatus was purchased from Amicon Inc. (Beverly, MA). Ultrafiltration membrane with a molecular weight cutoff 100 K was purchased from Millipore Corporation (Bedford, MA). Cellulase from *Trichoderma reesei* ATCC 26921 and Novozyme 188 (β-glucosidase) from *Aspergillus niger* were purchased from Sigma-Aldrich and used as received.

3.1.2 Biomass substrate

Baseline *Populus* (*trichocarpa x deltoides)* were harvested in 2008 and 2012 from area 0800 at Oak Ridge National Laboratory (ORNL), TN. Samples were shipped to National Renewable Energy Laboratory (NREL) in Golden, CO for room temperature air drying, debarking, and size-reduction using Model 4 Wiley Mill (Thomas Scientific, Swedesboro,

NJ) through a 1 mm screen size. Samples were stored in a freezer to maintain the moisture content and shipped to Georgia Tech upon request. Samples were further milled through a 20-80 mesh screen to produce particles with diameters of 0.20 mm to 0.80 mm (Thomas-Wiley Laboratory Mill Model 4, Arthur H. Thomas Company, Philadelphia, PA). Milled sample was stored at -20 ^{o}C for further analysis and treatments.

3.2 Experimental procedures

3.2.1 Soxhlet extraction

Extractives were removed by placing the biomass samples into an extraction thimble in a Soxhlet apparatus (Foss, Soxtec^{TM} 2050). The extraction flask was filled with dichloromethane and then refluxed with boiling rate of 24 solvent cycles per h for ~8 h. The extractive-free solids were air dried overnight in fume hood, and sealed in bag and stored in refrigerator for further analysis

3.2.2 Biomass pretreatment

3.2.2.1 Dilute acid pretreatment

Dilute acid pretreatment were applied on lignocellulosic using different sulfuric acid concentration and temperature. Samples were first prepared by presoaking in a ~0.15 mol/L dilute sulfuric acid solution for 4 h at room temperature. The presoaked slurry was then filtered to remove the solid material and washed with an excess of deionized (DI) water. A mass of 3.00 g of the presoaked samples was transferred to a 300 mL mini-Parr reactor with ~0.15 mol/L sulfuric acid solution at 5% dry solids. The reactor was then

sealed under ambient atmospheric conditions, and heated to 150 ^{o}C over ~30 min (~6 ^{o}C min^{-1}). The Parr reactor was held at this temperature (±2 ^{o}C) for two specified residence time ±30 s (10 min and 60 min), and then quenched in an ice bath for ~5 min. The pretreated slurry was filtered to remove the solid material and washed with an excess of deionized water. Other dilute acid pretreatments were done using similar procedures, with different temperature (120 ^{o}C and 160 ^{o}C) and residence times (10 min and 60 min).

3.2.2.2 Steam explosion

The steam explosion pretreatment was done in University of California, Riverside, and samples were used as received. Milled biomass was placed into a woven metal mesh basket, which was then suspended in a 4L Hastelloy steam reactor. Steam for pretreatment was provided by a Fulton steam boiler (FB-075-L, Fulton Companies, Pulaski, NY), which was controlled by setting the boiler pressure to the saturated steam pressure corresponding to the target temperature of 150 ^{o}C. Pretreatments were performed at 150°C for ~10 min (the heating time was less than 15 s), after which the temperature and pressure were suddenly dropped by opening a valve at the bottom of the vessel, discharging all pretreatment liquid. After cooling, the metal basket was removed from the steam reactor, and the pretreated milled biomass was recovered.

3.2.2.3 Alkaline pretreatment

For sodium hydroxide pretreatment, 2% (w/v) solution hydroxide aqueous solution was added to lignocellulosic substrate at 5% dry solids to liquor (w/w) ratio in a 4560 mini-Parr 300 mL pressure reactor. The mixture was allowed to remain at 120 ^{o}C in the reactor

for 2, 10, and 60 min and the impeller speed was set about 100 rpm. After quenching in an ice bath for ~10 min, the pretreated slurry was filtered to remove the solid material and washed with an excess of DI water. Other sodium hydroxide pretreatments were done using similar procedures, with different concentration (1% w/w), temperature (80 ^{o}C), and residence times (10 min and 60 min). For lime pretreatment, 0.10 M lime was added to *Populus* in a Parr reactor and the mixture was allowed to remain at 120 ^{o}C for 10 and 60 min. The pretreated slurry was filtered to move the solid material and washed with an excess of DI water. Paramagnetic impurities were removed by washing the solids with a dilute aqueous solution of 10 mM ethylenediaminetetraacetic acid (EDTA) and DI water. For the soaking ammonia pretreatment, *Populus* samples were immersed in a 30 wt. % of aqueous ammonia solution in screw-capped reagent glass bottles at 75 ^{o}C for 24 h and at room temperature for 5 days in 5% (w/v) solid to liquid ratios. After soaking, the solids were filtered, washed with DI water until its pH was near neutral, and stored in refrigerator at 4 ^{o}C until used.

3.2.2.4 Hot water pretreatment

Hot water pretreatment were performed in similar procedure compared with dilute acid pretreatment using water as the solvent. It was performed at 120 ^{o}C and 160 ^{o}C in a 4560 mini-Parr 300 mL pressure reactor for 10 and 60 min. The reactor was sealed under ambient atmospheric conditions, and heated to target temperature at a ramp rate of ~6 ^{o}C/min from room temperature.

3.2.3 Dye preparation for Simons' stain

Original staining method developed by Simons utilized both the orange and blue dye as received [153], later studies suggested that only the high molecular weight fraction of the Direct Orange dye was responsible for the increased affinity for cellulose, whereas the low molecular weight part had a very similar affinity for cellulose as the Direct Blue dye did [154]. Therefore an ultrafiltration of the orange dye to remove the low molecular weight part is necessary, and it is done by filtering a 1% solution of orange dye through a 100 K membrane using an Amicon ultrafiltration apparatus (Amicon Inc., Beverly, MA) under ~200 kPa nitrogen gas pressure [155]. Orange dye solution was poured into the Amicon container and filtered through until about 20% of the original volume remained. ~1.0 mL of the dye retained on the filter was dried in a 50 ^{o}C oven for at least 5 days and the weight of the solid residue was measured to determine the concentration of the top fraction in the filter. The ultrafiltrated dye with known concentration was then used as the concentrated stock solution for further dilution to the concentration required for the staining procedure.

3.2.4 Sample preparation for NMR cryoporometry and relaxometry

Hydrated biomass sample were never frozen and stored at 4 ^{o}C prior to conditioning. Untreated and pretreated materials were conditioned in a sealed desiccator at 25 ^{o}C and ~100% relative humidity over a 0.01 (w/v) NaN_3 solution for 14 days. The moisture contents in all samples were found to be 60 ± 3 %.

3.2.5 Holocellulose pulping

Biomass samples (~0.60 g) were mixed with peracetic acid (~2.10 g) and DI water (~5.80 mL). This mixture was then stirred at 25 ^{o}C for 24 h in the absence of light followed by repeated centrifugation and washing with DI water to isolate the holocellulose samples. The samples were then dried in vacuum oven at 40 ^{o}C overnight.

3.2.6 α-Cellulose isolation for GPC

α-Cellulose was isolated from holocellulose samples following Tappi method T-203 cm-09 with a slight modification [156]. Holocellulose samples (~0.10 g) were suspended in 17.5 wt% NaOH solution (~5.00 mL) at 25 ^{o}C for 2 h. The mixture was then diluted to 8.75% NaOH solution by adding ~5.00 mL of DI water and allowed to stir for additional 2 h. The isolated α-Cellulose samples were then collected by centrifugation, washed with 50 mL of 1% acetic acid and an excess of DI water until the pH of the filtrate was close to 7, and then air-dried overnight in fume hood.

3.2.7 Cellulose isolation for CP/MAS ^{13}C NMR

The cellulose samples for NMR analysis were prepared from holocellulose samples (~1.00 g) by acid (2.5 M HCl) hydrolysis for 4 h as reported elsewhere [43]. The isolated cellulose samples were then collected by filtration and rinsed with an excess of DI filtered water. The moisture content of isolated cellulose was adjusted to ~55-60% prior to ^{13}C NMR analysis.

3.2.8 Enzymatic hydrolysis

Enzymatic hydrolysis of different samples was performed at a consistency of 1% (w/v) in 50 mM citrate buffer (pH 4.8) and with cellulase and β-glucosidase loadings of 20 FPU/g and 40 CBU/g, respectively. The activities of cellulase and β-glucosidase were determined to be 91.03 FPU/ml and 387.70 CBU/ml, respectively, according to the literature methods [157]. The substrate and buffer mixtures were placed on the shaking incubator for 10 min to allow the substrate to disperse uniformly in the buffer prior to the addition of enzymes. The mixture was then incubated at 50 °C under continuous agitation at 150 rpm for 72 h. A sample of hydrolysis liquid (1.00 mL) was withdrawn after 2, 4, 8, 24, 48 and 72 h and the hydrolysis was quenched by submersion for 10 min in a vigorously boiling water bath. The liquid samples were then immediately frozen to -20 ^{o}C until analysis on an Agilent 1200 series HPLC system equipped with an auto sampler and an Aminex HPX-87H column and pre-column (Bio-rad Laboratories). The analysis was carried out at 65 ^{o}C using 10 mM nitric acid as eluent at a flow rate of 0.6 mL min^{-1} and with refractive index detection. The calibration of the system was performed with glucose standards. Substrate digestibility is expressed as mg glucose/g dry biomass, and the calculation is based on the dry weight of untreated and pretreated biomass.

3.2.9 Protease treatment

Cellulase hydrolyzed biomass samples were taken from enzymatic hydrolysis system after different residence times (2, 4, 8, 12, 24, 48, and 72 h), thoroughly washed with DI water then heat treated in boiling water for 10 min. Samples were then incubated overnight at 37 ^{o}C in phosphate buffer (50 mM, pH 7), containing 1 U/mL of protease

(Sigma, USA) to hydrolyze any remaining cellulases. Samples were thoroughly washed with DI water, heat treated, and stored in refrigerator for further analysis.

3.3 Analytical procedures

3.3.1 Carbohydrate and acid-insoluble (Klason) lignin analysis

The chemical composition of each of the substrates was determined by the Klason protocol according to TAPPI standard method T-222 om-88 with slight modification [11]. In brief, the extractive-free samples were treated with 72% sulfuric acid for 4 h at 30 ^{o}C and then diluted to 3% sulfuric acid using deionized water and subsequently autoclaved at 121 ^{o}C for ~1 h. The resulting solution was cooled to room temperature and the precipitate was then filtered through a G8 glass fiber filter (Fisher Scientific, USA), dried, and weighed to get the Klason lignin content. The resulting filtrate was diluted 50-fold, filtered and injected into high-performance anion exchange chromatography with pulsed amperometric detection (HPAEC-PAD) using Dionex ICS-3000 (Dionex Corp., USA) with an conductivity detector, a guard CarboPac PA1 column (2 × 50 mm, Dionex), a CarboPac PA1 column (2 × 250 mm, Dionex), a AS40 automated sampler and a PC 10 pneumatic controller at room temperature. 0.2 M and 0.4 M NaOH was used as the eluent and post-column rinsing effluent. The total analysis time was 70 min, with a flow rate 0.4 mL/min. Calibration was performed with standard solutions of Glucose, xylose, arabinose, mannose and galactose, and fucose was used as an internal standard.

3.3.2 Simons' stain

Lignocellulosic substrates (~100 mg) were weighed into five centrifuge tubes, and 1.00 mL of phosphate buffered saline (PBS) solution (pH 6, 0.3M PO_4, 1.40M NaCl) was also added to each tube. A set of tubes containing 1:1 mixture of DB and DO dyes at increasing concentrations were prepared by adding same amount of DB and DO dyes in a series of increasing volumes (0.25, 0.5, 0.75, 1.00, 1.50 mL), which can be then used to measure the dye adsorption isotherm. Distilled water was added to each tube to make up the final volume to 10.00 mL. All these centrifuge tubes were incubated at 70 ^{o}C for ~6 h with shaking at 200 rpm. After that, the absorbance of the supernatant solution was obtained on a Lambda 35 UV-vis spectrophotometer at 455 nm and 624 nm which represent the wavelength of maximum absorbance for DO and DB, respectively. The maximum amount of dye adsorbed to the lignocellulosic substrates was calculated using the Langmuir adsorption equation:

$$[C]/[A] = 1/(K_{ads}[A]_{max}) + [C]/[A]_{max}$$

where $[C]$ (mg/mL) is the free dye concentration, $[A]$ (mg/mg) is the amount of dye adsorbed by the substrate, K_{ads} is Langmuir adsorption constant, and $[A]_{max}$ is the maximum amount of dye adsorbed. The Langmuir isotherm plot, which is prepared by plotting $[C]/[A]$ versus $[C]$, yields a slope = $1/[A]_{max}$. The maximum amount of dye adsorbed by the substrate can be then obtained from the Langmuir isotherm curves. To conserve dye and substrates, the procedure was scaled down by a factor of 10 when there are not enough samples left.

3.3.3 Nuclear magnetic resonance (NMR) spectroscopy

3.3.3.1 NMR cryoporometry

The ^{1}H experiments were carried out in a Bruker static probe at frequencies of 300.13 MHz on a Bruker DSX-300 spectrometer. To completely remove all the possible ice signals, the ^{1}H NMR signals were collected using a standard Carr-Purcell-Meiboom-Gill (CPMG) sequence with a 5 μs (90°) ^{1}H pulse, 10 μs (180°) ^{1}H pulses, 16 scans, 10 s recycle delay, n = 8 echoes leading to an effective echo time of 0.00168 s prior to the acquisition of the free induction decay (FID). The hydrated sample was cooled to -50 °C slowly to completely freeze all the adsorbed water, and then the intensity of the NMR signal, which represents the amount of unfrozen water at a specific temperature, was recorded at intervals of 5 °C from -50 °C to -20 °C and then 1 °C from -20 °C to 0 °C. At each temperature increment, samples were allowed to equilibrate for 10-20 min. The intensities measured at each temperature T were corrected according to Curie's law under the assumption of a linearized Boltzmann distribution [158].

3.3.3.2 ^{1}H spin-spin (T_2) NMR experiments

^{1}H spin-spin (T_2) NMR measurements were carried out in a Bruker static probe at frequencies of 300.13 MHz on a Bruker DSX-300 spectrometer. Experiments were conducted using the Bruker Topspin software environment at a constant temperature of 25 ^{o}C. The spin-spin relaxation times were determined using a standard two-dimensional Carr-Purcell-Meiboom-Gill (CPMG) sequence with a 5 μs (90°) ^{1}H pulse, 10 μs (180°) ^{1}H pulses, 16 scans, 10s recycle delay and τ = 0.0002 s, 16 data points were recorded between n = 4 - 1024 echoes (0.00164 – 0.41984 s) [117].

3.3.3.3 ^{1}H spin-lattice (T_1) NMR experiments

^{1}H spin-lattice (T_1) NMR measurements were carried out in a Bruker static probe at frequencies of 300.13 MHz on a Bruker DSX-300 spectrometer. Experiments were conducted using the Bruker Topspin software environment at a constant temperature of 25 ^{o}C. The inversion recovery experiments utilized a 5μs (90°) ^{1}H pulse, 10μs (180°) ^{1}H pulse, 10s recycle delay and 128 scans [117].

3.3.3.4 ^{1}H diffusion NMR experiments

^{1}H diffusion NMR measurements were carried out in the Bruker Micro-25 NMR accessories at frequencies of 400.13 MHz on a Bruker DSX-400 spectrometer. The radiofrequency coil used with this accessory had a diameter of 10 mm and an active length of about 30 mm. The *Populus* sample was placed inside a 10 mm NMR tube with the gradient-composition axis parallel to the long axis of the tube, and wet cotton in the cap to maintain a ~100% RH environment. Experiments were conducted using the XWINNMR software at a constant temperature of 25 ^{o}C. Diffusion coefficients were measured using a pulse field gradient (PFG) simulated echo sequence utilized a 10 μs (90°) ^{1}H pulse and 10 s recycle delay with 128 scans, Δ = 25, 50, 100, and 200ms, taking 64 points varying δ between 0.0001 – 0.003 s [117].

3.3.3.5 Solid-state ^{13}C CP/MAS NMR experiments

Moisture equilibrated isolated cellulose samples (~35% water content) were packed in 4 mm cylindrical ceramic MAS rotors. Repetitive steps of packing sample into the rotor were performed to fully compress and load the maximum amount of sample. Solid state

NMR measurements were carried out on a Bruker Avance 400 spectrometer operating at a frequency of 100.55 MHz for ^{13}C in a Bruker double resonance MAS probe at spinning speeds of 10 kHz. CP/MAS experiments utilized a 5-μs (90^{o}) proton pulse, 1.5-ms ramped contact pulse, 4-s recycle delay, and 4-8 K scans.

3.3.4 Gel permeation chromatography (GPC) analysis of cellulose

The number-average molecular weight (M_n) and weight-average molecular weight (M_w) was determined by GPC after tricarbanilation of cellulose as described previously [46]. α-Cellulose samples (~15 mg) was placed in separate test tubes equipped with micro stir bars and dried overnight under vacuum at 40 ^{o}C. Anhydrous pyridine (4.00 mL) and phenyl isocyanate (0.50 mL) were added sequentially via syringe. The test tubes were then placed in an oil bath at 70 ^{o}C and allowed to stir for 48 h. The reaction was quenched by anhydrous methanol (1.00 mL). Methanol and water mixture (7:3, v/v) was added drop-wise to each test tube to promote precipitation of the cellulose derivative. The solids were collected by filtration and then washed with the methanol and water mixture (50 mL), followed by water (50 mL). The cellulose derivative was then dried overnight under vacuum at 40°C. Prior to GPC analysis the cellulose derivative was dissolved in tetrahydrofuran (1.0 mg/mL), filtered through a 0.45 μm filter, and placed in a 2 mL auto-sampler vial. The molecular weight distributions were analyzed by Agilent GPC SECurity 1200 system equipped with four Waters Styragel columns (HR0.5, HR2, HR4, HR6), Agilent refractive index (RI) detector and Agilent UV detector (270 nm). Tetrahydrofuran was used as the mobile phase (1.0 ml/min) and the injection volume was 30.0 μl. A calibration curve was constructed based on 10 narrow polystyrene standards

ranging in molecular weight from 1.2 x 10^3 to 5.5 x 10^4 g/mol. Data collection and processing were performed by Polymer Standards Service WinGPC Unity software (Build 6807). The M_n and M_w were calculated by the software relative to the universal polystyrene calibration curve. DP_n and DP_w were obtained by dividing M_n and M_w by 519 g/mol, the molecular weight of the tricarbanilated cellulose repeat unit.

3.3.5 Fourier transform infrared (FTIR) spectroscopy

Spectrum One FTIR system (Perkin Elmer, Wellesley, MA) with a universal attenuated total reflection (ATR) accessory was used to characterize the lignocellulosic samples. Each sample was pressed uniformly and tightly against the diamond surface using a spring-loaded anvil. FTIR spectra were obtained by averaging 64 scans from 4,000 to 800 cm^{-1} at 4 cm^{-1} resolution. Baseline and ATR corrections for penetration depth and frequency variations were carried out using the Spectrum One software supplied with the equipment.

3.4 Error Analysis

Error analysis was conducted by performing carbohydrate and acid-insoluble lignin analysis in triplet, and the results represented the mean values of three independent experiments. The error bar represents the standard error, which is calculated by divide the standard deviation by the square root of the sample size. The standard deviation associated with the compositional analysis was ± 0.5-3.2%, and ± 0.3-0.9% for carbohydrate and Klason lignin, respectively. Enzymatic hydrolysis, GPC analysis and

Simons' stain experiment was performed in duplicate, and the results represented the mean values of two independent experiments. Mercury porosimetry analysis was repeated on selected samples, and results showed that data is quite reproducible with a 1.5% error. For other NMR analysis, error analysis was conducted by at least two individual line-fit data processing or integration analyses.

Chapter 4

DETERMINATION OF POROSITY OF *POPULUS* BEFORE AND AFTER STEAM EXPLOSION AND DILUTE ACID PRETREATMENT[†]

4.1 Introduction

The demand for renewable fuel sources continues to grow, in part due to the diminishing supply of fossil fuel resources as well as growing concerns about environmental stewardship and energy security. Lignocellulosic biomass, composed of cellulose, hemicellulose, and lignin, is one of the most abundant potential sustainable sources for renewable fuel production [1]. Undoubtedly, biofuels derived from this renewable resource, biomass, will play a key role in reducing the world dependence on fossil fuels. Bioconversion of lignocellulose is significantly hindered by the innate recalcitrance of biomass. As a result, achieving reasonable conversion rate and yield profiles necessitates the inclusion of the pretreatment stage. Commonly cited goals of pretreatment, which is usually done prior to enzymatic deconstruction of cellulose, are (1) to remove/redistribute hemicellulose/lignin, (2) to disrupt the ultrastructure of cellulose, and (3) to open the lignin and hemicellulose matrix encapsulating cellulose, ultimately increasing the proportion of enzyme accessible surface area [8]. Dilute acid pretreatment (DAP) and steam explosion (SE) are two of the leading technologies that have included significant research efforts over the past few decades. DAP can significantly reduce biomass

[†] This manuscript was accepted for publication in Bioresource Technology, 2013. It is entitled as "Determination of porosity of lignocellulosic biomass before and after pretreatment by using Simons' stain and NMR techniques. The other authors are Marcus Foston, Johannes Leisen, Jaclyn Demartini, Charles E. Wyman, and Arthur J. Ragauskas. The copyright permissions will be submitted to the thesis office of Georgia Tech.

recalcitrance and it has been successfully applied to a wide range of feedstocks, including hardwood, softwood, and agricultural residues [159,160,161]. Among a variety of acids that have been employed, sulfuric acid has been recognized as one of the most widely used acids. DAP is usually performed over a temperature range of 120 to 210 ^{o}C, with acid concentration typically less than 4 wt%, and residence time from a few seconds to an hour [130]. In SE, biomass is treated with high-pressure saturated steam followed by a sudden pressure reduce, which makes the materials undergo an explosive decompression. It is typically initiated at a temperature of 160-260 ^{o}C for several seconds to a few minutes before the biomass is exposed to atmospheric pressure [162]. This research has been conducted in the areas of pretreatment optimization and scale-up; however, for significant future improvements to occur an improved understanding of the fundamentals of biomass recalcitrance must be obtained.

Lignocellulosic substrate characteristics, e.g., crystallinity, degree of polymerization, accessible surface area (ASA), and lignin/hemicellulose distribution, have been all thought to influence the efficiency of enzymatic hydrolysis [84]. The porosity of lignocellulosic biomass or the ASA of exposed cellulose in lignocellulosic biomass has been identified as a particularly important factor in influencing enzymatic deconstruction rate and yield. This dependence between cellulose accessibility and enzymatic deconstruction is associated with intimate contact between cellulose and cellulases, such as exo-1,4-β-D-glucanase, as a prerequisite step for enzymatic hydrolysis to occur. Some research on the relationship between biomass pore size and enzymatic hydrolysis suggest that small pores (i.e., those with diameters smaller than the diameters of cellulase

enzymes) hinder and large pores enhance enzymatic hydrolysis [163]. In the case of small pores, only small cellulase components can diffuse slowly inside the pores and consequently may become trapped there, causing a (1) decrease in molecular movement, (2) decrease in synergistic interaction, and (3) ultimately lowering the rate of solubilization. However, when large pores dominate the biomass pore system, the probability of that the entire enzyme will have access and that synergistic catalytic action will occur becomes so high that the influence of the diffusion inside small pores becomes negligible and subsequently that the enzymatic hydrolysis yield and rate becomes significant [117]. This was supported by the fact that the initial rate of hydrolysis of steam pretreated mixed hardwood, poplar and white pine is linearly correlated with the pore volume of the substrate accessible to a nominal diameter of 5.1 nm representative of the size of the cellulase from *Trichoderma reesei* [110]. This is also consistent with the fact that if cellulases are spherical, they were from 2.4 to 7.7 nm in diameter, with mean of 5.9 nm [163].

Historically, considerable amounts of work have been done in developing accessible surface area measurement techniques performed on cellulosic substrates, including electron microscopy [164], gas (e.g., nitrogen or water) adsorption [165], and mercury porosimetry [166]. However, most of these techniques require a prior drying of the substrate which makes it typically less effective in determining the pore volume due to the fact that water removal from nonrigid porous materials could produce partial irreversible collapse of pores [167]. Other techniques such as solute exclusion, can measure the substrate in its wet state, but it requires significant experiment time and it

only measures the interior surface of the cellulose [92]. In addition, gas adsorption methods typically result in an over-estimation of cellulose accessibility due to the fact that molecular size of the probe gas is much smaller than cellulase enzymes. For all these reasons, the best techniques for surface area measurement are those (1) that can be directly applied to wet materials, and (2) that measure the overall surface area in a relative short time. Most of the current studies only use one technique for evaluating biomass accessibility. However, it is our opinion that this is inadequate, different techniques are based on different principles of measurement and their results reflect different physical measurement associated with accessibility, consequently, utilizing only one method will often provide incomplete information, and accounts for conflicting result or data interpretations.

In the present study, a modified Simons' stain (SS) method along with several NMR techniques was utilized to measure the cellulose accessibility/porosity of various pretreated *Populus* samples. The pretreatment techniques used in this study include DAP and steam explosion. Using calculated dye adsorption, cryoporometry pore size distribution (PSD) curves, nuclear relaxation time distributions, and diffusion coefficient distributions, information about changes in the accessibility of lignocellulosic substrate upon pretreatment was resolved. This work was done in an effort (1) to generate a more accurate description of cellulose accessibility via multiple methods, (2) to further test the changes in the accessibility of lignocellulosic substrate upon pretreatment, thus yielding a better understanding of the biomass recalcitrance

4.2 Experimental Section

4.2.1 Biomass substrates

Hybrid *Populus* (*Populus trichocarpa x deltoides*) was harvested in 2008 from area 0800 at Oak Ridge National Laboratory (ORNL), TN, and prepared as described in Chapter 3 (3.1.2 Biomass substrate).

4.2.2 Extractive-free poplar preparation

Extractive was removed by placing the biomass samples into an extraction thimble in a Soxhlet apparatus (Foss, Soxtec^{TM} 2050) as described in Chapter 3 (3.2.1 Soxhlet extraction).

4.2.3 Biomass pretreatment

Dilute acid pretreatment and steam explosion were directly applied on extractive-free *Populus* as described in Chapter 3 (3.2.2.1 Dilute acid pretreatment and 3.2.2.2 Steam explosion). The temperature of pretreatment was 150 ^{o}C, and dilute acid pretreatment was done for 10 and 60 min while steam explosion is done for only 10 min.

4.2.4 Chemical composition analysis

Carbohydrate profiles and acid-insoluble lignin (AIL) content in untreated and pretreated *Populus* were determined as described in Chapter 3 (3.3.1 Carbohydrate and acid-insoluble lignin analysis). Acid soluble lignin (ASL) content in the filtrate was measured

from the absorbance at 205 nm using a UV-vis spectroscopy according to TAPPI methods T-222 om-88.

4.2.5 Simons' stain

Direct Blue 1 was used as received, and an ultrafiltration of Direct Orange 15 was used to remove the low molecular weight part of the orange dye as described in Chapter 3 (3.2.3 Dye preparation for Simons' stain). Blue and orange dye with a concentration of 10 mg/mg was used as the stock solution. Simons' Stain was applied on untreated and pretreated *Populus* to estimate the accessible surface area of cellulose as described in Chapter 3 (3.3.2 Simons' stain).

4.2.6 NMR cryoporometry

Samples for cryoporometry measurement were prepared as described in Chapter 3 (3.2.4 Sample preparation for NMR cryoporometry and relaxometry). Pore size distribution of untreated and pretreated *Populus* was determined by NMR cryoporometry as described in Chapter 3 (3.3.3.1 NMR cryoporometry).

4.2.7 NMR relaxometry

Samples were prepared as described in Chapter 3 (3.2.4 Sample Preparation for NMR cryoporometry and relaxometry). ^{1}H spin-spin (T_2) NMR measurements were carried out in a Bruker static probe as described in Chapter 3 (3.3.3.2 ^{1}H spin-spin (T_2) NMR experiments). ^{1}H spin-lattice (T_1) NMR measurements were carried out in a Bruker static probe as described in Chapter 3 (3.3.3.3 ^{1}H spin-lattice (T_1) NMR experiments).

4.2.8 NMR diffusometry

^{1}H diffusion NMR measurements were carried out in the Bruker Micro-25 NMR accessories as described in Chapter 3 (3.3.3.4 ^{1}H diffusion NMR experiments).

4.2.9 NMR data processing

Inverse Laplace transforms (ILT) were accomplished by a Matlab 7.13 program written at Victoria University of Wellington (Wellington, New Zealand) by P. T. Callaghan to process 1- and 2-dimensional ASCII data measuring either diffusion or relaxation characteristics of heterogeneous proton systems. This program is based on unconstrained regularization, non-negative least squared fit and singular value decomposition algorithms. The routine was tested using a series of multi-exponential and stretched-exponential functions of varying component weights, widths and characteristic decay times demonstrating fairly good accuracy, resolution and stability in the corresponding distributions produced. To assess the effect of noise, relaxation curves were generated using a multi-exponential function, and each data point was allow to increase or decrease by a maximum of 10% of its only value. The particular variance at each data point was controlled by a random number generator to simulate a randomly noisy relaxation curve.

4.3 Results and discussion

4.3.1 Chemical composition analysis

The chemical composition of *Populus* including carbohydrate and lignin distribution before and after pretreatment is presented in Table 4.1, with glucose representing the major monosaccharide. The majority of the hemicellulose, typically characterized by xylose, mannose, arabinose, and galactose contents, was removed within 10 min of DAP. However, there are still significant amounts of xylose and mannose left in the *Populus* sample after 10 min SE pretreatment. In terms of acid insoluble lignin content, results indicate that both DAP and SE are ineffective at the removal of the majority of lignin, and the acid insoluble lignin content actually increases after dilute acid pretreatment due to the formation of pseudo-lignin [156].

Table 4.1 Chemical composition of untreated, dilute acid, and steam explosion pretreated *Populus.*

Substrate	Arabinan	Xylan	Glucan	Galactan	Mannan	AIL*	ASL**
Untreated *Populus*	0.3	11.5	50.3	0.6	1.9	34.7	0.5
10 min DAP *Populus*	0.0	3.5	58.1	0.0	0.1	36.9	0.6
60 min DAP *Populus*	0.0	0.2	56.5	0.0	0.2	42.6	0.4
10 min SE *Populus*	0.2	6.0	61.4	0.2	1.5	30.1	0.5

*AIL: Acid Insoluble Lignin. **ASL: Acid Soluble Lignin

4.3.2 Characterization of cellulose accessible surface area

Simons' stain method evaluates the accessibility of a substrate by applying two different dyes: a direct orange (DO) and a direct blue (DB). Dyes are well known as sensitive

probes for the characterization of cellulose structure, and direct dyes are particularly appropriate because of their linear structures and outstanding substantively toward cellulose [168]. Direct blue 1 has a well-defined chemical formula with a molecular weight of 992.82 g/mol and a molecular diameter of ~1 nm. Direct orange 15 is a condensation product of 5-nitro-o-tolueesulfonic acid in aqueous alkali solution, with a molecular diameter in the range of ~5-36 nm [153]. When lignocellulosic biomass is treated with a mixed solution of the direct orange and blue dye, the blue dye enters all the pores with a diameter larger than ~1 nm, while the orange dye only populates the larger pores. After a pore size increase either by physical or chemical action, the orange dye will gain further access to the enlarged pores because of the higher affinity of the orange dye for the hydroxyl groups on a cellulosic surface. The ratio and amount of DO and DB dye adsorbed into the biomass can be used to indicate the amount of large pores to small pores and subsequently cellulose accessibility in lignocellulosic biomass for enzymatic deconstruction [114].

Chandra et al. found that the use of SS dyes, more specifically the O/B ratio, as a molecular probe is a good indicator of the total surface area of cellulose available to the enzymes [114]. It was also evident that the higher the O/B ratio, the lower the protein loading required for efficient hydrolysis [93]. As mentioned above, the adsorbed O/B ratio has been related to cellulose accessibility and cellulase activity; however, it can be helpful to also analyze the total amount of dye adsorbed. For example, as ASA become significant and large proportions of pores are small in size, large amounts of the smaller DB dye are adsorbed by a substrate and cause a decrease in the overall O/B ratio. In this

case, there may be a significant amount of large pore and cellulose accessibility, but analysis based solely on the low O/B ratio may skew data interpretation. An increase in the adsorbed O/B ratio accompanied by a minimal increase in total dye adsorption generally indicates larger accessible surface area, and in the case of comparison before and after treatment, is indicative of expanding existing pore distributions. Again, when comparing SS results before and after treatment, a minimal increase in the adsorbed O/B ratio with large increases in total dye adsorption suggests pore generation is occurring.

As shown in Table 4.2, *Populus* showed an increase of the total amount of adsorbed dye after pretreatment, for all conditions, when compared to the untreated sample. Table 4.2 also indicates that total dye adsorption increases with pretreatment severity with the smallest increase shown for the 10 min SE sample, then 10 min DAP, and finally with the largest increase for the 60 min DAP sample. Both the adsorption of DO and DB dye increased after pretreatment, but the adsorption of the orange dye increased to a higher extent than the adsorption of the blue dye after pretreatment. This asymmetrical increase caused the O/B ratio to increase with pretreatment severity, increasing from 0.19 (untreated sample) to 0.25 (10 min SE sample), 0.39 (10 min DAP sample), and 0.54 (60 min DAP sample), respectively. These results suggest that both DAP and SE increase SSA by generating new pores and expanding existing pore distributions, and DAP increases SSA as a function of pretreatment severity. The results also indicate, despite explosive decompression that occurs during SE, under a similar time and temperature profile DAP is more effective in terms of the overall accessible surface area increasement.

As shown previously, both DAP and SE are ineffective at the removal of the majority of lignin, and the acid insoluble lignin content actually increases after DAP. The SS results showed that in spite of higher lignin content, pretreatment especially DAP results in a much larger accessible cellulosic surface area. Hsu et al. suggested that this was not only caused by hemicellulose removal but also by hydrolysis and rearrangement of the lignin structure during DAP [169]. Wiman et al. also found that although the lignin content of the steam-pretreated spruce increased at higher pretreatment temperature and residence time, the initial rate of enzymatic hydrolysis increased, and the DR 28 (Congo Red) stain and Simons' stain indicated that pretreatment did not result in larger total cellulosic surface areas but rather in a larger accessible cellulosic surface area [121]. So the positive effects of cellulose accessibility thus dominate over the negative effects of lignin for steam-pretreated spruce. However, highly selective lignin removal is also important to pinpoint the lignin effect on biomass digestibility but has rarely been reported for application of delignification to pretreated biomass, and the chemical reagents employed to delignify pretreated biomass are known oxidizing agents (sodium chlorite-acetic acid, peracetic acid) and, therefore, can affect cellulose structure features such as crystallinity, DP and subsequently accessibility [48].

Table 4.2 The maximum amount of direct orange and blue dye adsorbed by untreated and pretreated *Populus* expressed as mg dye/g substrate using Simons' stain.

Substrate (*Populus*)	Maximum Adsorbed Orange Dye (mg/g sample)	Maximum Adsorbed Blue Dye (mg/g sample)	Total adsorbed Dye (mg/g sample)	O/B Ratio
Untreated	10.6	56.4	67.0	0.19
10 min SE	16.1	64.6	80.7	0.25
10 min DAP	28.3	71.8	100.1	0.39
60 min DAP	44.8	83.3	128.1	0.54

4.3.3 Characterization of biomass pore size distribution

NMR cryoporometry is a technique for non-destructively determining Pore size distribution (PSD) in porous media through the observation of the depressed melting point of a confined liquid. It takes advantage of the fact that small crystals formed from liquid within pores melt at a lower temperatures than bulk liquid, which is known as melting point depression. For a liquid confined within a pore in which a crystal is forming, the melting point depression of the liquid can be related to pore size through the Gibbs-Thompson equation [170]:

$$\Delta T = T_m - T_m(x) = k/x$$

where T_m is the normal melting point, $T_m(x)$ is the melting point of a crystal in pores of diameter x, and k is a characteristic constant of the liquid. The pore volume v is a function of pore diameter x, so the melting temperature of the liquid $T_m(x)$ can be related to the pore size distribution by:

$$\frac{dv}{dx} = \frac{dv}{dTm(x)} \frac{dTm(x)}{dx}$$

From Gibbs-Thompson equation, $dT_m(x)/dx = k/x^2$, so the pore size distribution can be rewrite as:

$$\frac{dv}{dx} = \frac{dv}{dTm(x)} \frac{k}{x^2}$$

The NMR cryoporometry data contains signal intensity proportional to the integral pore fluid volume v, which varies as a function of temperature T (Figure 4.1). At each temperature, v is the volume of liquid in cell wall pores with a dimension less than or equal to x. So the measurement of $dv/dT_m(x)$ which can be obtained from the slope of the

curve of *v* against T, provided *k* is known for the liquid used (50.0 K·nm for water) will allow the pore size distribution curve to be determined.

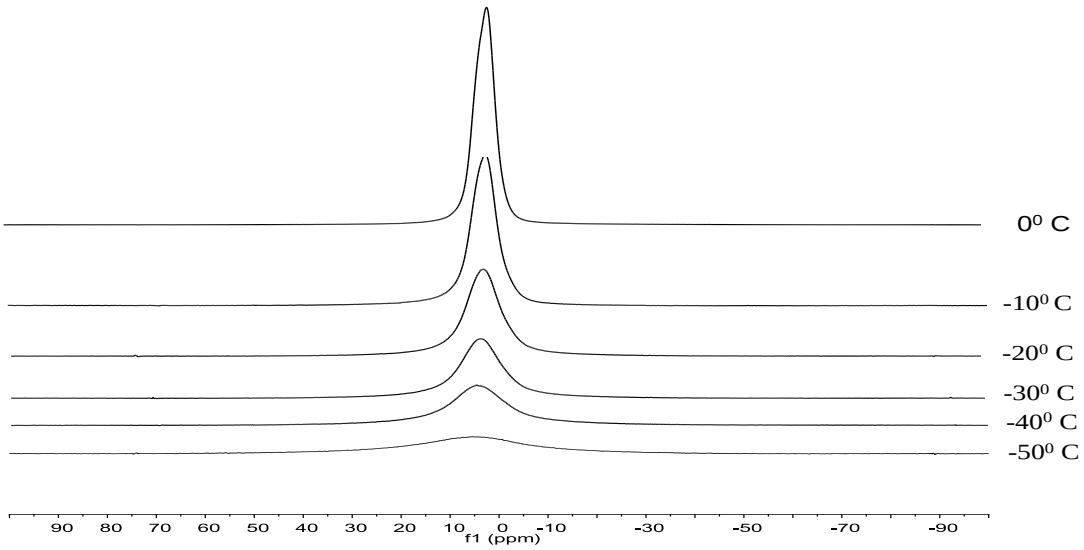

Figure 4.1 ^{1}H NMR cryoporometry spectra of 60 min DAP *Populus* from -50 ^{o}C to O ^{o}C.

Figure 4.2 shows the melting curves (e.g., the temperature dependences of the NMR signal intensity) of all the samples in the range of temperatures between 220 and 280 K. The intensities measured at each temperature T were corrected according to Curie's law by multiplication with the factor T/T_o to account for the temperature dependence of the occupation of the spin levels under the assumption of a linearized Boltzmann distribution. The corrected intensities are normalized to the value just below T_o = 280 K, where all pore water as well as excess water are in the liquid state. A step-like intensity increase in the vicinity of the bulk melting point of water 273 K was observed for all the samples, which is attributed to the bulk liquid component. The smooth increase of the signal intensity with temperature in the region of pore melting indicates a transition of water in the pores. According to the Gibbs-Thompson equation, liquid melting depression is

inversely proportional to the pore diameter; therefore, liquid in smaller pores has a lower melting point which means as temperature increases, liquid in smaller pores starts melt first. As shown in Figure 4.2, as the temperature increases, the NMR intensity for untreated sample starts to increase first, and this change refers to the melting of water in small pores of the untreated material.

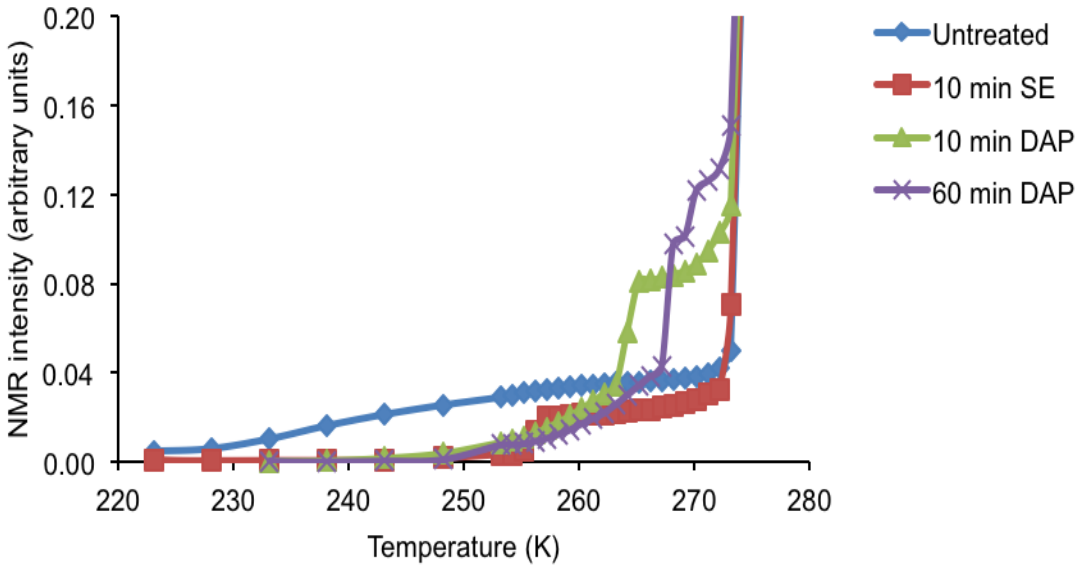

Figure 4.2 Melting curves (temperature dependence of NMR signal intensity) of untreated, dilute acid, and steam explosion pretreated *Populus* samples.

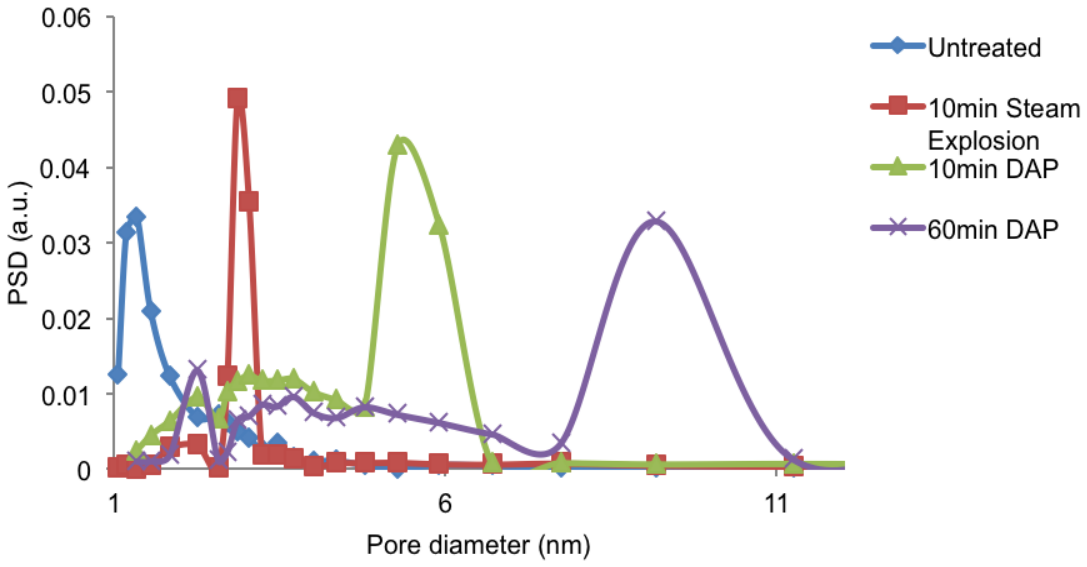

Figure 4.3 Pore size distributions of untreated, dilute acid, and steam explosion pretreated *Populus* samples calculated using the Gibbs-Thompson equation.

The pore size distribution of these lignocellulosic biomass samples calculated based on Gibbs-Thompson equation using the first derivative of the intensity with respect to temperature ($dv/dT_m(x)$) from the melting curve is shown in Figure 4.3. A representative pore diameter can be roughly estimated from peak maximums. The positions of the main peaks attributed to meso-scale pores in the PSD for untreated, 10 min SE, 10 min DAP, and 60 min DAP sample are 1.5 nm, 3 nm, 6 nm, and 9 nm, respectively. Only DAP samples seems to have the nominal size required for cellulase (diameter ~ 5.1 nm) access and diffusion. Obviously, all the pretreated samples display a larger pore diameter than the untreated sample. In addition, the two 10 min pretreatments (of both SE and DAP) have a broad pore diameter polydispersity with a broader distribution of pore diameters observed for DAP than for SE. However, due the lack experimental points at temperature near 0 °C this broadening effect could be a result of noise. The pore size shows up in bimodal distribution after pretreatment in the mesoporous range. All the pretreatments

cause the formation of an additional peak, centered around 2.2 nm, which again indicates pretreatment most likely causes pore expansion.

4.3.4 ^{1}H spin-spin (T_2) measurements

Like NMR cryoporometry, there are other NMR based techniques which can be used to track changes in accessibility upon treatment of biomass, such as proton NMR relaxometry. Adsorbed water can be found spatially localized within lignocellulosic biomass on and within cellulosic microfibrils, existing as capillary water in the lumen, or between fibers and within the lignin-hemicellulose matrix [171]. The nature and strength of the association between the probe molecule, water, and the cell wall is directly related to the ultrastructural and chemical state of the biomass [116]. Therefore by monitoring the amount and the relative nature of nuclear relaxation seen in the adsorbed water, information about changes in biomass pore surface area to volume ratio and chemistry can be inferred.

In this work, ^{1}H T_2 data measured with the CPMG sequence and analyzed via inverse Laplace transformation (ILT) were used to investigate the change in the nature of biomass–water interactions and subsequent accessibility as a result of DAP and SE. Biomass, for example, with a more hydrophilic pore surface chemistry and/or reduced pore size distributions will contain a higher proportion of bound to unbound water. This would be reflected in NMR cryoporometry by greater melting point temperature depression. NMR relaxation experiments can provide information pertaining to the molecular mobility within a system. In a spin-spin or T_2 relaxation curve, the signal

intensity decays as a function of local inhomogeneities in the magnetic field mainly due to perturbation by nuclei through space or dipolar interactions [172]. This attenuation is described by a characteristic relaxation time referred to as the T_2 relaxation time (Figure 4.4). Basically, as the T_2 relaxation time of adsorbed water increase the degrees of freedom or average local mobility of the water in the pores also increases. Similarly, an increase in T_2 relaxation time of adsorbed water can be correlated with a decrease in the proportion of bound to unbound water or amount of water located at pore surface versus the pore interior. Therefore, in systems of increasing average pore size, the pore surface area to volume ratio will decrease and is therefore detected by an increase in the T_2 relaxation time. As determined by a CMPG experiment the T_2 time of free water is ~3 s

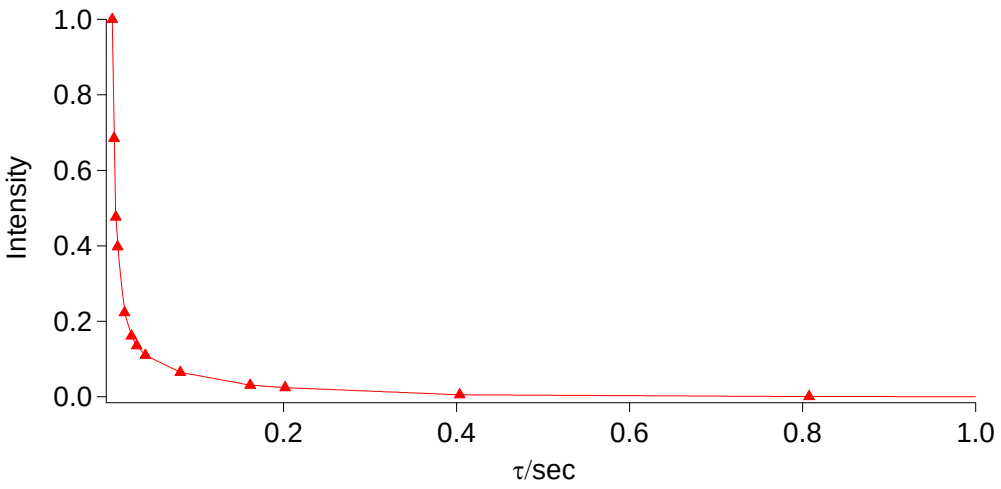

Figure 4.4 Spin-spin T_2 attenuation curve of water in 10 min DAP *Populus* with a moisture content of 60 ± 3%.

A common technique to extract information for comparison on systems having wide distributions of nuclear relaxers or T_2 decays utilizes an inverse Laplace transforms (ILT) routine [116]. Figure 4.5 (a) depicts the relaxation time distributions of adsorbed water in

untreated and pretreated *Populus* wood as a result of ILT. The T_2 distribution of adsorbed water in the untreated wood chip sample shows the existence of at least two pools of adsorbed water with T_2 peaks centered at 11.5 and 40.5 ms. The exact location in the cell wall of these pools of water is difficult to determine; however, based on studies investigating relaxation rates of plant cell wall physiological water distributions in wood during drying, water within the cellulose fibrils and lignocellulosic matrix represent the downfield and upfield peaks [171]. Despite the exact location of the water distributions, Figure 4.5 (a) indicates significant expansion of the larger cell wall water pool seen in the untreated sample centered at ~40.5 ms with pretreatment. Interestingly, increasing DAP time from 10 to 60 min only causes on a slight increase in T_2 times, whereas upon SE, even for a short residence time, a much larger increase is observed. This would suggest the mechanism related to a decrease in the pore surface area to volume ratio and to an increase in accessibility as a result of DAP pretreatment occurs primarily in the first 10 min of pretreatment, and though continues through the remaining 50 min of pretreatment, happens at a significantly slower rate. The results also show SE is much more effective at decreasing pore surface area to volume ratios, at least for the cell wall water pools detected by changes in T_2 relaxation times.

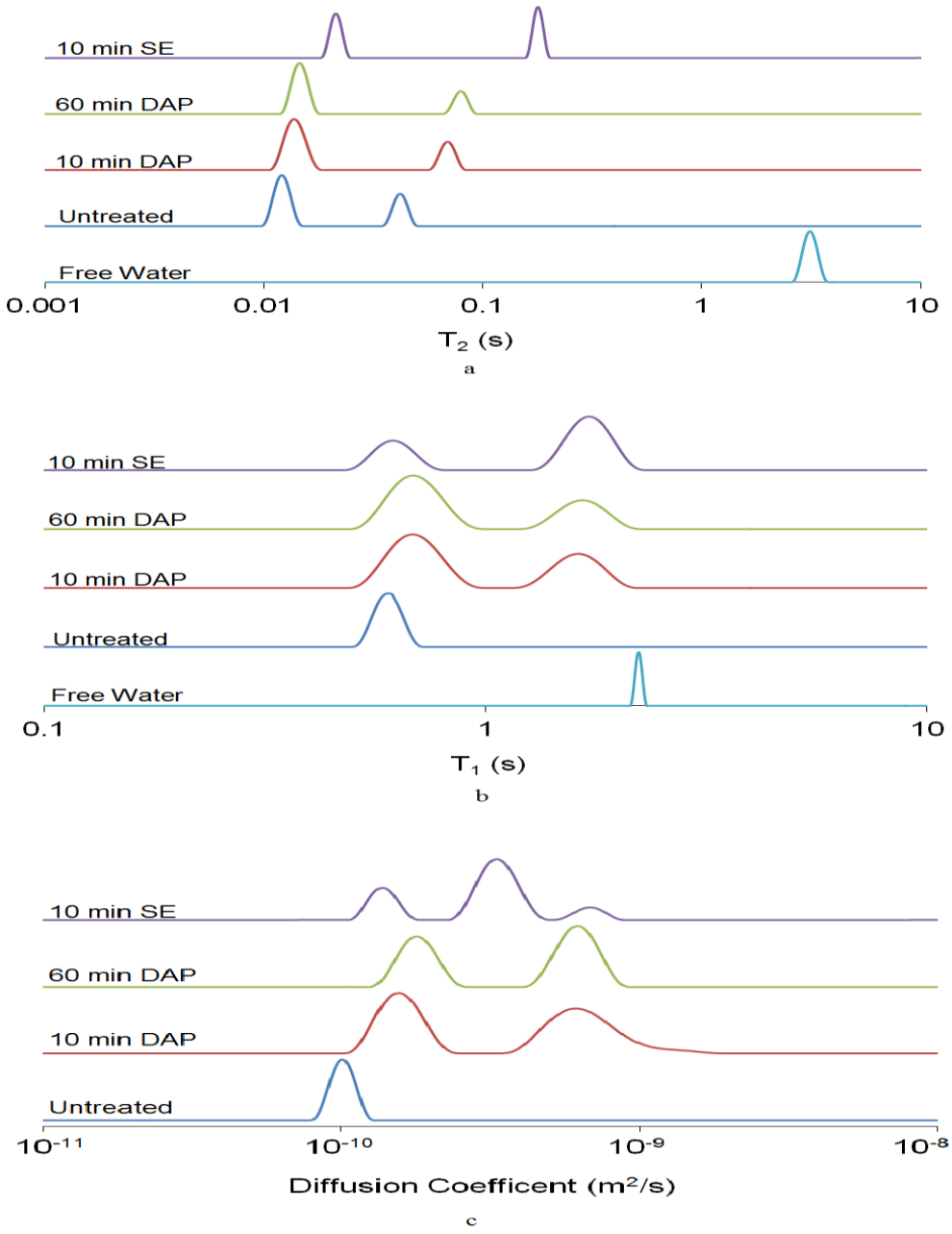

Figure 4.5 (a). Distribution of spin-spin relaxation times of absorbed water within untreated and pretreated *Populus* biomass produced via ILTs of CMPG T_2 experiments at a moisture content of 60 ± 3 %. (b). Distribution of spin-lattice relaxation times of absorbed water within untreated and pretreated *Populus* biomass produced via ILTs of inversion recovery T_1 experiments at a moisture content of 60 ± 3 %. (c). Diffusion coefficient distribution of water adsorbed in untreated and pretreated *Populus* biomass at a moisture content of 60 ± 3 % with an observation window Δ=100 ms.

4.3.5 spin-lattice (T_1) NMR measurements

It is also well known that liquid molecules near a solid surface will have different spin-lattice or T_1 relaxation profiles from that of the bulk liquid because of interactions at the solid-liquid interface [173,174]. As a result, in porous biomass that contains water the observed average T_1 time of the adsorbed water is influenced by the surface area to volume ratio of the pores. Under fast exchange conditions, there are models describing the change in T_1 relaxation, based on a two-component system, where the observed T_1 is the weighted sum of relaxation times of free and surface bound water. However, T_1 relaxation is more sensitive to higher frequency relaxation and molecular dynamics than T_2 relaxation, the consequence being a lowered ability to detect (1) pore surface bound water and (2) differences in pore sizes, especially for larger pore systems. Nevertheless, analyzing T_1 relaxation of adsorbed cell wall water can be informative particularly in light of the well-developed model describing changes in T_1 relaxation due to fast exchange between pore surface bound and unbound water. Much like the T_2 analysis above, ^{1}H inversion recovery experiments (Figure 4.6) and ILT of T_1 relaxation curves were generated and used to investigate the changes in accessibility as a result of pretreatment.

ILT of the T_1 relaxation curve of the untreated *Populus* biomass shows the existence at least one pool of cell water adsorbed into biomass with T_1times centered at ~0.60 s. All pretreatments cause the development of the second upfield distribution and a slight increase in the T_1times of the peak seen in the untreated sample. As in T_2 relaxation, increases in T_1time suggest that more free water exist within the biomass, with free water

having a T_1 time of ~2.2s. Figure 4.5 (b) seems to indicate a similar significant decrease in the pore surface area to volume ratio occurs in the cell wall of *Populus* biomass upon pretreatment. The relative intensities of the two water distributions suggest the SE sample has more water in the larger dimension cell wall water pool than in the DAP samples.

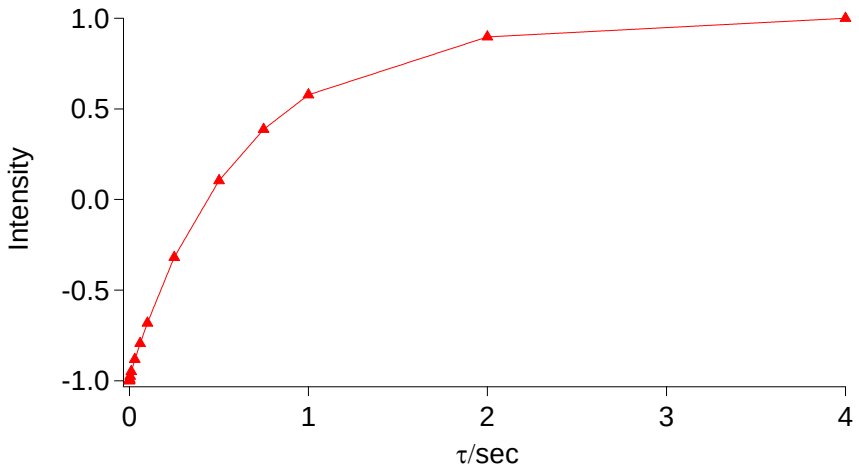

Figure 4.6 Spin-lattice T_1 inversion recovery curve of water in 10 min DAP *Populus* with a moisture content of 60 ± 3%.

4.3.6 NMR diffusometry and q-space imaging

Another property of the solvent probe molecule that can be gathered in a fairly straightforward manner by NMR measurement is the self-diffusion coefficient. An increase in pore size distributions can be reflected by the increase of diffusion coefficient due to increased unrestricted diffusion path lengths and decreased fractions of pore surface bound water. Pulsed gradient spin echo (PGSE) experiments have been in wide use to investigate molecular diffusion of fluids in various porous systems (e.g., biomass)

[175]. Typically, this method is used to determine the apparent self-diffusion coefficient (D_s) of a molecule. This can be done using the following equation:

$$\frac{I}{I_o} = \exp\left[-(\gamma G\delta)^2 D_s\left(\Delta - \frac{\delta}{3}\right)\right] = \exp\left[-(2\pi q)^2 D_s\left(\Delta - \frac{\delta}{3}\right)\right]$$

where γ is the nuclear gyromagnetic ratio, G is the gradient strength, δ is the amount of time the gradient is applied ($q=G\delta\gamma/2\pi$) and Δ is delay between the application of the gradients [176]. By systematically varying either G, δ, or Δ the D_s of a system can be determined. Also, by using a well-defined ($\Delta-\delta/3$) interval or period of observation PGSE experiments can probe the diffusion of a molecule over various length scales. The larger the interval, the longer the technique "observes" or the larger the root-mean distance of observation in which the diffusion coefficient is determined over [117,177]. As done above, ^{1}H PGSE experiments and ILT of diffusion attenuation curves were generated and used to investigate the changes in accessibility as a result of pretreatment. The resulting distribution of D_s, detected with an observation window of Δ=100 ms, for water adsorbed in untreated and pretreated *Populus* biomass is shown in Figure 4.5 (c). In general, an increase in pore size distributions could cause the average D_s to increase due to a lower fraction of pore surface bound water or larger unobstructed root-mean diffusion path (D_s of bulk free water is ~2.27×10^{-9} m^2 s^{-1}). The D_s distributions, seen in Figure 4.5 (c) indicate there is at least one resolvable D_s within the untreated *Populus* biomass centered at ~1.06×10^{-10} m^2 s^{-1}. All pretreatments cause the development of additional fast diffusion coefficients and a slight increase in the D_s of the peak seen in the untreated sample. SE pretreatment specifically causes the development of two new

distributions, which seems to suggest the explosive decompression results in a more complex pore system.

An alternative method of analyzing PGSE techniques utilizes q-space NMR imaging to characterize the average pathway of liquid molecules imbibed in a micro-porous medium, the plant cell wall [177]. Water displacement probability profiles can be obtained by Fourier transform of the spin-echo attenuation profiles measured as a function of the changing gradient amplitude or *q*. The displacement probability profiles describe the probability water undergoing random diffusive motion will encounter a wall. These water displacement probability profiles were collected on untreated and pretreated *Populus* biomass for varying diffusion observation times (Δ = 25-200 ms). Several studies have demonstrated that water translational displacement probability profiles can be obtained directly by Fourier transform of the spin-echo attenuation profiles (E[q]) recorded as a function of the magnitude of the pulsed field gradient at a fixed gradient spacing for both cellulose fiber and wood pulps [178].

$$E(q) = \iint \rho(r) Ps(r|r', \Delta) \exp\left[i 2\pi q (r' - r)\right] dr' \, dr$$

where r'- r represents the displacement distance. This type of q-space imaging experiments can provide a novel method to produce data of microscopic spacing in porous media, at a higher spatial resolution than k-space images generated from more traditional NMR imaging. Figure 4.7 shows characteristic diffusion NMR data sets plotted as the echo intensity verses the magnitude of the wave number vector q (spin-echo attenuation profiles). This was done for four different diffusion observations or Δ-values 25, 50, 100 and 200 ms (only Δ=100ms curves are shown in Figure 4.7). One data

processing option is to determine apparent diffusion coefficient. In this case the result from the diffusion attenuation curves can be affected by cross-relaxation with the biomass, anisotropic diffusion, and pore tortuosity.

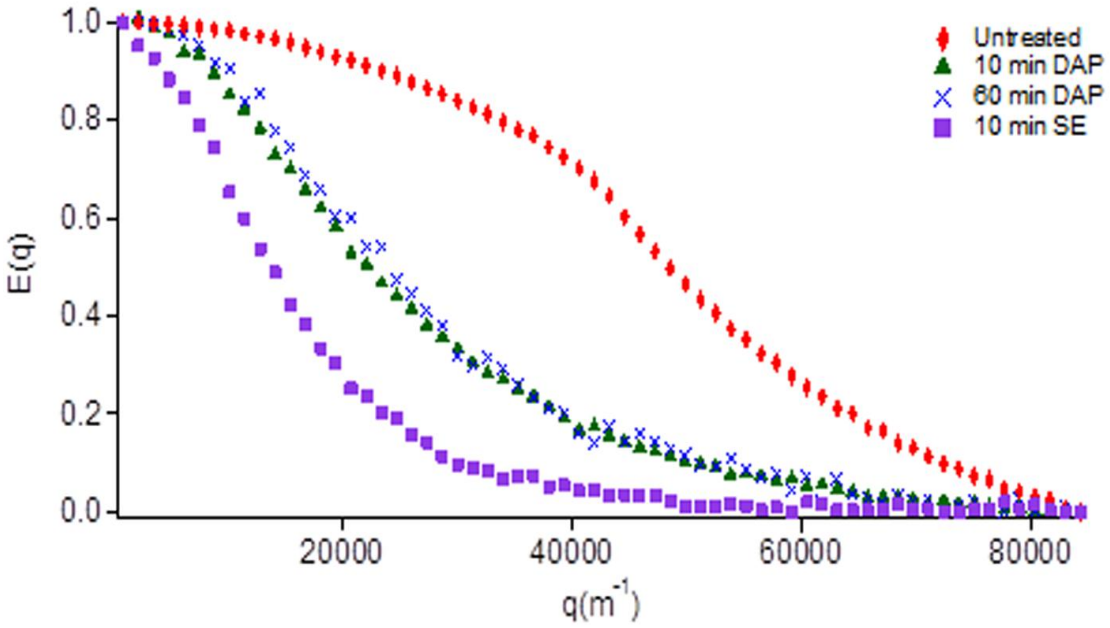

Figure 4.7 Echo amplitude as a function of q=Gδγ/2π at Δ=100ms of water in untreated and pretreated *Populus* biomass at a moisture content of 60 ± 3%.

However, in an effort to extract a distribution which can represent the pore sizes on a macro-scale, the spin-echo attenuation profiles were converted to a complex form, zero filled to 256 points, and inverted using a Fourier transform algorithm using Matlab software. The resulting distribution is a water displacement probability profile, which describes the probability water undergoing random diffusive motion will encounter a pore wall. Based on the Figure 4.8, an average diffusion displacement plot at an observation window of Δ =100 ms, it is clear that the untreated *Populus* biomass has a much more relative intensity centered at shorter displacement probability values than

pretreated samples, with the lowest relative intensity for the SE sample. This clearly shows a difference in micron related pores as a result of difference pretreatment. Again there is little difference between 10 min and 60 min DAP sample, suggesting the majority of increases in accessibility occurs in the first 10 min of DAP and that the cell wall expansion in SE pretreatment, at least in cell wall water pools, is more effective. Other average diffusion displacement plots at observation windows of Δ =25, 50, and 200ms are shown in Figure 4.9, 4.10 and 4.11, and display similar results as Figure 4.8.

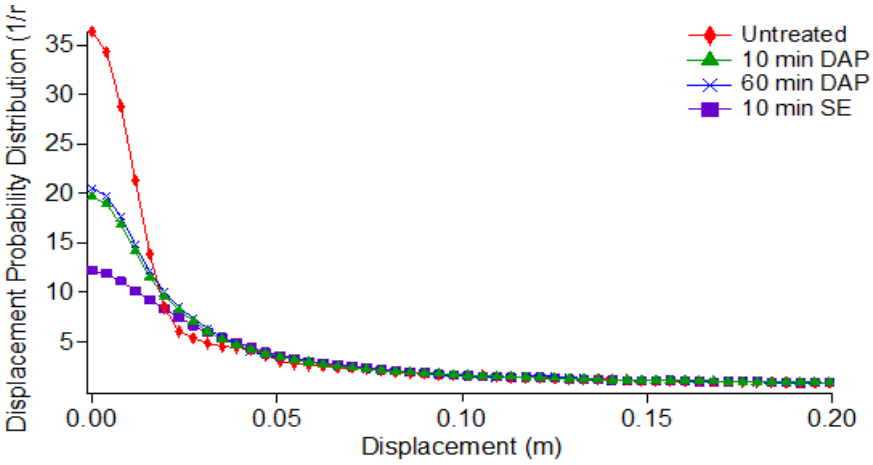

Figure 4.8 Average diffusion displacement of water in untreated and pretreated *Populus* biomass at a moisture content of 60 ± 3 % (Δ = 100 ms).

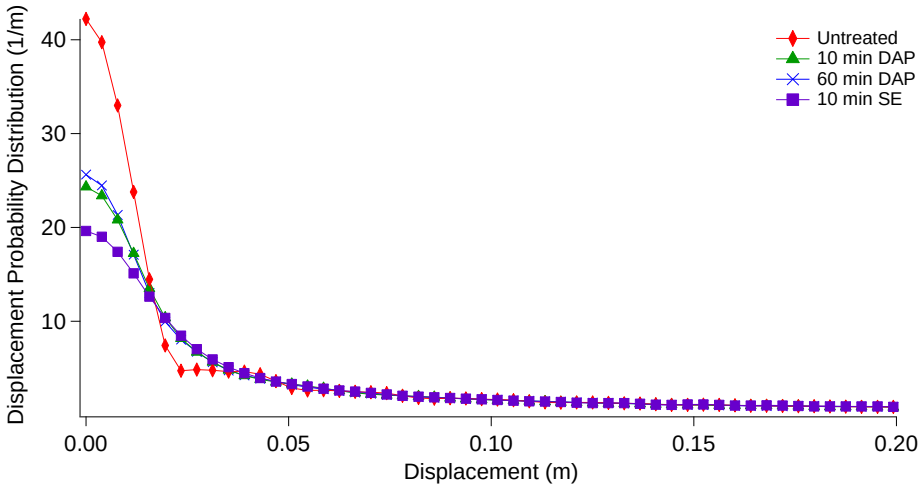

Figure 4.9 Average diffusion displacement of water in untreated and pretreated *Populus* biomass at a moisture content of 60 ± 3 % (Δ = 25ms).

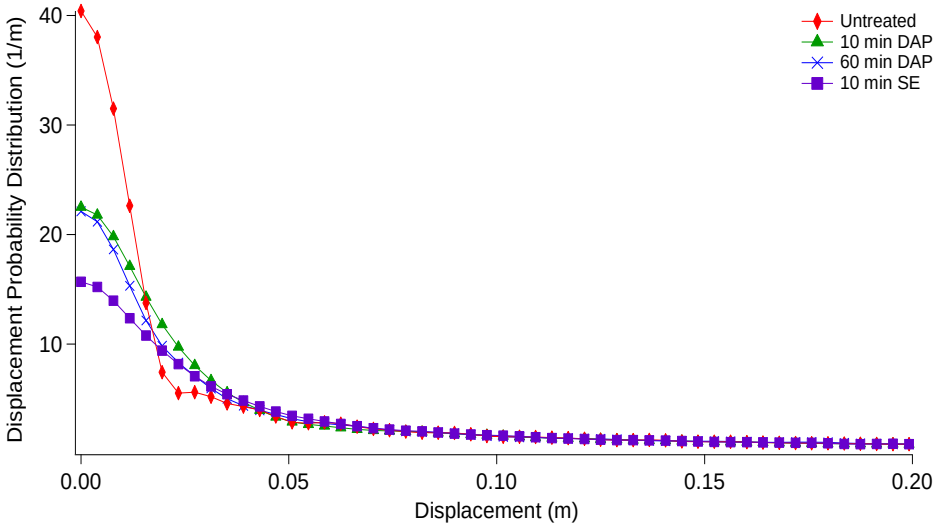

Figure 4.10 Average diffusion displacement of water in untreated and pretreated *Populus* biomass at a moisture content of 60 ± 3 % (Δ = 50 ms).

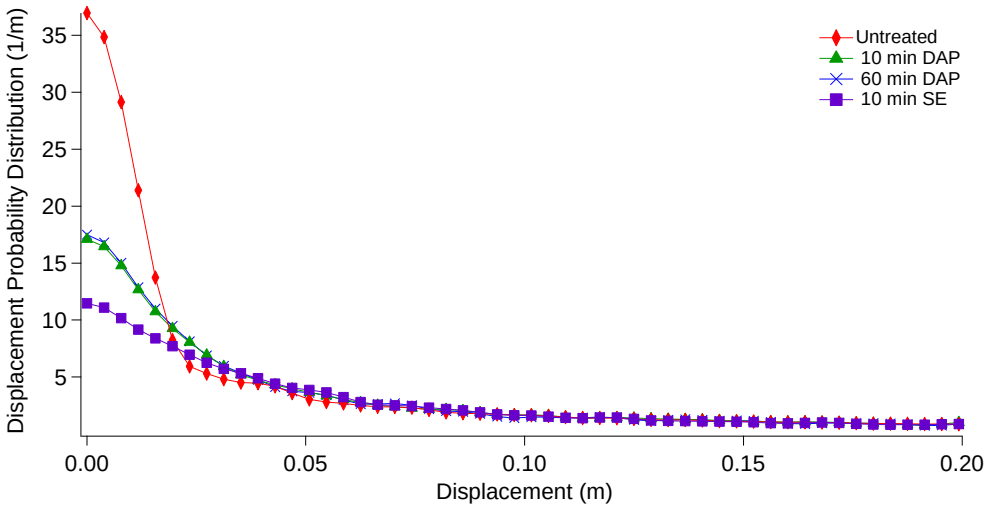

Figure 4.11 Average diffusion displacement of water in untreated and pretreated *Populus* biomass at a moisture content of 60 ± 3 % (Δ = 200 ms).

Displacement probability profiles should be Gaussian and have been shown to follow the form:

$$P(R,\Delta) = A * \exp((r'-r)^2 / Ds)$$

where $A = \frac{1}{2\sqrt{\pi \Delta Ds}}$ and *Ds* is the measure diffusion coefficient for water in the plant cell wall accounting for the perturbing effect of the porous system. Figure 4.12 shows the Gaussian fit to the water displacement probability profile on 10 min steam explosion pretreated wood sample at a diffusion time of 100 ms. This analysis was done on all sample for all diffusion times and tabulated in Table 4.3. In general the trend show the D_s slows with increase diffusion time and increases from the untreated sample to the pretreated samples. This again suggests pretreatment significant increases in the sizes of pores with respect to untreated samples.

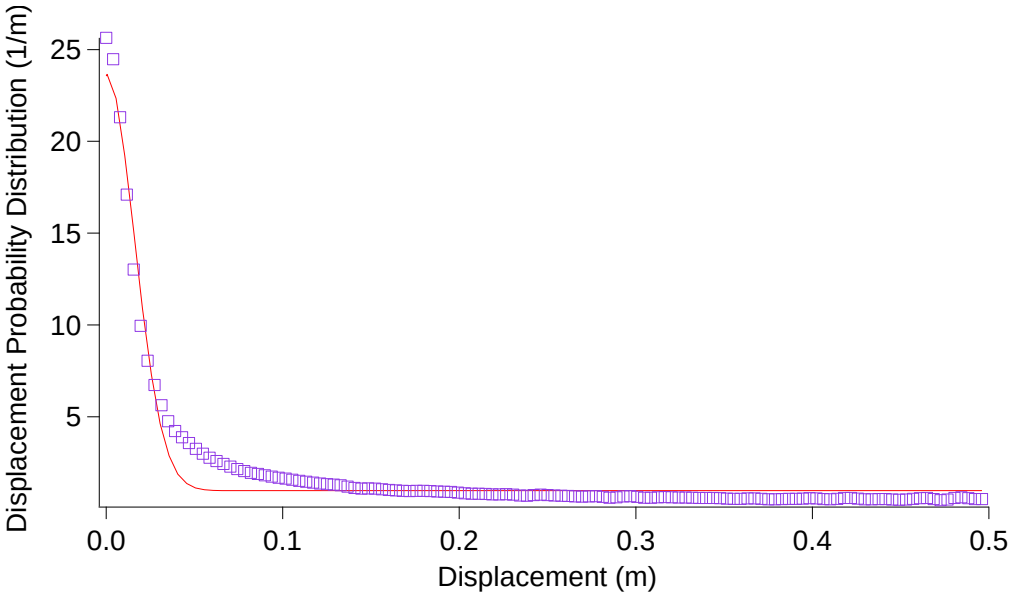

Figure 4.12 Average diffusion displacement of water in steam explosion pretreated *Populus* biomass at a moisture content of 60 ± 3 % (Δ =100ms). The red line represents a Gaussian distribution fit of the displacement probability profile.

Table 4.3 The apparent self-diffusion (D_s) coefficient of water as a result of the perturbing effect of pore in the plant cell wall of untreated and pretreated *Populus* in m^2/s.

Substrate	**Δ = 25 ms**	**Δ = 50 ms**	**Δ = 100 ms**	**Δ = 200 ms**
Untreated	$1.9*10^{-6}$	$9.1*10^{-7}$	$6.6*10^{-7}$	$3.2*10^{-7}$
10 min DAP	$6.7*10^{-6}$	$4.0*10^{-6}$	$3.0*10^{-6}$	$2.0*10^{-6}$
60 min DAP	$6.2*10^{-6}$	$4.5*10^{-6}$	$2.7*10^{-6}$	$2.0*10^{-6}$
10 min SE	$1.1*10^{-5}$	$9.4*10^{-6}$	$8.2*10^{-6}$	$5.2*10^{-6}$

4.4 Conclusion

To further investigate the effect of DAP and steam SE on the change in cellulose accessibility, several techniques were applied including a Simons' stain (SS) technique along with several NMR methods (i.e., NMR cryoporometry, ^{1}H spin-lattice (T_1) and ^{1}H spin-spin (T_2) relaxometry, and diffusometry). These methods were utilized to probe biomass porosity and thus assess cellulose accessibility on untreated and pretreated *Populus.* The results show DAP is more effective that SE in terms of increasing SSA, and that as DAP severity is increased so is SSA. NMR relaxometry and diffusometry indicate that pore expansion for DAP pretreatment occur primarily in first 10 min of pretreatment, but SE is more effective at pore expansion for the cell wall water pools detected by changes in relaxation times.

In terms of the techniques used in this study, the PSD generated by cryoporometry show that the 10 min and 60 min DAP *Populus* has mean diameter around 6 and 9 nm, both should have enough large pores accessible to the orange dye used in SS. However, SS results show that the increase of pretreatment time from 10 min to 60 min causing orange dye adsorption increases from 28.3 to 44.8 mg/g. Cell wall expansion could obviously increase the cellulose accessible surface area. However, considering the fact that both 10 min and 60 min DAP sample have enough large pores accessible to the orange dye, this increased dye adsorption may be due to the extensive remove of hemicellulose causing by increased pretreatment time. In other words, the significant increase of orange dye adsorption may not be due to a result of significant pore expansion, in fact, the NMR

relaxometry and diffusometry revealed that pore expansion for DAP occur primarily in first 10 min. The cryoporometry only indicates pores up to 10 nm in this study, there are clearly larger pores than that exist which SS, T_1, T_2 and diffusion test all can detect. However, SS test is sensitive to pore inlet size. If a pore is large but the entrance to that pore is small, the SS methodology will not reflect the existence of that large pore. Relaxometry and diffusometry indicate that SE is more effective at pore expansion, while SS results show that orange dye adsorption for 10 min SE is only 16.1 mg/g. As mentioned before, the content of hemicellulose obviously plays an import role here, and another explanation could be the possible generation of some "ink-bottle" shaped pores caused by the explosive decompression that occurs during SE makes it hard for orange dye to access as reflected by SS results. However, that large pore is more than likely inaccessible to cellulolytic enzymes as well. Lastly, the effect of lignin rich pore surfaces on dye adsorption during this modified SS testing is fairly unclear. On the other hand, NMR technique typically measure the ratio of surface bound to unbound water within the plant cell wall, as a result NMR techniques are not affected by pore inlet size or shape. However, NMR techniques also have serious limitation with respect to detecting larger pores. This limitation is in some way related to the fact that the proportion of surface bound to unbound water becomes small, so small that accurate detection is impossible.

CHAPTER 5

THE EFFECT OF ALKALINE PREATMENT ON CELLULOSE STRUCTURE AND ACCESSIBILITY[‡]

5.1 Introduction

In recent years, renewable energy resources such as wind, solar, and biomass, are of particular interest as a way to lower fossil fuel consumption and to meet the ever-increasing energy demands [1]. Amongst the various renewable sources being explored, cellulosic ethanol is being pursued as one of the most promising solutions that are being investigated to complement the usage of conventional fuels [179]. Currently, bioethanol is being produced from the fermentation of edible food crops resources such as corn starch and sugar cane which can have several environmental and socioeconomic impacts [180]. In contrast, cellulosic ethanol derived from abundant and non-edible lignocellulosic biomass such as poplar, switchgrass, and eucalyptus do not compete with the food crops while being capable of providing clean sustainable energy and fuels, and frequently referred as second generation bioethanol. Among all of these substrates, poplar is a potential lignocellulosic feedstock for cellulosic ethanol production because of its fast growth properties and the ability to produce high biomass yields in various types of soil and climate conditions [31,181]. However, biomass recalcitrance is the biggest obstacle in the development of large-scale second-generation cellulosic ethanol production and

[‡] This manuscript was accepted for publication in ChemSusChem, 2014. It is entitled as "The effect of alkaline pretreatment methods on cellulose structure and accessibility". The other authors are Garima Bali, Jacob I. Deneff, Qining Sun, and Arthur J. Ragauskas. The copyright permissions will be submitted to the thesis office of Georgia Tech.

use. Biomass recalcitrance hinders the effectiveness and accessibility of enzymes during the bioconversion process and mostly arises from the complex structure and ultrastructure of lignocellulosics, predominantly composed of cellulose, hemicellulose, and lignin network matrix [68]. Amongst the components of biomass, cellulose is an unbranched polymer made up of D-glucose subunits linked by β-(1,4)-glycosidic bonds and able to interact through hydrogen bonding to form fibrils packed into cellulose bundles. Cellulose has crystalline regions, which are more difficult to break down and to contribute to recalcitrance, while the amorphous regions in cellulose are known to be more easily hydrolyzed [182]. In contrast to cellulose, the hemicellulose present in lignocellulosic is amorphous in nature and consists of a variety of branched polysaccharides that protects cellulose fibrils and making it less accessible to the enzymatic hydrolysis. In addition, under high severity dilute acid and autohydrolysis biomass pretreatment, the hydrolyzed fragments of xylan are converted into furfural or HMF, which also inhibits the saccharification process and further reduces fermentation yields [10]. The next major component of biomass is lignin: a complex phenolic polymer made up of a variety of phenyl propane subunits that contribute to plant recalcitrance by blocking the access of enzymes to cellulose. In overall, the complex interactions and structural properties of biomass components make lignocellulosic biomass recalcitrant, and so it requires pretreatment before it can be enzymatically deconstructed into simple sugars. Pretreatment has several aims, such as disrupting the physical structure of the biomass by breaking the lignin barriers, disrupting cellulose crystallinity, and removing non-cellulosic components in order to increase cellulose accessibility [183,184].

Previous studies indicated that the structural parameters related to cellulose, mainly degree of polymerization (DP), and cellulose CrI affect the biomass recalcitrance and subsequent enzymatic saccharification [185], however, in many cases, it is not very clear whether these features are the major rate limiting substrate characteristics for the cellulose hydrolysis [134]. Further, improving cellulose accessibility by pretreatment is also critical as it directly affects the efficiency of the cellulose hydrolysis [91,93]. Several recent studies also revealed the correlation of accessibility of pretreated biomass with the rate of enzymatic hydrolysis [186,187]. Nevertheless, pretreatment is always a necessary and an important step, to improve the substrate accessibility and enzymatic hydrolysis for the overall biofuels conversion pathway [188].

Over the past few decades, various pretreatment methods such as mechanical, physiochemical and chemical treatments often using alkali, acid, organosolv, ionic liquids or steam have been developed with the goal of increasing enzymatic digestibility of biomass [189]. Many of these pretreatment methods involve high temperatures and high pressures to disrupt the lignin carbohydrate complex, however, alkaline pretreatment methods commonly use lower temperatures and pressures compared to other pretreatment methods [188]. The widely used reagents for alkali pretreatment are sodium hydroxide [190], ammonia [191], and calcium hydroxide [192]. At this point, sodium hydroxide pretreatment is one of the most common alkaline pretreatment methods which has been extensively studied in the bioconversion of lignocellulosics by maximizing swelling and solubilization of lignin, deacetylation, disrupting the lignin-hemicellulose network and subsequently enhancing the cellulose digestibility. As previously reported, the NaOH

treatment was significantly effective in increasing the digestibility of hardwood and agriculture residue with low lignin content [193]. Furthermore, Xu et al. reported that NaOH pretreatment offers great potential because it works at reduced temperatures and also exhibits a remarkable delignification capacity relative to its severity [194]. Another effective alkaline process is pretreatment with lime. Lime pretreatment removes lignin, which improves the enzymes effectiveness because that eliminates nonproductive adsorption sites and increases access to cellulose and hemicellulose [195]. Ammonia pretreatment is an alternative alkaline pretreatment process, which involves the use of an ammonia solution either under high-pressure conditions (AFEX process) or under ambient conditions of soaking biomass in aqueous ammonia [196]. The various alkaline pretreatment conditions described above have the common effect of increasing the digestibility of the lignocellulosics by changing the lignin-hemicellulose complex network, however, few reported studies demonstrated the potential effects of alkaline pretreatment on pure cellulose substrates other than that obtained from complex lignocellulosic.

This chapter examines the effects of various alkaline pretreatment methods on cellulose structure and its accessibility in milled hybrid poplar (*Populous trichocarpa x deltoids*). The study not only reveals the changes that occur in cellulose structure and accessibility upon a variety of low cost and mild alkaline treatments but also helps in determining the key factors responsible for biomass recalcitrance. Ultimately, characterizing and understanding these substrate changes and the subsequent relationship between these

substrate factors and lowered recalcitrance will enable the development of a more effective lower cost pretreatment system.

5.2 Experimental section

5.2.1 Biomass substrates

Hybrid *Populus* (*Populus trichocarpa x deltoides*) was harvested in 2012 at Oak Ridge National Laboratory (ORNL), TN, and prepared as described in Chapter 3 (3.1.2 Biomass substrate).

5.2.2 Extractive-free *Populus* preparation

Samples were extracted with dichloromethane in a Soxhlet apparatus (Foss, Soxtec™ 2050) as described in Chapter 3 (3.2.1 Soxhlet extraction).

5.2.3 Biomass pretreatment

Various alkaline pretreatments including sodium hydroxide, lime, and soaking in ammonia were directly applied on extractive-free *Populus* as described in Chapter 3 (3.2.2.3 Alkaline pretreatment). Pretreatment conditions were chosen according to previous literature with slightly modified to produce comparable time and temperature scale as shown in Table 5.1 [49,182,197]. The *Populus* yields after pretreatment ranged between 75 and 85% (w/w) by the dry weight of biomass.

Table 5.1 Alkaline pretreatment conditions for *Populus*.

Sample name	Temperature (^{o}C)	Time	Conditions
NaOH 2 min	120	2 min	2% sodium hydroxide
NaOH 10 min	120	10 min	2% sodium hydroxide
NaOH 60 min	120	60 min	2% sodium hydroxide
$Ca(OH)_2$ 10 min	120	10 min	0.1 M calcium hydroxide
$Ca(OH)_2$ 60 min	120	60 min	0.1 M calcium hydroxide
SA 5 days	25	5 days	Soaking in 30% ammonia solution
SA 24 h	75	24 h	Soaking in 30% ammonia solution

5.2.4 Chemical composition analysis

Carbohydrate profiles and acid-insoluble lignin content in untreated and various alkaline pretreated *Populus* were determined as described in Chapter 3 (3.3.1 Carbohydrate and acid-insoluble lignin analysis).

5.2.5 Gel Permeation Chromatography (GPC) analysis of cellulose

Holocellulose samples were prepared as described in Chapter 3 (3.2.5 Holocellulose pulping). α-Cellulose was isolated from holocellulose samples as described in Chapter 3 (3.2.6 α-Cellulose isolation for GPC). The weight-average molecular weight (M_w) and number-average molecular weight (M_n) were determined by GPC as described in Chapter 3 (3.3.4 Gel permeation chromatography (GPC) analysis of cellulose). Polydispersity index (PDI) was calculated by dividing M_w by M_n.

5.2.6 ^{13}C CP/MAS NMR analysis of cellulose

Holocellulose samples were prepared as described in Chapter 3 (3.2.5 Holocellulose pulping). The cellulose samples for NMR analysis were prepared as described in Chapter 3 (3.2.7 Cellulose isolation for CP/MAS ^{13}C NMR). Solid state NMR measurements were

carried out on a Bruker Avance 400 spectrometer as described in Chapter 3 (3.3.3.5 Solid-state ^{13}C CP/MAS NMR experiments).

5.2.7 Simons' stain

Simons' Stain was applied on untreated and various alkaline pretreated *Populus* to estimate the accessible surface area of cellulose as described in Chapter 3 (3.3.2 Simons' stain).

5.2.8 Enzymatic hydrolysis

Enzymatic hydrolysis of untreated and various alkaline pretreated samples were performed as described in Chapter 3 (3.2.8 Enzymatic hydrolysis). A sample of hydrolysis liquid after 48 and 72 h was withdrawn and analyzed by an Agilent 1200 series HPLC system for sugar analysis.

5.3 Results and Discussion

5.3.1 Chemical composition analysis

The amounts of carbohydrates and lignin in untreated and alkaline pretreated *Populus* are given in Figure 5.1. The carbohydrates in *Populus* were mainly composed of glucan and xylan with minor amounts of mannose, arabinose, and galactose. There was a significant increase in glucan content, 12%, 35%, and 40%, after 2, 10, and 60 min of sodium hydroxide pretreatment, respectively. As compared with above alkaline pretreatments, less percentage increase in the glucan proportion (~5-8%) was observed in case of lime

pretreatment for 60 min and soaking ammonia at higher temperature, with respect to untreated sample, most probably because of less lignin removal under those particular conditions. Pretreatment with lime for 10 min increased the glucan content by 12%, while soaking in ammonia for 5 days increased the glucan content by 14%. However, pretreatment by soaking in ammonia remained the most effective method for solubilizing most of the hemicellulose (~41%). For untreated *Populus*, the Klason lignin content was 29.9% of the total biomass, which agree with the typical lignin content found in Populus species (20-30%) [31]. For pretreated samples, lignin content varied from 19.5% to 26.0%. Samples pretreated with sodium hydroxide showed the lowest content of lignin (19-21%), indicating that the pretreatment is fairly effective at removing the majority of lignin under the conditions studied.

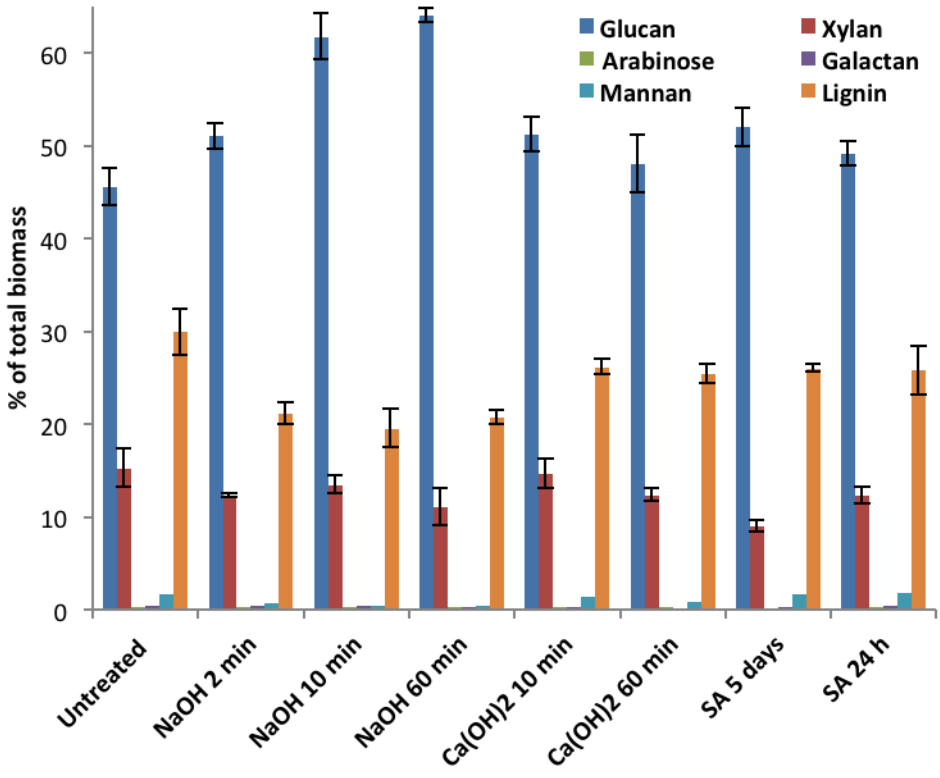

Figure 5.1 Carbohydrate and Klason lignin contents of untreated and various alkaline pretreated *Populus*.

5.3.2 Molecular weight analysis of cellulose

The molecular weight distributions of cellulose isolated from different pretreated alkaline *Populus* samples are shown in Table 5.2. Measurements of the molecular weights of the cellulose samples indicated that highest level of degradation occurred in samples pretreated with sodium hydroxide, and increasing the severity of pretreatment further degrades the cellulose. Pretreatment with sodium hydroxide for 2 min led to a ~8% decrease in cellulose DP_w and as the residence time was increased to 10 min and 60 min degradation in cellulose DP_w increased to 61 and 76%, respectively. For samples pretreated with lime for about 10 min, the DP_w of cellulose exhibited a decrease of 7% while a pretreatment time of 60 min caused more cellulose degradation, leading to a decrease in DP_w of 15%. For samples pretreated in ammonia at room temperature and a residence time of 5 days, the observed decrease in cellulose DP_w was 23% whereas, for a relatively shorter time of 24 h but a higher temperature, 65% decrease in cellulose DPw was observed.

Table 5.2 Degree of polymerization of cellulose isolated from alkaline pretreated *Populus*.

Sample	DP_w	DP_n	PDI
Untreated	2504	342	7.3
NaOH 2 min	2312	173	13.3
NaOH 10 min	963	115	8.3
NaOH 60 min	578	77	7.5
$Ca(OH)_2$ 10 min	2312	154	15.0
$Ca(OH)_2$ 60 min	2119	169	12.5
SA 5 days	1926	134	14.3
SA 24 h	867	115	7.5

DP_w = weight-average degree of polymerization
DP_n = number-average degree of polymerization
PDI = polydispersity index

5.3.3 Crystallinity analysis of cellulose

The crystallinity index (CrI) of cellulose isolated from alkaline pretreated *Populus* samples was determined by ^{13}C CP/MAS measurements. In a typical ^{13}C CP/MAS spectrum of cellulose isolated from pretreated *Populus* as shown in Figure 5.2, the carbon atoms corresponding to C1 through C6 of the cellulose glucopyranose unit were labeled accordingly. The peaks from 82.5 ppm to 92.5 ppm correspond to the C-4 carbon region of the cellulose in which the broad peak at 86-92.5 ppm is attributed to crystalline cellulose [198]. The integration ratio between the crystalline cellulose region and the total C-4 region provided the crystallinity index (CrI), which was evaluated for all alkaline pretreated *Populus* samples and is shown in Figure 5.3. The alkaline pretreated cellulose showed significant change in the CrI as compared to cellulose isolated from untreated *Populus*, however not much variation in CrI was observed among various pretreatment methods. The CrI data for alkaline pretreated *Populus* samples, ranged from 50 % to 54 %, which is lower than that of the untreated *Populus* exhibiting 55% cellulose crystallinity. The percent decreases in cellulose crystallinity in various alkaline pretreated samples with respect to untreated cellulose sample were 5-7 %, 7-9 % and 5-9 % in sodium hydroxide, lime and ammonia pretreatment respectively. This indicates that the alkaline pretreatment methods may slightly disrupt the crystalline cellulose structure. The crystallinity index of *Populus* cellulose remained almost unchanged during the sodium hydroxide pretreatment time of 2–10 min. As the pretreatment time increased to 60 min, the cellulose isolated from *Populus* had a slight increase of CrI by 3 percentages. Similarly, no considerable variation in CrI was observed in the lime pretreatment at 10 to 60 min residence time. However, soaking ammonia pretreatment at higher temperature

exhibited relatively higher CrI than that of ammonia treatment at room temperature. The slight increase in crystallinity of *Populus* cellulose at longer pretreatment time is presumably due to the dissolution of amorphous cellulose, which is more susceptible to hydrolysis; however at shorter pretreatment time the different pretreatment conditions appeared to have no notable preference of alkaline hydrolysis of cellulose amorphous regions.

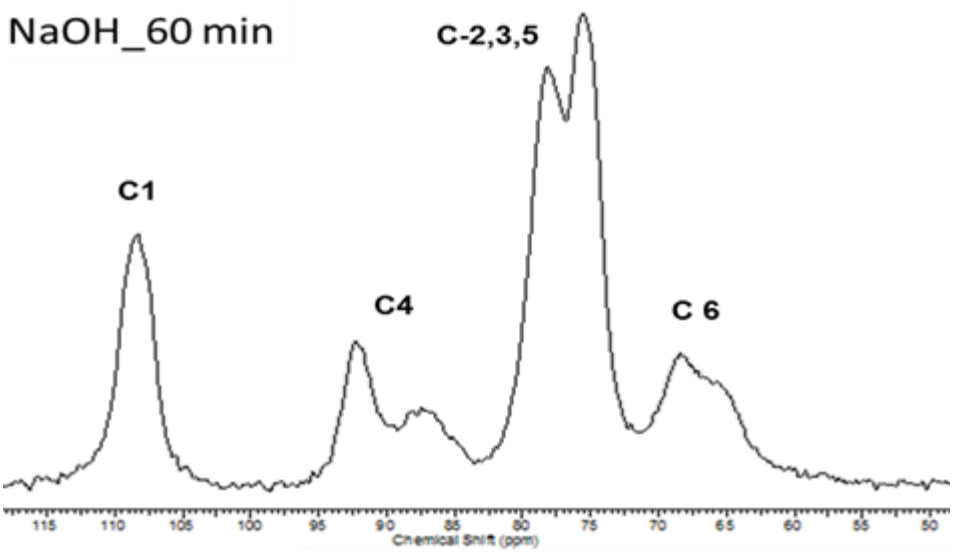

Figure 5.2 Representative spectra of cellulose isolated from 60 min sodium hydroxide pretreated *Populus*.

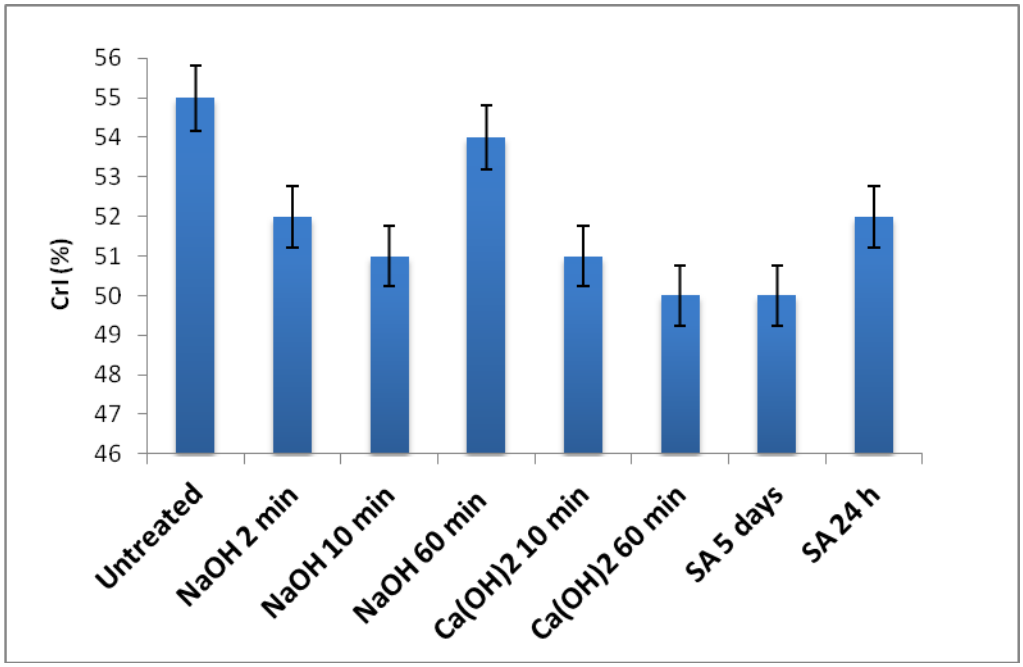

Figure 5.3 Crystallinity results for untreated and alkaline pretreated *Populus*.

As reported earlier, high-severity conditions induce the thermochemical changes by breaking hydrogen bonds of cellulose and making amorphous cellulose more amenable to dissolve at higher temperature or longer residence time [41]. Further, treatment of pure cellulose samples with NaOH and ammonia usually alters their crystalline structures, which has also been shown to impact their enzymatic digestibility. While treatment with NaOH produces less-crystalline cellulose II, liquid ammonia pretreatment transforms cellulose I to the cellulose III allomorph [199]. In present study, the singlet (C-1) at 105.o ppm in ^{13}C CP/MAS spectra of isolated cellulose samples indicates that the cellulose is predominantly in cellulose I form in all alkaline pretreated *Populus* samples.

5.3.4 Accessible surface area analysis of cellulose

The Simons' Stain technique was used to evaluate the porosity of the biomass. The method involves the use of a dye mixture comprised of direct blue 1 (DB), which has a molecular diameter of ~1 nm, and direct orange 15 (DO) with a molecular diameter in the range of 5-36 nm. The DB has a low affinity to cellulose while DO has a high affinity to cellulose initially. In general, DB enter all the pores with a diameter larger than 1 nm, while DO only populates the larger pores. An increase of pore size for *Populus* would facilitate of DO dye gaining access to enlarged pores and displacement of DB because of the higher affinity of DO for the cellulose hydroxyl groups. The ratio and amount of DO and DB absorbed into the biomass indicates the number of large pores and small pores and subsequently cellulose accessibility in lignocellulosic biomass for enzymatic deconstruction [114]. The amount of dye adsorbed by the substrates as well as the orange/blue (O/B) ratio is shown in Figure 5.4.

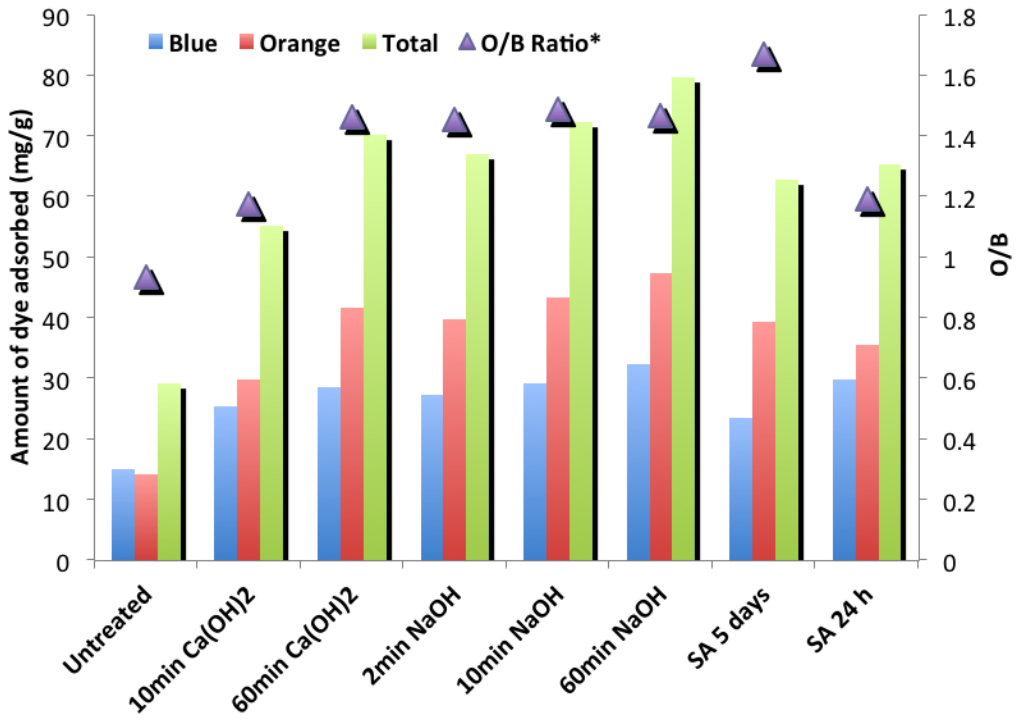

Figure 5.4 Dye adsorption diagram of untreated, NaOH, $Ca(OH)_2$, and soaking in ammonia pretreated *Populus*. Primary y axis represents the dye adsorption, mg dye / g of dry biomass, while secondary y axis indicates the orange/blue ratio.

All the alkaline pretreatments significantly increased the cellulose accessibility, as revealed by the increased amount of orange dye adsorbed as well as O/B ratio. As pretreatment severity extended, so did cellulose accessibility. It has been shown that analysis based solely on the O/B ratio may skew data interpretation, as larger amounts of blue dye adsorbed by a substrate can cause a decrease in the overall O/B ratio. In this particular study, the amount of orange dye adsorbed alone might provide an even simpler and better indicator of the cellulose accessibility. In addition, although Simons' Stain has successfully been utilized to assess the accessible surface area of cellulose in pretreated substrates, the specificity of the dyes for cellulose, when compared to lignin, still needs to be more fully resolved.

For dilute sodium hydroxide pretreated *Populus*, although the O/B ratio did not increase as the temperature time increased, there was an obvious increase in the amount of orange dye adsorbed, which indicates increased cellulose accessibility. Sodium hydroxide was also found to be much more effective than lime pretreatment in terms of increased cellulose accessibility. At equivalent pretreatment times, sodium hydroxide pretreated *Populus* always adsorbed larger amount of orange dye, and in fact pretreatment with sodium hydroxide for 10 min was more effective than pretreatment with lime for 60 min. Pretreatment by soaking in ammonia at room temperature and with long treatment times is lightly more effective than pretreatment for 24 h at higher temperatures, as indicated by the amount of orange dye adsorbed (39.3 vs. 35.6 mg/g substrate). In addition, the biggest increase in cellulose accessibility upon alkaline pretreatment occurs in the first 10 min the pretreatment, although the accessibility continues to increase through the remaining 50 min of pretreatment but at a significantly slower rate. The exact same trend was also reported in a previous published report, employing NMR relaxometry technique on increasing accessibility by dilute acid pretreatment [11].

5.3.5 Enzymatic hydrolysis

To evaluate the potential of alkaline pretreatment of biomass for ethanol production, enzymatic hydrolysis of all pretreated and untreated *Populus* samples were performed and the glucose yield after 48 h and 72 h are shown Figure 5.5. The maximum glucose yields were obtained for the NaOH treated biomass samples followed by 60 min lime pretreated samples. The sodium hydroxide pretreatment resulted in a 3-4 fold increase in

cellulose to glucose conversion yield than the untreated *Populus*. Ammonia pretreatment also resulted in two-fold increase in glucose yield.

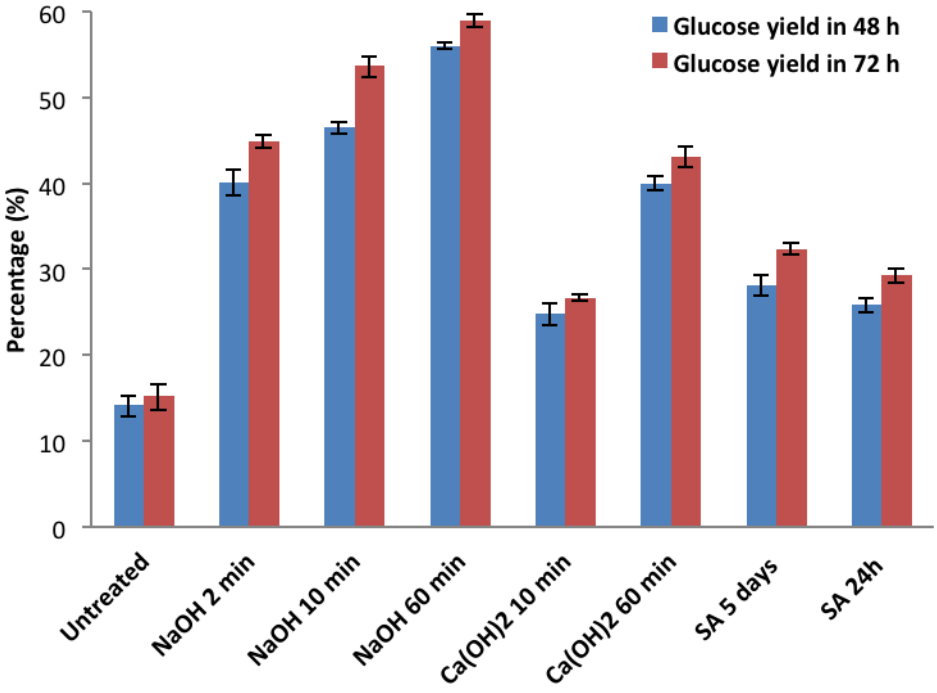

Figure 5.5 Glucose yields after 48 and 72 h from enzymatic hydrolysis of various Populus samples pretreated with alkali.

The glucan yields obtained from *Populus* by different pretreatments could be directly correlated to compositional analysis data and other cellulose structural parameters such as, DP, crystallinity and cellulose accessibility. The results of characterization experiments demonstrated that significant changes had occurred regarding the DP and crystallinity of the cellulose – both of these parameters are considered as very important for effective enzymatic conversion of cellulose to glucose [199]. A lower DP is a sign of an increased number of cellulose reducing ends and consequently a higher exoglucanase activity can be expected during enzyme hydrolysis. This in turn exposes further sites of

endoglucanase attack and it weakens the networks to permit better access for the enzymes, making the cellulose more amenable to enzymatic deconstruction [10]. In the present study, the *Populus* samples pretreated with dilute sodium hydroxide and ammonia show significantly reduced DP_w and DP_n, resulting in a notable reduction of the biomass recalcitrance of these samples.

In addition, the alkaline pretreatment methods studied herein reduced the crystallinity of the cellulose, although only a very slight change was found in the sample pretreated by sodium hydroxide for 60 min. Short residence times (e.g. 2 and 10 min) in NaOH, lime, and ammonia revealed a reduced crystallinity, indicating possible recrystallization of the cellulose, while 60 min of treatment in dilute NaOH had a very slight change. However, in contrast, the sample pretreated with sodium hydroxide for 60 min released the highest amount glucose, which indicates that crystallinity may not be playing a very important role in determining sugar release. As revealed by the modified SS technique, NaOH pretreatment led to the highest increase in cellulose accessibility and was more effective than any other tested alkaline pretreatment method. Lignin removal has been shown to increase the yield of enzymatic hydrolysis; however, the direct effect of lignin removal on cellulose accessibility is still not fully clear. In this study, the Simons' stain method indicated that substrates pretreated with sodium hydroxide for 10 min and 60 min had the lowest lignin content and highest cellulose accessibility. However, samples pretreated with ammonia had the highest lignin content among all the alkaline pretreatments, but still showed higher cellulose accessibility data compared to samples pretreated with lime for 10 min. This is likely due to the fact that soaking ammonia pretreatments are much

more effective at removing xylan. The effect of xylan removal on cellulose accessibility could also be explored by comparing these two soaking ammonia pretreatments. Soaking ammonia pretreatments at lower and higher temperature showed very similar lignin contents (26.0% and 25.7%), however, pretreatment at lower temperature was more effective than that at higher temperature in terms of xylan removal, thereby leading to higher cellulose accessibility. This suggests that hemicellulose, which is normally found to the outer surface of fibers as well as in interfibrillar spaces, is another physical barrier that limits cellulose accessibility. Nevertheless, a strongly positive relationship between cellulose accessibility and sugar release could be established (Figure

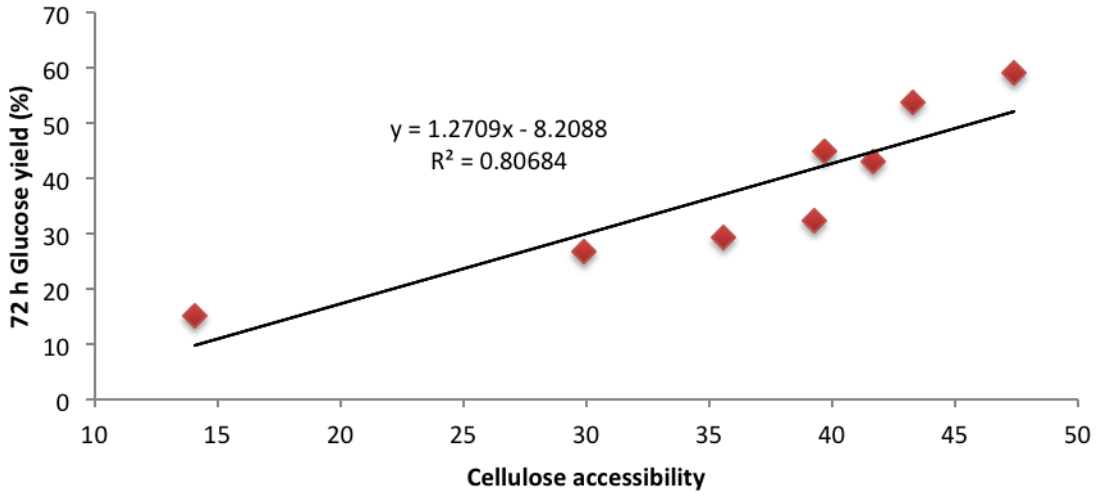

Figure 5.6 Relationship between cellulose accessibility of untreated and alkaline pretreated *Populus* as determined by Simons' Stain and 72 h glucose release.

5.4 Conclusion

The present study provides key insights into the biomass recalcitrance specifically those associated with cellulose structure and accessibility arising from various alkaline pretreatment methods. A comparison of various alkaline pretreatment methods on milled poplar revealed that the sodium hydroxide and lime pretreatments increase the relative glucan content of biomass possibly by removing a portion of the hemicellulose and lignin, especially sodium hydroxide being more effective in that respect. Further, cellulose content increased with the severity of the sodium hydroxide pretreatments, but in the lime as well as in ammonia pretreatments, relative cellulose content decreased as the severity increased, suggesting that the pretreatment may have initiated the glucose solubilization. Decreasing the degree of polymerization of cellulose, removal of lignin, and altered cellulose accessibility contributes to a reduced recalcitrance of biomass and results in cellulose that can be easily digested by enzymes. The Simons' stain showed that porosity and hence, the cellulose accessibility was improved by each pretreatment, and increased further with the severity of the treatment. For sodium hydroxide pretreatments the porosity as well as proportion of large and small pores increased faster with time while for other alkaline pretreatment methods, the same increased at a comparatively slower rate. The most significant cellulose degradation was observed for sodium hydroxide pretreatment that possibly increases the cellulose accessibility and consequently showed maximum cellulose to glucose conversion. However, it is difficult to evaluate the exact effect of each of individual factors independently because pretreatment modifies many parameters at the same time. Nonetheless, the present study

provides key insight into biomass recalcitrance, specifically aspects associated to cellulose structure and accessibility arising from various alkaline pretreatment methods.

CHAPTER 6

INSIGHTS INTO THE EFFECT OF LIGNIN AND HEMICELLULOSE REMOVAL ON ACCESSIBLE SURFACE AREA AND ENZYMATIC OF CELLULOSE[§]

6.1 Introduction

Rapid developments in biotechnology, engineering, and plant genetics are leading to a manufacturing concept for converting lignocellulosic biomass, representing the most abundant carbon-neutral renewable resources, to biofuels and biomaterials [1]. However, this process is significantly hindered by innate biomass recalcitrance which refers to the characteristics of lignocellulose to protect its carbohydrates from degradation by cellulases [6]. In an effort to assess the effects of the substrate characteristics, such as hemicellulose and lignin content, cellulose crystallinity, cellulose degree of polymerization, intensive research has focused on modifying and correlating these substrate characteristics to biomass recalcitrance [68, 200]. Some of the literature, however, reports conflicting trends on the individual effects of these characteristics, which are mainly due to the fact that biomass recalcitrance does not come from a single structural factor and interactive effects naturally exist between these factors [9]. Unlike other factors, the accessible surface area of cellulose also known as cellulose accessibility has been consistently recognized as one of the most critical factors effect enzymatic

[§] This manuscript was accepted for publication in Green Chemistry, 2015. It is entitled as "Insights into the effect of dilute acid, hot water or alkaline pretreatment on the cellulose accessible surface area and the overall porosity of *Populus*". The other authors are Tyrone Jr. Wells, Qining Sun, Fang Huang, and Arthur J. Ragauskas. The copyright permissions will be submitted to the thesis office of Georgia Tech.

hydrolysis yield and rate [12,119,201]. Grethlein reported a linear relationship between the initial cellulase reaction rate and pore volume of the substrate accessible to a nominal diameter of 5.1 nm, which representative of the diameter of a typical cellulase [90,110]. Several pretreatment technologies have been developed to change the structure of lignocellulosic biomass physically, chemically, biologically, or in combination. Though the fundamental mechanisms for each pretreatment, particularly how it alters the chemical compositions or physical structures of biomass are not yet fully understood, the final objective of pretreatment is always to render biomass more accessible to enzymes for efficient and rapid sugar generation using low protein loading.

The ideal pretreatment should fractionate cellulose, hemicellulose, and lignin cost effectively so that cellulase can react with pure cellulose, and at the same time minimize the loss of sugars and formation of degradation products that inhibit enzymatic hydrolysis and fermentation. Dilute acid (DA), hot water (HW) and dilute alkaline pretreatment are three most commonly used pretreatment technologies that have included significant research efforts over the past few years. Hemicellulose, located on the outer surface of cellulose fibers as well as inter-fibrillar space, has been shown to be the most subject to changes in pretreatment conditions [202]. Lignin could also act as a protective matrix making the target polysaccharides inaccessible to microbes, hence slowing down the deconstruction process. Obviously, the content of lignin and hemicellulose in plant cell wall affect the degree of substrate digestibility, and understand the relative importance of the removal of one of these two components over the other is critical for further optimization of the current pretreatment techniques [203]. Comparisons of pretreatment

effectiveness in terms of increasing cellulose accessibility or reducing biomass recalcitrance based on literature data are hindered by the fact that various studies use different feedstock, enzyme loading and pretreatment conditions. At the same time, majority of the studies that tried to highlight the importance of cellulose accessibility made use of highly digestible pure cellulosic substrates such as filter paper which are not really indicative of how the realistic heterogeneous lignocellulosic biomass might behave [93].

In this study, *Populus* was pretreated by DA, HW and NaOH at three different pretreatment severities, producing substrates differing substantially in the composition and structure. Considerable amounts of work have been done to develop surface area measurement techniques that can be performed on cellulosic substrates [11]. One of the approaches that can be used as an alternative to represent the amount of accessible surface area of substrate is the measurement of porosity using probing molecules, such as water in NMR cryoporometry and relaxometry technique, mercury in mercury porosimetry technique and a set of dextran molecules in solute exclusion technique [92]. Other techniques such as nitrogen adsorption, water retention value (WRV) method, Simons' stain and protein adsorption method directly measures the adsorption of a given molecule to a lignocellulosic substrate [92]. Some of these techniques such as nitrogen adsorption require prior drying of the substrates which makes it typically less effective due to fiber hornification, while other techniques such as WRV suffer from the fact that size of water molecular is much smaller than cellulase enzymes resulting in over-estimation of cellulose accessibility [11]. Solute exclusion and NMR techniques can

measure lignocellulosic substrates in its wet state, but they are laborious and expensive [119]. A recent study by Wang et al. measured the total substrate accessibility to cellulase based on the maximum adsorption capacity of cellulose for a non-hydrolytic fusion protein named TGC, containing a green fluorescent protein and a cellulose binding module, and results correlated quite well with classic solute exclusion technique [92]. Simons' stain and mercury porosimetry was used to measure different and complementary information on cellulose accessibility of substrates prepared by these pretreatments, providing insights into the effect of pretreatment on cellulose accessibility as well as the role of cellulose accessibility in the fundamentals of biomass recalcitrance (Figure 6.1).

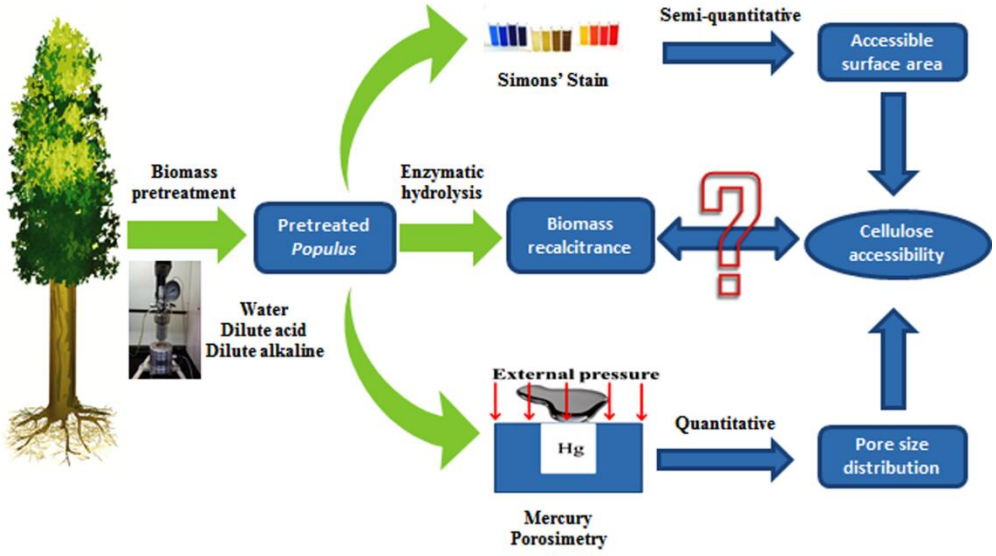

Figure 6.1 Objective and experimental approach.

6.2 Experimental Section

6.2.1 Biomass substrates

Hybrid *Populus* (*Populus trichocarpa x deltoides*) was harvested in 2012 at Oak Ridge National Laboratory (ORNL), TN, and prepared as described in Chapter 3 (3.1.2 Biomass substrate).

6.2.2 Extractive-free *Populus* preparation

Samples were extracted with dichloromethane in a Soxhlet apparatus (Foss, Soxtec^{TM} 2050) as described in Chapter 3 (3.2.1 Soxhlet extraction).

6.2.3 Biomass pretreatment

Various pretreatments including dilute acid (DA), hot water (HW), and dilute alkaline were directly applied on extractive-free *Populus* as described in Chapter 3 (3.2.2.1 Dilute acid pretreatment; 3.2.2.3 Dilute alkaline pretreatment; 3.2.2.4 Hot water pretreatment). Each pretreatment was done at three different severities as shown in Table 6.1.

Table 6.1 Conditions for dilute acid, hot water, and alkaline pretreatment of *Populus*

Pretreatment	Temperature (^{o}C)	Time (min)	Impregnation agent
Dilute alkaline	80	10	1% (w/w) NaOH at
	120	10	5% solid loading
	120	60	
Hot water	120	10	DI water at 5% solid
	160	10	loading
	160	60	
Dilute acid	120	10	1% (w/w) H_2SO_4 at
	160	10	5% solid loading
	160	60	

6.2.4 Chemical composition analysis

Carbohydrate profiles and acid-insoluble lignin content in untreated and various dilute acid, hot water, and dilute alkaline pretreated *Populus* were determined as described in Chapter 3 (3.3.1 Carbohydrate and acid-insoluble lignin analysis).

6.2.5 Simons' stain

Simons' Stain was applied on untreated and various alkaline pretreated *Populus* to estimate the accessible surface area of cellulose as described in Chapter 3 (3.3.2 Simons' stain)

6.2.6 Mercury porosimetry

Organic solvent exchange drying experiment was done in an effort to avoid irreversible pore collapse during typical biomass drying process. Samples were first soaked in deionized water for 24 h, and were then subsequently transferred to Soxhlet apparatus and solvent exchanged with wet methanol for 24 h, dry methanol for 24 h, and finally with dry toluene for 24 h. Molecular sieves (4 Å) were put in the round flask to adsorb the water diffusing from the biomass during the exchange process with dry methanol. Toluene saturated biomass were then transferred to a vacuum oven at 45 ^{o}C and dried for 5 h. Mercury intrusion porosimetry was used for the evaluation of pore size distributions. The measurements were performed with an AutoPore IV 9500 porosimeter using a pressure range from 1×10^{-1} to 6×10^{4} psia (Micromeritics Atlanta, Georgia, USA) on the organic solvent exchange dried sample immersed in the non-wetting mercury. During the analysis, the largest of pores fill at the lowest of the pressures; as pressure increasing,

mercury was intruded into smaller voids progressively. The pore volume can be determined based on the quantity of the intruded mercury, and the pore size distribution can be derived according to the Washburn equation, which gives the relationship between pore size and pressure:

$$r = -2\gamma\cos\theta/p$$

r = pore radius, γ = surface tension of mercury (0.485 N/m), θ = wetting angle of mercury (130^{o})

6.2.7 Enzymatic hydrolysis

Enzymatic hydrolysis of untreated and various alkaline pretreated samples were performed as described in Chapter 3 (3.2.8 Enzymatic hydrolysis). A sample of hydrolysis liquid after 24 h was withdrawn and analyzed by an Agilent 1200 series HPLC system for sugar analysis.

6.3 Results and Discussion

6.3.1 Chemical Composition Analysis

The chemical composition of each of the substrates was determined by Klason protocol according to TAPPI standard method T-222 (Figure. 6.2). The majority of the hemicellulose (98%), typically characterized by xylan, is removed within 10 min of DA pretreatment. The DA and HW pretreatment are ineffective at removal of lignin, and in fact the Klason lignin content actually increases after pretreatment due to the formation of pseudo-lignin [156]. On the other hand, 35% of lignin can be removed via 60 min

NaOH pretreatment at 120 ^{o}C while only 28% of xylan was degraded. Glucan content was increased after all pretreatments due to the removal of either xylan or lignin.

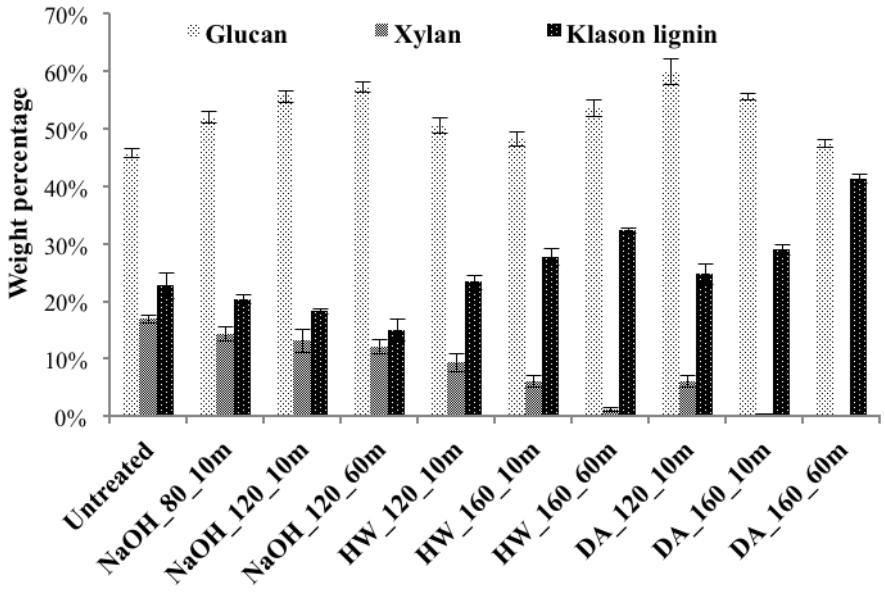

Figure 6.2 Glucan, xylan, and Klason lignin contents of untreated, dilute alkaline, hot water and dilute acid pretreated *Populus.*

6.3.2 Enzymatic hydrolysis

The native and pretreated *Populus* was subject to enzymatic hydrolysis for 24 h at a consistency of 1% (w/v) in 50 mM citrate buffer (pH 4.8) with *cellulase* and *β-glucosidase* loadings of 20 FPU/g and 40 CBU/g, respectively. The glucose and xylose yield (Figure 6.3) was analysed by high-performance anion exchange chromatography with pulsed amperometric detection. Severe DA pretreatment resulted in the highest glucose yield as compared to other pretreatments, and approximately 500 mg of glucose per grams of dry pretreated biomass could be released after 60 min 160 ^{o}C DA pretreatment. At the same pretreatment conditions (120 ^{o}C, 10 min), alkaline pretreated

Populus actually has the highest glucose release, approximately 320 mg/g of dry biomass. Alkaline pretreatment also released much more xylose compared the other two pretreatments, primarily due to the significant solubilization of xylan during HW and DA pretreatment.

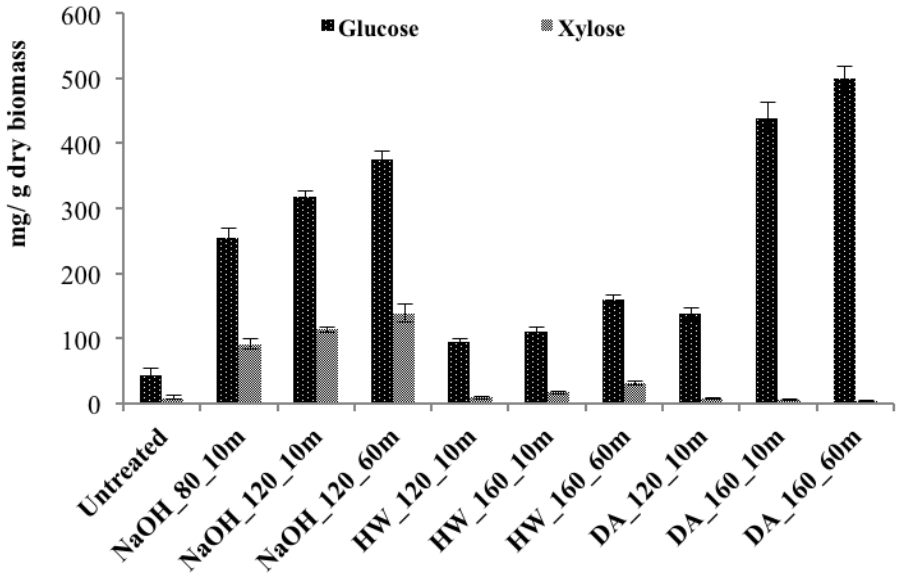

Figure 6.3 Glucose and xylose yield (mg/g dry biomass) after 24 h enzymatic hydrolysis of native, dilute alkaline, hot water and dilute acid pretreated *Populus.*

6.3.3 Accessible surface area analysis of cellulose

Simons' stain (SS), a two color differential stain technique, has been shown to be a semi-quantitative method for the estimation of the accessible surface area of lignocellulosic substrates by applying two dyes: Direct Orange (DO) 15 and Direct Blue 1 (DB) [114]. The ratio of DO and DB (O/B) adsorbed by the substrates can be therefore used to indicate the relative amount of large pores to small pores. In addition, because DO dye has a very similar diameter compared with a typical enzyme, the amount of DO dye

adsorbed (A_O) can be used to estimate the accessible surface area of cellulose [202]. A recent study has proposed that the use of A_O(O/B) as a correction factor for the shape of the pore size distribution curve contributing to the enzyme-accessible surface area shows better correlation with other accessibility measurement techniques such as water retention value [108]. A modified Simons' stain assay based on previously developed procedures was applied to provide insights into the pore surface area (Figure 6.4)

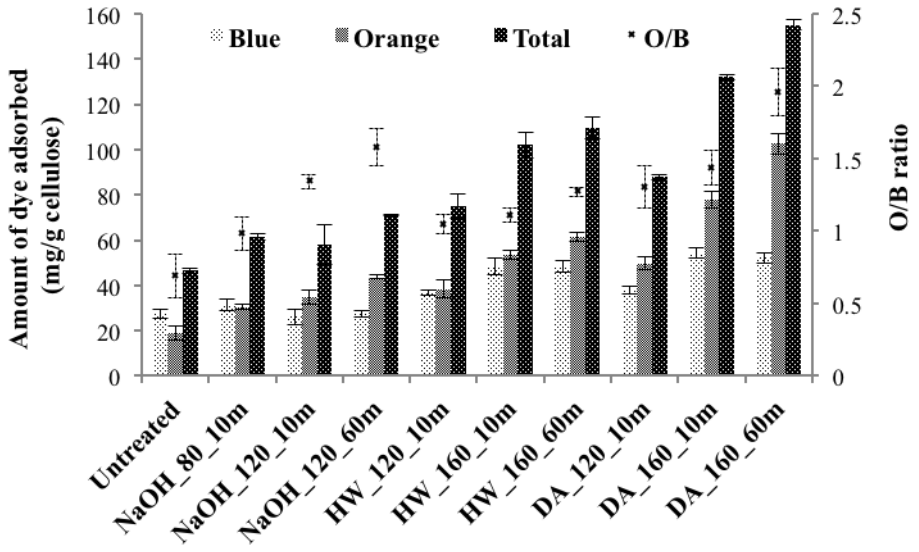

Figure 6.4 Simons' stain results for biomass accessible surface area represented by the amount of adsorbed dye (mg dye/g of cellulose) and relative biomass porosity represented by ratio of adsorbed large orange dye to small dye (O/B).

As indicated by the increase of O/B and orange dye adsorption, all these pretreatment significantly increases biomass porosity and the total accessible surface area of cellulose. For each type of pretreatment, as the pretreatment severity extended, so did the cellulose accessible surface area. For example, O/B and orange dye adsorption increased from 0.69 and 18.9 mg/g to 1.30 and 49.7 mg/g after 10 min 120 ^{o}C DA pretreatment. These numbers further increased to 1.44, 77.8 mg/g and 1.96, 102.5 mg/g as the pretreatment

temperature and time increased to 160 ^{o}C and 60 minutes. A very interesting finding is that 312% increase (18.9 to 77.8) in orange dye adsorption could be noticed after 10 min pretreatment, while only 32% increase (77.8 to 102.5) is obtained after the rest 50 minutes. This phenomenon also applies to the other two pretreatments, suggesting that the increase in accessible surface area of cellulose primarily occurs in the first 10 min of pretreatment and though continues through the rest pretreatment time, occurs at a significantly slower rate. In addition, DA pretreatment is found much more effective than the other two pretreatments in terms of accessible surface area increase, while HW and alkaline at same pretreatment conditions exhibits very similar data, 38.4 and 35.0 mg/g respectively.

6.3.4 Effect of xylan and lignin removal on cellulose accessibility

With compositional, accessibility and digestibility data available for a series of pretreated *Populus*, a comprehensive investigation of the effect of removal of each individual cell wall component by different pretreatment on cellulose accessibility as well as the relation between cellulose accessibility and substrate digestibility can be performed. Although current understanding of cell wall structure is quite limited, it has been generally recognized that elementary cellulose fibrils are coated with other non-cellulosic polysaccharides to form microfibrils, which are then cross-linked by hemicellulose/pectin matrixes to form macrofibrils [15]. The relative importance of removing lignin versus xylan was obtained by comparing the cellulose accessibility of *Populus* substrates produced by DA, HW and alkaline pretreatment as indicated by Simons' stain **(**Figure 6.5 and 6.6). Obviously, cellulose accessibility of *Populus*, pretreated by alkaline, HW and

DA under different pretreatment conditions, is inversely proportional to the amount of xylan retained (Figure 6.6), while the relationship between cellulose accessibility and Klason lignin content is not quite obvious (Figure 6.5). As a matter of fact, data shown in Figure 6.5 suggest that cellulose accessibility is inversely proportional to lignin content for the three alkaline pretreated substrates, but has a general trend of a positive relationship with lignin content for DA and HW pretreatments. This is mainly because the decrease of lignin content after alkaline pretreatment is accompanied by the decrease of xylan, while on the other hand, the increased lignin content after DA and HW pretreatments was accompanied with dramatic decrease of xylan content which helps increase the cellulose accessibility as shown in Figure 6.6. This is in consistent with a recent review with in-depth analysis of removal of lignin/hemicellulose content to improve substrate digestibility from last 5 years published literature work, which suggest that cellulose saccharification is linearly proportional to the amount of xylan removal but has a general trend of an inverse relationship with lignin removal for a serious of acid-based pretreatments due to the fact that this increased lignin removal is normally achieved at the expense of hemicellulose removal [12]. Jungnikl et al. investigated the implication of chemical extraction treatments on the cell wall nanostructure of spruce wood using small-angle X-ray scattering, indicating that delignification had only a moderate effect on the structural organisation of the cell wall, while further extraction of hemicellulose with NaOH induced considerable nanostructural changes [204]. An inverse relationship was also observed between the lignin content after alkaline pretreatment and the extent of xylan conversion in a 24 h period (Figure 6.7). Wang et al. also showed that the xylan conversion efficiency was more sensitively affected by the variation of NaOH

pretreatment conditions than glucan conversion efficiency [205]. It therefore can be concluded that lignin probably doesn't directly dictate cellulose accessibility but rather restricts xylan accessibility which in turn controls the access of cellulase to cellulose. However, it is worth mentioning that near complete removal of both lignin and xylan may cause aggregation of cellulose microfibrils resulting decreased cellulose accessibility [138].

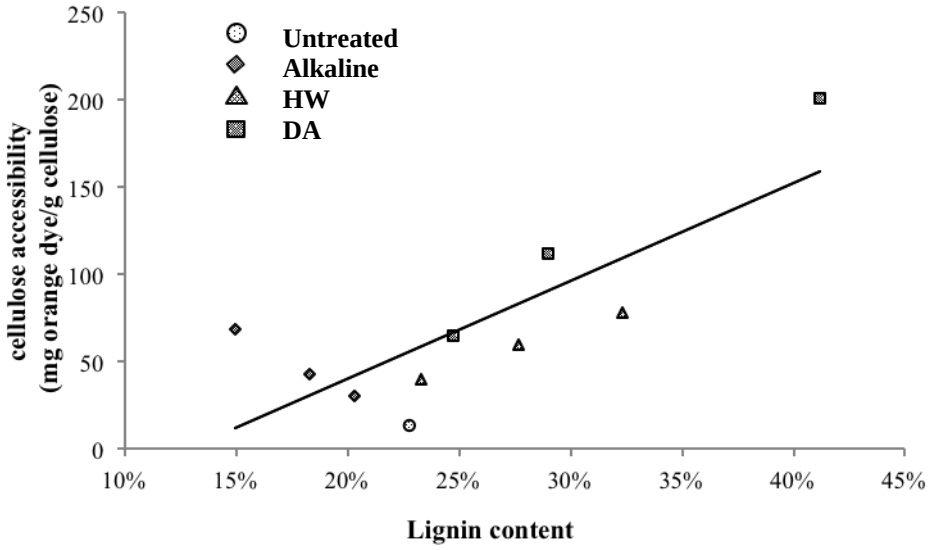

Figure 6.5 Effect of lignin removal by different pretreatments on cellulose accessibility for a series of alkaline, HW and DA pretreated *Populus*. A correction factor A_O(O/B) was used to represent the cellulose accessibility, where A_O is the orange dye adsorption, and O/B is ratio between Orange and blue dye adsorption.

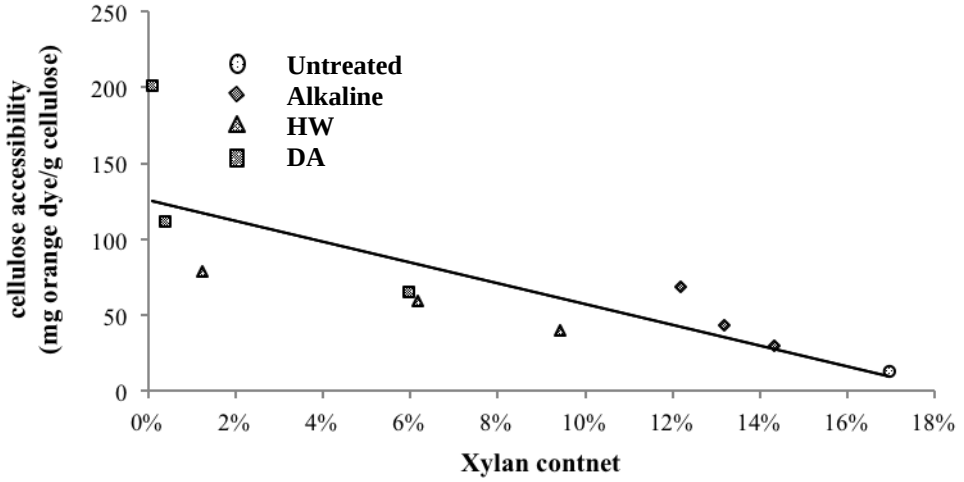

Figure 6.6 Effect of xylan removal by different pretreatments on cellulose accessibility for a series of alkaline, HW and DA pretreated *Populus*. A correction factor A_O(O/B) was used to represent the cellulose accessibility, where A_O is the orange dye adsorption, and O/B is ratio between Orange and blue dye adsorption.

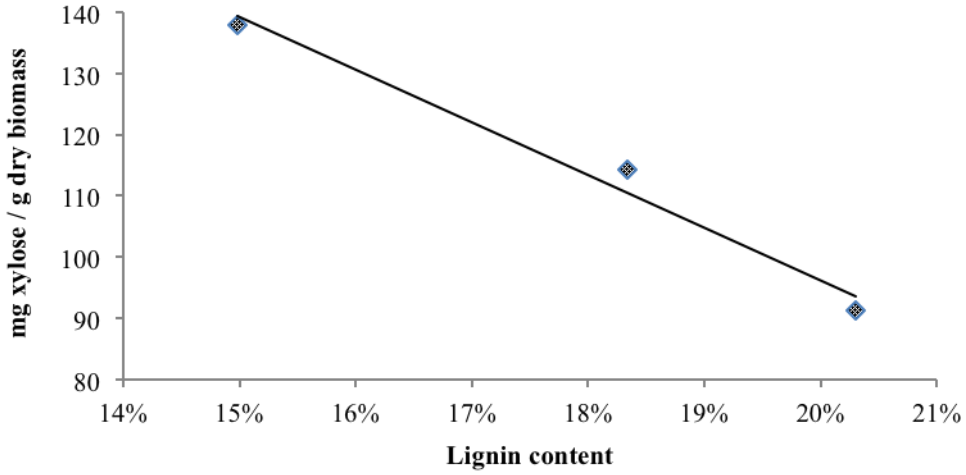

Figure 6.7 Effect of lignin removal by dilute NaOH pretreatment on xylose release for Populus substrates.

6.3.5 Effect of cellulose accessibility on enzymatic hydrolysis

The relation between cellulose accessibility and substrate digestibility was also analyzed to determine if accessibility is a dominant factor affecting saccharification of different pretreated lignocellulosic substrates (Figure 6.8). It was found that substrate digestibility is always proportional to the cellulose accessibility for each individual pretreatment technique under different pretreatment conditions, including DA, HW and alkaline pretreatment. Furthermore, for the same type of pretreatment that exhibits similar degradation mechanism, i.e., HW and DA pretreatment, a strong positive relationship between cellulose accessibility and substrate digestibility can be also obtained. However, when alkaline pretreatment is involved, this linear relationship becomes less obvious. The likely reason is that lignin can not only be physically limiting the cellulose accessibility but also bind to cellulase unproductively through functional groups such as lignin phenolic hydroxyl groups therefore reducing the effectiveness of the enzymatic hydrolysis, and the relative contribution of these two negative roles of lignin is not yet fully quantitively understood [206]. Several studies have shown that unproductive binding of enzymes to lignin could be responsible for the need of high enzyme loading [207]. However, a recent study also demonstrated that the effect of unproductive adsorption is minimal for most cases under typical hydrolytic reaction concentrations and the steric hindrance of lignin remained as a major limiting factor [208]. In our study, removal of lignin by alkaline pretreatment probably didn't increase cellulose accessibility to the extent that HW/DA did as shown previously by Simons' stain, however, the negative binding effect of lignin has been decreased to some extent during the subsequent enzymatic hydrolysis process, resulting in the highest sugar release when compared to

HW and DA pretreated substrate at same pretreatment conditions. In other words, although alkaline pretreatment increases the cellulose accessibility and substrate digestibility, it seems reasonable to argue that increase of cellulose accessibility by NaOH pretreatment is probably not the main reason causing the high substrate digestibility. However, as the DA pretreatment severity increasing, the accessibility increased to a certain level that the accessibility became the dominate factor, causing higher sugar release despite retaining a large lignin fraction. A recent study also showed that the lignin-binding cellulase can be potentially recovered by addition of a sufficient quantity of cellulosic substrate with an increased surface area [209]. It can be therefore concluded that the cellulose accessible surface area appears to be a strong indicator of the ease of enzymatic hydrolysis only when same or same type of pretreatment is applied, and this direct cause-effect relationship as discussed above, cannot be easily obtained for substrates produced using different type of pretreatments. Other biomass or cellulose structural relevant factors such as cellulose crystallinity, degree of polymerization, or herein this case, the irreversible enzyme adsorption by lignin might need to be considered in order to better predict the substrate digestibility. Kumar and Wyman reported that delignification of corn stover by peracetic acid greatly enhanced enzymatic hydrolysis, but had a very limited effect on cellulose accessibility [127]. In contrast, Rollin et al. showed that high levels of delignification by soaking in aqueous ammonia without a significant increase in cellulose accessibility did not results in a large increase in glucan digestibility of switchgrass [187]. All these published literatures support the conclusion that delignification may have a limited effect on cellulose accessibility; however, the exact roles of lignin content in biomass recalcitrance are much more complicated and

most of time depends on substrates and pretreatment methods being used. Therefore, different pretreatment strategies will need to be adopted when trying to engineer different plants for efficient reduced recalcitrance.

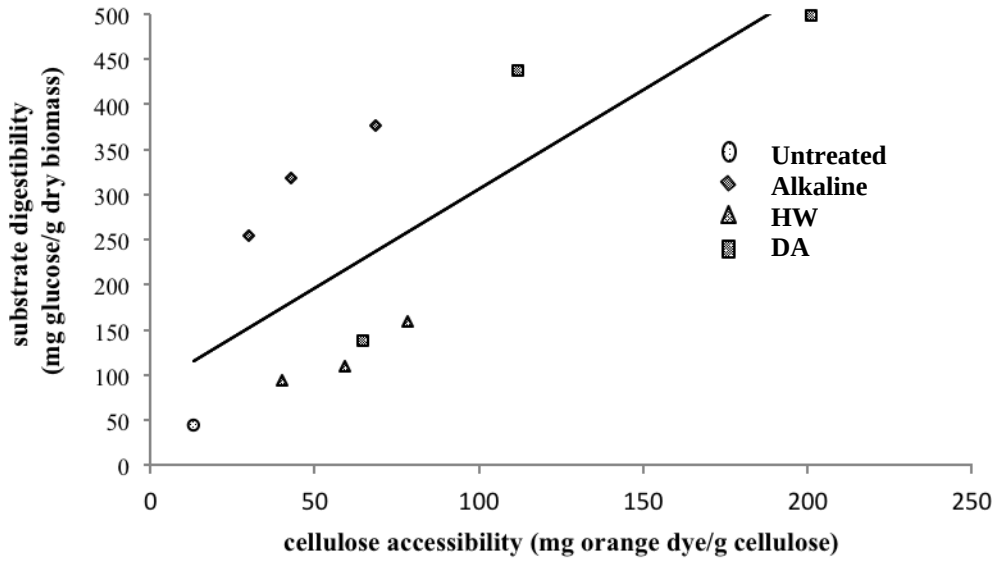

Figure 6.8 Relation between cellulose accessibility measured by Simons' stain (mg dye/g cellulose) and substrate digestibility (mg glucose/g dry biomass) for a series of alkaline, HW and DA pretreated *Populus*. A correction factor A_O(O/B) was used to represent the cellulose accessibility, where A_O is the orange dye adsorption, and O/B is ratio between Orange and blue dye adsorption.

6.3.6 Pore size distribution by mercury porosimetry

There are several porosity scales in biomass from the cell lumen, intercellular space, pits to the nano-pores formed between coated microfibrils [105]. The following classifications that comply better with the wood anatomy than IUPAC definition of pore-size classes was proposed: macropores comprise the cell lumina, approximately 5 to 400 µm; micropores include pit apertures, pit membrane voids, 100 nm to 5 µm; nanovoids include the pores in the cell wall and space between cell wall component range in diameter less than 100 nm [210,211]. With majority pore size data focused on the native

biomass or pure cellulosic pulp, the description of the exact effect of different pretreatment on different scales of biomass porosity ranging from nanometer to macrometer is still quite limited. From this perspective, a porosimetry technique that can generate the actual pore size distribution (PSD) curves other than Simon' stain would be necessary. However, most of these techniques require a prior drying of the substrate which makes it typically less effective in determining the pore volume due to the fact that water removal from non-rigid porous materials such as biomass could produce partial irreversible collapse of pores known as fiber hornification. Zauer et al. showed that the pore diameter of native hardwood range between 4 and 400 nm decreased considerably due to thermal drying at 200 ^{o}C for 4 h [212]. Organic solvent exchange drying is a technique that has been used in surface/pore size measurement such as nitrogen adsorption and mercury porosimetry, which shows minimal pore collapse upon drying of lignocellulosic substrates [117]. To avoid this pore collapse, the untreated and pretreated *Populus* were solvent exchanged in a Soxhlet apparatus with wet methanol, absolute dry methanol, and dry toluene using molecular sieves to absorb all water diffusing from the substrates before final oven dry. In this manner, water is removed from biomass step by step preserving the maximally swollen pore structure of the wood samples in absolutely dry state. Mercury porosimetry which can provide a wide range of information, e.g. the pore size distribution, total pore area and volume, average pore diameter, and the pore tortuosity was performed on these organic solvent exchanged untreated and pretreated substrates. Briefly, non-wetting liquid mercury was penetrated into the pore under external pressure, and the mercury volume infiltrated into the pore was measured as a function of the external pressure with an AutoPore IV 9500 porosimeter (Micromeritics

Atlanta, Georgia, USA). Intrusion pressure was then directly converted to the corresponding pore size by using the Washburn equation. The pore size distribution curves for dilute alkaline, HW and acid pretreated samples along with untreated *Populus* were shown in Figure 6.9, 6.10 and 6.11.

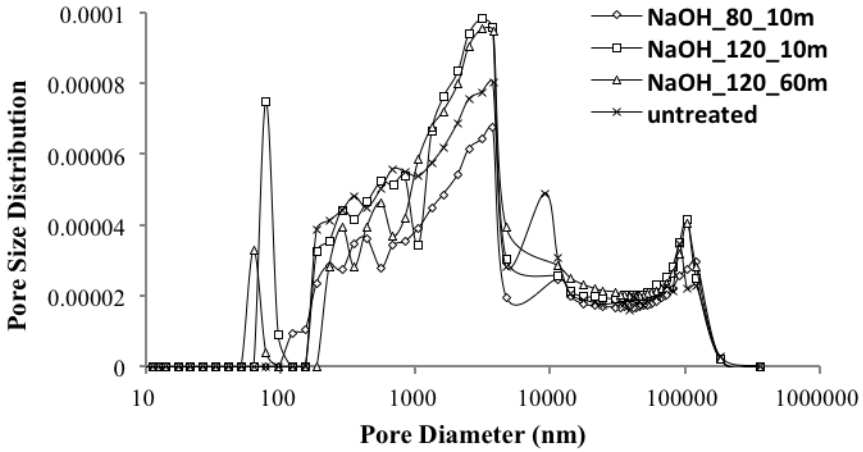

Figure 6.9 Pore size distributions of *Populus* before and after alkaline pretreatment. Pore size distribution is represented using the fundamental theorem of calculus, dv/dx, where the pore volume v is a function of the pore diameter x given by Washburn equation.

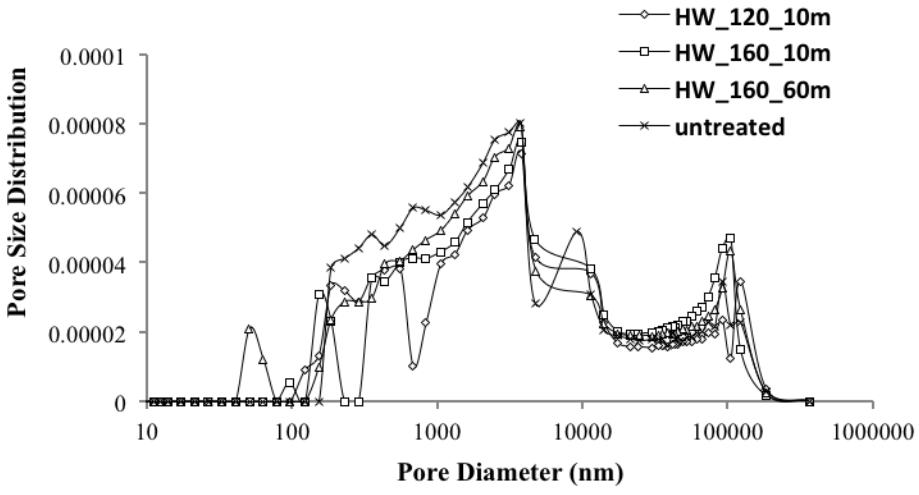

Figure 6.10 Pore size distributions of *Populus* before and after hot water pretreatment. Pore size distribution is represented using the fundamental theorem of calculus, dv/dx, where the pore volume v is a function of the pore diameter x given by Washburn equation.

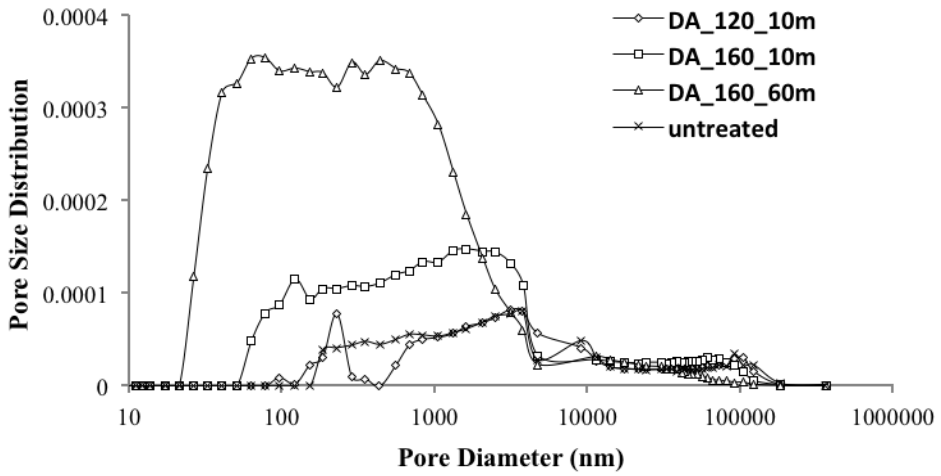

Figure 6.11 Pore size distributions of *Populus* before and after dilute acid pretreatment. Pore size distribution is represented using the fundamental theorem of calculus, dv/dx, where the pore volume v is a function of the pore diameter x given by Washburn equation.

The PSD of alkaline and HW pretreated samples present multi-modal hierarchical pore distributions with similar average diameters, while DA pretreatment results a wide unimodal distribution. The pores with a diameter of ~100000 nm are probably due to inter-particle space of granules [213]. The major part of macropores and micropores shown for alkaline and HW pretreated sample has diameter of about 1000-10000 nm, and their distribution of all three HW pretreated sample and one of the NaOH pretreated sample with the lowest severity is actually narrower than that of untreated biomass. The untreated biomass also has much greater volumes of pore with diameter around 10000 nm compared pretreated sample. After pretreatment, fiber cells were separated from each other and cell wall was destroyed into fragments, which can block the fiber cell lumen and pit in the cell wall, decrease the corresponding pore volume [214]. Moreover, some volumes of nanopores between 50-100 nm were also observed on the distribution curves

of all pretreated samples, while no pores with diameter lower than 100 nm can be found for untreated sample. This increase of pore size in nano-space is much more obvious for DA pretreatment compared the other two pretreatments. Indeed, 160 ^{o}C DA pretreatment significantly increases the pore volume between 10-1000 nm, primarily due to its near completely removal of hemicellulose and great redistribution of lignin. Xu et al. also investigated the effect of acid treatment on fiber structure by small-angle X-ray scattering, suggesting microvoids representing a needle-shaped space adjacent to cellulose increases from 790 nm to 1319 nm after 40 min 160 ^{o}C DA pretreatment for sorghum, likely due to "peeling-away" of the plant cell wall components such as xylan [215]. At the most fundamental level, enzymatic hydrolysis only occurs when enzymes diffuse, bind and react on readily activate cellulose fibrils, and synergism can only occur when great amounts of enzymes with complementary activities occupy the same reaction volume [216,217]. Therefore, this significant nano-pore expansion by severe DA pretreatment could increase the synergistic activities, causing a high sugar release. Table 6.2 summarizes the major pore characteristics of these substrates, of which the pretreated samples always have larger total pore area. Meanwhile, DA pretreatment has the largest pore area among these three pretreatments while HW and alkaline results very similar pore area, which are in accordance with the Simons' stain results. Both HW and alkaline pretreatments slightly increases the average pore diameter, while the two DA pretreatments at 160 ^{o}C actually significantly decrease the average pore diameter, e.g., 90% decrease of average pore diameter was observed after 60 min 160 ^{o}C DA pretreatment. Results also indicated that DA pretreatment increased the pore tortuosity which is consistent with literature results by Foston and Raguaskas using water self-

diffusion experiments [117]. The importance of pore size distribution in enzymatic hydrolysis of biomass has also been highlighted in literatures. Luterbacher et al. proposed a pore-hindered diffusion and kinetic model that can be used to predict cellulose hydrolysis with time using pore size distribution and initial composition data [218]. Chundawat et al. reported that nanoporous tunnel-like networks as visualized by 3D-electron tomography can be formed within the cell wall after ammonia fiber expansion, and the shape, size (10 to 1000 nm), and spatial distribution of pores depended on their location within the cell wall and the pretreatment conditions [139]. To the best of our knowledge, it is the first report showing that the unique significant nano-pore expansion caused by severe DA pretreatment despite its small average pore size should be responsible for the high sugar release, therefore suggesting this nano-pore space formed between coated microfibrils is probably the most fundamental pore-scale barrier for efficient enzymatic hydrolysis.

Table 6.2 Pore area, diameter and tortuosity of the tested untreated and pretreated *Populus* from mercury intrusion porosimetry

Substrates	Total Pore Area (m^2/g)	Average Pore Diameter (nm)	Tortuosity
Untreated	0.86	17427.2	1.723
NaOH_80_10m	1.12	22983.4	1.585
NaOH_120_10m	1.23	17827.0	1.706
NaOH_120_60m	1.36	21111.1	1.639
HW_120_10m	0.94	22480.5	1.507
HW_160_10m	1.01	20768.7	1.847
HW_160_60m	1.04	21245.3	1.671
DA_120_10m	1.99	18068.2	1.949
DA_160_10m	2.34	6998.9	2.439
DA_160_60m	5.85	1627.4	3.649

6.4 Conclusion

Pretreatment is known to render biomass more reactive to cellulase by altering the chemical compositions as well as physical structures of biomass. A comprehensive investigation of the effect of DA, HW and alkaline pretreatment on cellulose accessibility of *Populus* was performed in this study. Simons' stain technique along with mercury porosimetry were applied on the acid, neutral, and alkaline pretreated materials to measure the accessible surface area of cellulose and pore size distribution of *Populus.* Results indicated accessible surface area of cellulose is an important factor governing the extent of hydrolysis, however, effectiveness of different type of pretreatment cannot be simply judged on this solely common basis. Delignification through alkaline-based pretreatment is found less effective than removal of hemicelluloses using acid in terms of cellulose accessibility increase. Lignin also plays a negative role in the processes of enzymatic hydrolysis by binding to cellulases, and this negative effect of lignin could be dominated by the positive effect of cellulose accessibility, especially at severe DA pretreatment conditions. Pore size distribution analysis indicated that the most fundamental barrier in terms of biomass porosity scale for efficient enzymatic hydrolysis is the nano-pore space formed between coated microfibrils, despite some of the porous architecture such as cell lumen and pit could be severely destroyed after pretreatment. Cellulose structural relevant factors such as crystallinity and degree of polymerization might also play some roles, but the relative contribution of these factors compared cellulose accessibility and whether some side effects from these factors can be avoid with the significant increase of cellulose accessibility after pretreatment need further analysis.

CHAPTER 7

CHANGES IN CELLULOSE ACCESSIBILITY AND DEGREE OF POLYMERIZATION OF ACID AND ALKALINE PRETREATED BIOMASS DURING ENZYMATIC HYDROLYSIS[**]

7.1 Introduction

Driving forces including the diminishing availability of fossil fuels, potentially higher fossil fuel prices, and growing concerns about environmental stewardship have catalyzed scientists to develop renewable fuel sources, such as lignocellulosic biomass, for the production of biofuels [9]. Enzymatic hydrolysis of lignocellulose refers to a process in which the structural cellulose polysaccharides are effectively broke down to its component sugar using a multi-component enzyme system that typically contains endoglucanase, cellobiohydrolase, and β-glucosidase [219]. However, enzymatic hydrolysis of native lignocellulose is a very slow process due to the innate biomass recalcitrance refers to the complex characteristics of lignocellulose to protect its carbohydrate from degradation by cellulase [6]. Pretreatment is a process that can alter chemical composition such as lignin/hemicellulose content, biomass structure-relevant factors such as particle size, specific surface area (SSA), porosity and cellulose structure-relevant factors including cellulose crystallinity and degree of polymerization (DP), increase the accessible surface area (ASA), therefore enhance enzymatic hydrolysis [10]. To date, numerous physical or chemical pretreatment techniques have been developed,

[**] This manuscript will be submitted in a peer review journal. It will be entitled as "Changes in cellulose accessibility and degree of polymerization of acid and alkaline pretreated biomass during enzymatic hydrolysis". The other authors are Yunqiao Pu, Qining Sun, Fang Huang, and Arthur J. Ragauskas.

including dilute acid (DA), hot water, alkali, organic solvent, ammonia fiber expansion (AFEX) and ionic liquid (IL) pretreatment [130]. While years of research have focused on modifying these characteristics and correlating the substrate alterations to the extent and rate of enzymatic hydrolysis, information about the change of cell wall substrate characteristics, such as cellulose DP and accessibility, during enzymatic hydrolysis is still quite limited.

Changes in structure and properties of cellulose caused by cellulase treatment depend on the composition, the type of enzyme, and the treatment conditions. It was reported that cellobiohydrolase gave only a slight diminution in cellulose DP due to the fact that it only degrades cellulose by an endwise attack, while the endoglucanase, on the other hand, cleaves the cellulose chains randomly, provoking a relative strong degradation therefore has a much more pronounced effect on the decrease of DP [220]. It was also found that the crystalline index of cellulose increased during hydrolysis which indicated that the amorphous portion of the cellulose is more readily hydrolyzed than the crystalline [32]. After enzymatic hydrolysis, a portion of hydrogen bonds is also broken.

As a result of enzymatic hydrolysis, the pore size and accessible surface area of the substrate are also expected to change. Li et al. reported that the concentration of pores smaller than 6 nm in cotton fabric decreased after enzyme treatment as measured by size exclusion liquid chromatography, but no significant changes were observed for the concentration of pores larger than 6 nm [221]. However, Buschle-Diller et al. found porosity of the hemp fibers increased to approximately 270% for the first 4 hours

treatment, then continuously dropped to about the original value of the untreated sample after 24 hours of incubation [222]. Lee et al. reported the specific surface area increased from 8.50 to 9.34 m^2/g cellulose during the first hour of the hydrolysis which may be partly attributed to the particle size reduction, followed by a slow decrease to 7.70 m^2/g due to the hydrolysis of amorphous cellulose result in a larger crystalline fraction that is highly ordered with a lower specific surface area, and then gradually leveled off [223]. In addition, Santa-Maria and Jeoh reported two important observations of cellulose microstructure change during enzymatic hydrolysis: the untwisting of cellulose microfibrils early in the reaction at high hydrolysis rates and the appearance of channels along the microfibril length and thinning of cellulose microfibrils at late stages of the hydrolysis [224].

It is repeated observed that enzymatic hydrolysis proceeds at an initial fast rate followed by a rapid decrease in conversion rates at longer times. Substrate characteristics such as composition, ASA, porosity, DP, crystallinity as well as enzyme related features including enzyme inactivation/inhibition, fractal and jamming effects, diffusion constraints, clogging and imperfect processivity are all suggested to be responsible for this slowdown of the reaction rate, but so far the exact mechanisms leading to this decrease are not fully understood and in most of cases controversial. Nevertheless, it has been hypothesized that the increased recalcitrance of the substrate is probably the reason gradually decreases the rate at which cellulose is hydrolyzed [225]. The decline in hydrolysis rate is suggested to result from (a) depletion of hydrolysable material within the cellulose surface area accessible to a single cellulase through obstacle-free movement

on the surface area and (b) the apparent inaptitude of the enzyme to escape local restrictions through chain release and surface desorption processes [226]. In this study, poplar and switchgrass were pretreated by dilute acid and alkaline and subjected to enzymatic hydrolysis for 72 h. The reducing sugar yield was measured by high performance liquid chromatography at different hydrolysis time points. Hydrolyzed biomass samples were isolated from the hydrolysis system and the cellulose accessible surface area and degree of polymerization were characterized to understand the limitations occurring during enzymatic hydrolysis of lignocellulosic substrates that might be responsible for the gradual slowing down of the reaction. The results obtained should provide insight into the mechanism of enzymatic hydrolysis, which in turn will be extremely helpful for the selection or development of the most effective biomass pretreatment for different biomass substrates.

7.2 Experimental section

7.2.1 Biomass substrates

Hybrid poplar (*Populus trichocarpa x deltoides*) and switchgrass were harvested in 2012 at Oak Ridge National Laboratory (ORNL), TN, and prepared as described in Chapter 3 (3.1.2 Biomass substrate).

7.2.2 Extractive-free *Populus* preparation

Samples were extracted with dichloromethane in a Soxhlet apparatus (Foss, Soxtec^{TM} 2050) as described in Chapter 3 (3.2.1 Soxhlet extraction).

7.2.3 Biomass pretreatment

Various pretreatments including dilute acid (DA), and dilute alkaline were directly applied on extractive-free poplar and switchgrass as described in Chapter 3 (3.2.2.1 Dilute acid pretreatment; 3.2.2.3 Dilute alkaline pretreatment). The pretreatment conditions are shown in Table 7.1.

Table 7.1 Conditions for dilute acid and alkaline pretreatment of poplar and switchgrass.

Biomass	Pretreatment	Temperature (^{o}C)	Time (min)	Impregnation agent (5% loading)
poplar	Dilute acid	120	60	1% (w/w) H_2SO_4
	Dilute alkaline	120	60	1% (w/w) NaOH
Switchgrass	Dilute acid	120	60	1% (w/w) H_2SO_4
	Dilute alkaline	120	60	1% (w/w) NaOH

7.2.4 Chemical composition analysis

Carbohydrate profiles and acid-insoluble lignin content in untreated and various dilute acid and dilute alkaline pretreated poplar and switchgrass were determined as described in Chapter 3 (3.3.1 Carbohydrate and acid-insoluble lignin analysis).

7.2.5 Enzymatic hydrolysis

Enzymatic hydrolysis of untreated and various alkaline pretreated samples were performed as described in Chapter 3 (3.2.8 Enzymatic hydrolysis). Besides measuring the sugar release after different time intervals (2, 4, 8, 12, 24, 48, and 72 h), solid samples were also taken and thoroughly washed then heat treated in boiling water for ~ 10 min at the same time periods.

7.2.6 Protease treatment

Protease treatment was applied on each isolated hydrolyzed samples to remove any remaining enzymes as described in Chapter 3 (3.2.9 Protease treatment).

7.2.7 Simons' stain

Simons' stain was applied on untreated, dilute acid and alkaline pretreated, and enzymatic hydrolyzed poplar and switchgrass to estimate the accessible surface area of cellulose as described in Chapter 3 (3.3.2 Simons' stain). ~10 mg of samples was used instead of ~100 mg due to the limited amount of samples available, and amount of dye, phosphate buffered saline solution added to the solution were also scaled down accordingly.

7.2.8 Gel permeation chromatography analysis of cellulose

Holocellulose samples were prepared as described in Chapter 3 (3.2.5 Holocellulose Pulping). α-Cellulose was isolated from holocellulose samples as described in Chapter 3 (3.2.6 α-Cellulose isolation for GPC). The weight-average molecular weight (M_w) and number-average molecular weight (M_n) were determined by GPC as described in Chapter 3 (3.3.4 Gel permeation chromatography (GPC) analysis of cellulose).

7.2.9 Fourier transform infrared (FTIR) spectroscopy

FTIR spectra of untreated, pretreated, and hydrolyzed samples were analyzed as described in Chapter 3 (3.3.5 Fourier transform infrared spectroscopy).

7.3 Results and Discussion

7.3.1 Chemical composition analysis

The chemical composition of each of the substrates was determined by Klason protocol according to TAPPI standard method T-222 (Figure 7.1). Untreated poplar has higher glucose and lignin content, 51.3% and 23.4% respectively; while untreated switchgrass has higher xylan content (25.5%). Xylan was almost completely removed after DAP for both poplar and switchgrass, while only ~20.2% and 19.2% of xylan was removed after alkaline pretreatment for poplar and switchgrass, respectively. Partial delignification was observed after alkaline pretreatment, and much more lignin was removed for switchgrass than poplar (66.3% vs. 14.5%).

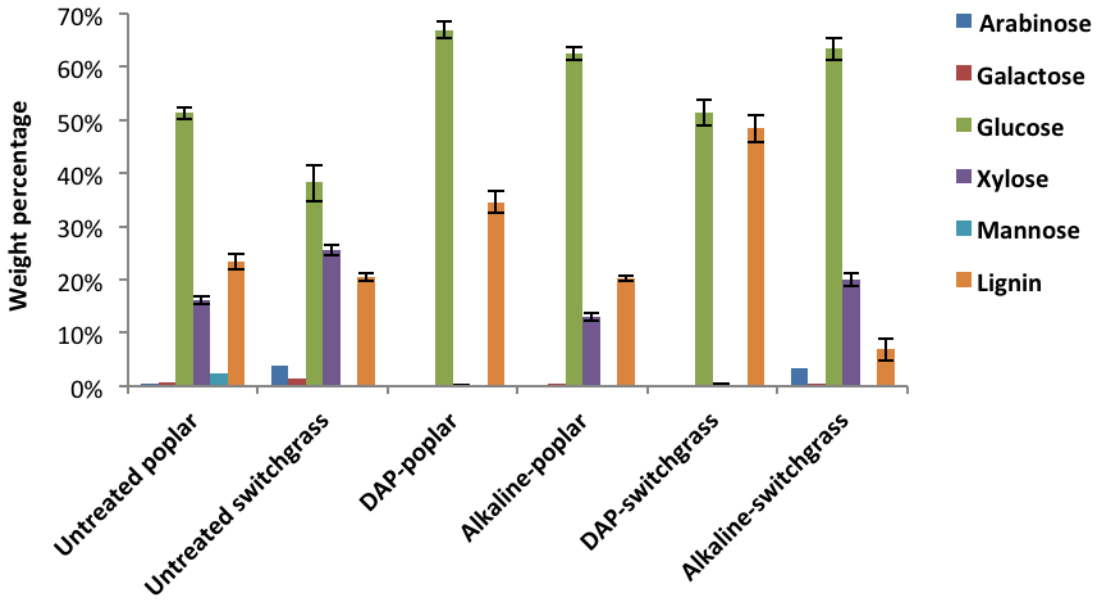

Figure 7.1 Carbohydrate and Klason lignin content of untreated, DAP, and dilute alkaline pretreated poplar and switchgrass.

7.3.2 Enzymatic hydrolysis

The native and pretreated poplar and switchgrass were subject to enzymatic hydrolysis for 72 h at a consistency of 1% (w/v) in 50 mM citrate buffer (pH 4.8) with *cellulase* and *β-glucosidase* loadings of 20 FPU/g and 40 CBU/g, respectively. Figure 7.2 shows the time course of glucose conversion of various samples after 72 h of enzymatic hydrolysis. The hydrolysis rate was relatively fast at the beginning and then gradually decreased with time thus following a typical patter widely reported in literature. Significantly higher glucose yields were obtained for pretreated poplar and switchgrass than for the corresponding untreated materials. Switchgrass always had higher glucose yield compared poplar before and after pretreatment. The glucose yields for the untreated materials were low for both poplar (<15%) and switchgrass (<25%) after 72 h. For the hydrolysis times of 2 and 4 h, DAP poplar and alkaline pretreated poplar has almost identical glucose yield, and as hydrolysis time extended to 48 h, DAP poplar exhibited slightly higher glucose yield. After 72 h, DAP and alkaline pretreated poplar again has almost identical glucose yield around ~50% conversion. Unlike poplar, alkaline pretreated switchgrass always has higher glucose yield from very beginning of the hydrolysis all the way to the end of hydrolysis. Alkaline pretreated switchgrass has ~90% glucose conversion yield, while DAP switchgrass only has 78% of cellulose being converted to glucose after 72 h enzymatic hydrolysis.

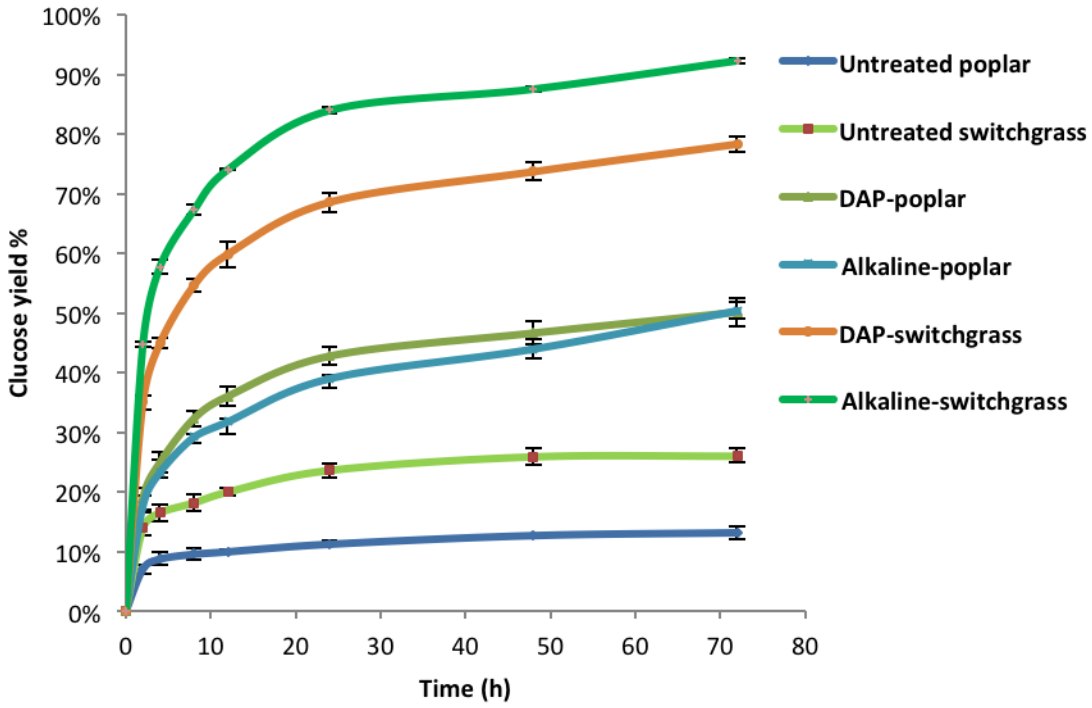

Figure 7.2 Glucose yields during enzymatic hydrolysis of untreated, DAP, and alkaline pretreated poplar and switchgrass.

7.3.3 Structural characterization of biomass substrates

The chemical fingerprinting of untreated, various pretreated and cellulase treated poplar and switchgrass were characterized by ATR-FTIR, and their spectra were presented in Figure 7.3 and 7.4. Table 7.2 shows some common FTIR absorption bans from biomass. Peak near 3350 cm^{-1} represents OH stretching of the hydrogen bonds of cellulose, and the band position at 2900 cm^{-1} is attributed to C-H stretching within the methylene of cellulose. The width of bands between 3000 cm^{-1} and 3600 cm^{-1} became narrower after DAP and alkaline pretreatment for both poplar and switchgrass, suggesting pretreatment could destroy the intermolecular hydrogen bonds in cellulose [227]. However, after enzymatic hydrolysis, this band became broader than untreated and pretreated samples due to fact that enzymatic hydrolysis might produce more hydroxyl groups which enable

the formation of new intermolecular hydrogen bonds. Peak around 1740 cm^{-1} have been proposed to be associated with the alkyl ester of the acetyl group in hemicellulose, and the intensity significantly decreased after both alkaline and DA pretreatment of poplar and switchgrass, due to the hemicellulose removal by DA and acetyl group removal by NaOH [47]. This is also supported by the fact of decreasing peak intensity around 1245 cm^{-1} which represents C-O adsorption resulting from acetyl group cleavage after alkaline pretreatment of switchgrass (Figure 7.4). Reduction and shift in the 1595 cm^{-1} band position (Figure 7.3) assigned to aromatic ring stretch after NaOH pretreatment is probably attributed to the condensation reactions and splitting of lignin aliphatic side chains [228]. Peak near 1100 cm^{-1} and 900 cm^{-1} is associated with the crystalline and amorphous cellulose, respectively. The intensity of the peak around 1100 cm^{-1} is increased after DA pretreatment for both poplar and switchgrass, suggesting an increase of cellulose crystallinity when compared with untreated samples. Guaiacyl ring-related IR spectra could be observed in all untreated materials at around 1505-1510 cm^{-1}, and this peak is decreased after NaOH pretreatment due to the lignin removal, but still can be seen after DA pretreatment and enzymatic hydrolysis [229]. Bands around 1460 cm^{-1} could be attributed to C-H methyl and methylene deformation common in hardwoods such poplar, and band at 1315 cm^{-1} is attributed to C-O absorption of syringyl rings in lignin of poplar (Figure 7.3) [230]. The presence of syringyl units in switchgrass is evident from the bands at 1315 cm^{-1}, which is well defined in untreated and pretreated material, but almost disappears after enzymatic hydrolysis especially for the NaOH pretreated switchgrass (Figure 7.4). Peak around 1708 cm^{-1} (Figure 7.3 and 7.4) become sharper after all pretreatment indicating the presence of an unconjugated carbonyl group

probably in the lignin fraction [231]. The peak around 1640 cm^{-1} (Figure 7.4) represents the C=O groups in the alkyl groups of the lignin side chains that conjugate with the aromatic structure, and the intensity of this peak decreased after DAP and alkaline pretreatment due to either partial delignification caused by alkaline or lignin redistribution caused by acid-catalyzed reaction [169].

Table 7.2 Assignment of FTIR absorption bands for biomass

Band position (cm^{-1})	Assignment
3200-3400	O-H stretching
2850-2940	C-H stretching
1735-1750	C=O ester; carbonyl groups in branched hemicellulose
1595	Aromatic ring stretch associated with lignin
1509-1512	C=C related to lignin; guaiacyl ring of lignin
1465	C-H methyl and methylene deformation
1417-1423	C-H deformation (asymmetric) of cellulose
1370-1380	C-H stretching of cellulose
1330	O-H in-plane deformation, syringyl ring breathing deformation
1215	C-C and C-O stretch associated with lignin
1160	C-O-C asymmetrical stretching
1100	C-O vibrations of crystalline cellulose
900	Amorphous cellulose vibration

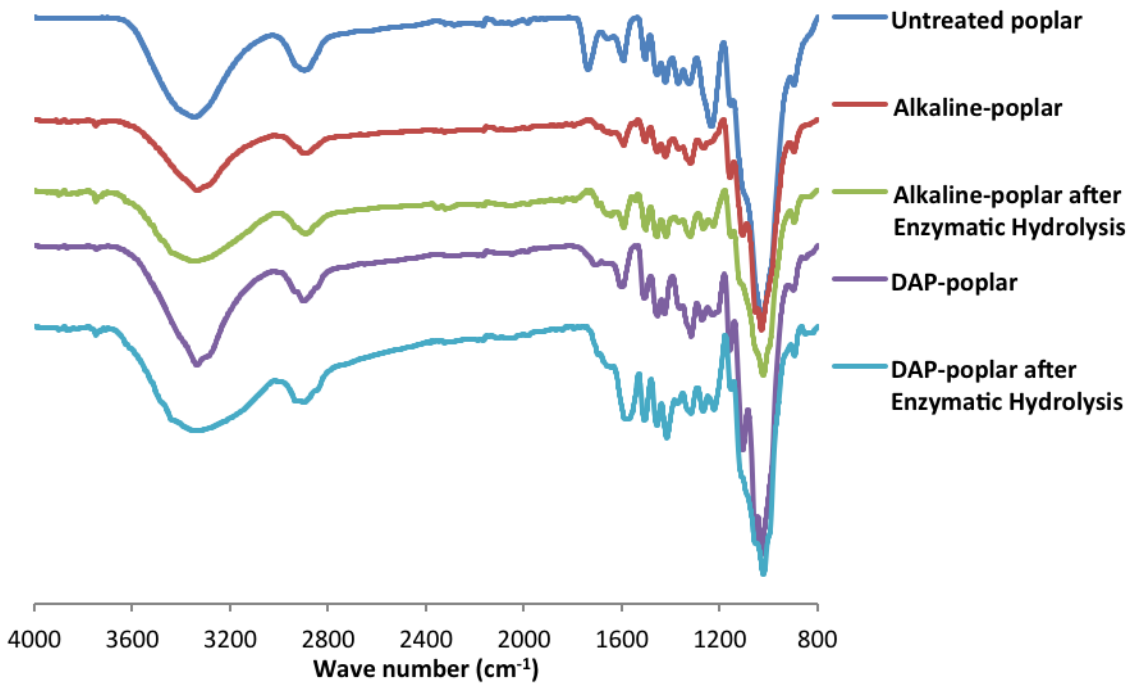

Figure 7.3 Chemical changes in poplar as determined by FTIR after pretreatment and enzymatic hydrolysis

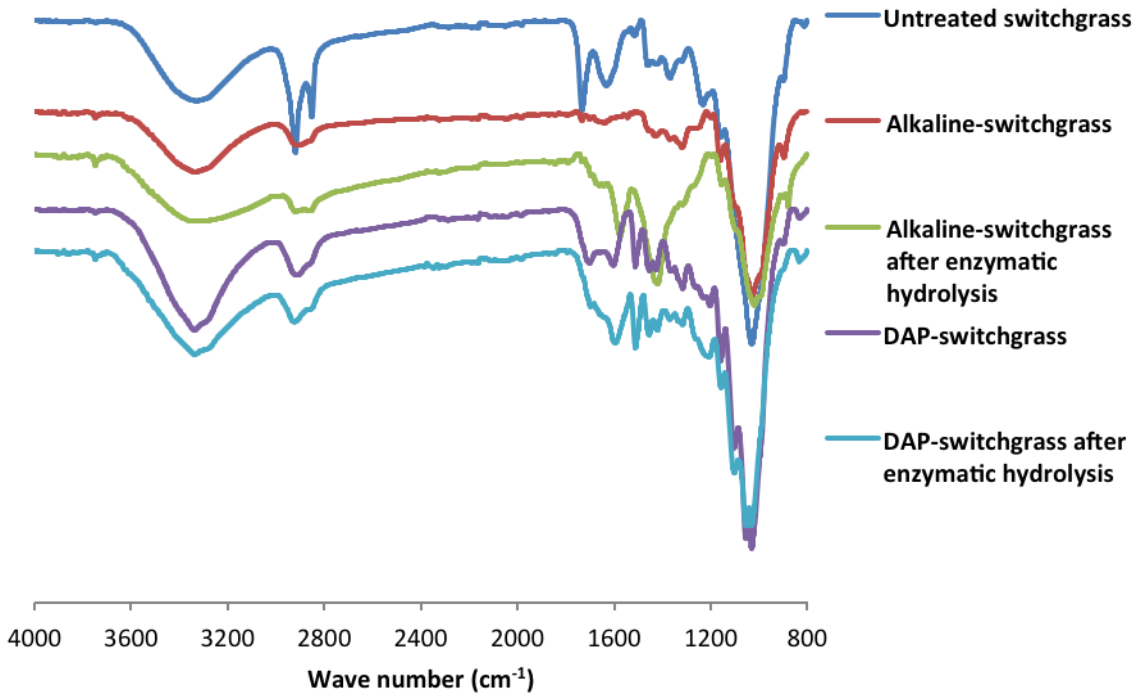

Figure 7.4 Chemical changes in switchgrass as determined by FTIR after pretreatment and enzymatic hydrolysis

7.3.4 Change of cellulose degree of polymerization upon pretreatment and enzymatic hydrolysis

Although the effect of cellulose DP on enzymatic hydrolysis is still under debate, it is generally believed that cellulose with lower DP which has more reducing ends available to provide sites of cellulase to begin cleavage favors enzymatic hydrolysis [232]. GPC is frequently employed to determine the molecular weight of cellulose in lignocellulosic substrates. Figure 7.5 illustrates the effect of different pretreatments on weight average cellulose degree of polymerization (DP_w) determined by GPC. Native poplar has a DP_w around 5400, while switchgrass has a DP_w of ~4600. A substantial reduction in DP_w was found for both poplar and switchgrass after pretreatment. However, the extent of reduction for DAP is much larger than that of alkaline pretreatment. Different substrates decreased to a similar DP_w upon pretreatment with acid or alkaline. The DP_w of cellulose decreased ~27% and ~25% after alkaline pretreatment for poplar and switchgrass, respectively. After DAP, ~89% and ~88% reduction of cellulose DP_w was observed for poplar switchgrass. In an effort to determine the effect of cellulose DP_w on biomass digestibility, 72 h enzymatic hydrolysis sugar release was plotted versus the DP_w of untreated and various pretreated poplar and switchgrass (Figure 7.6). Results suggested that cellulose DP_w was probably not the main factor affecting cellulose saccharification. However, there is no doubt that pretreatment increases cellulose digestibility partially due to the reduction of cellulose molecular weight.

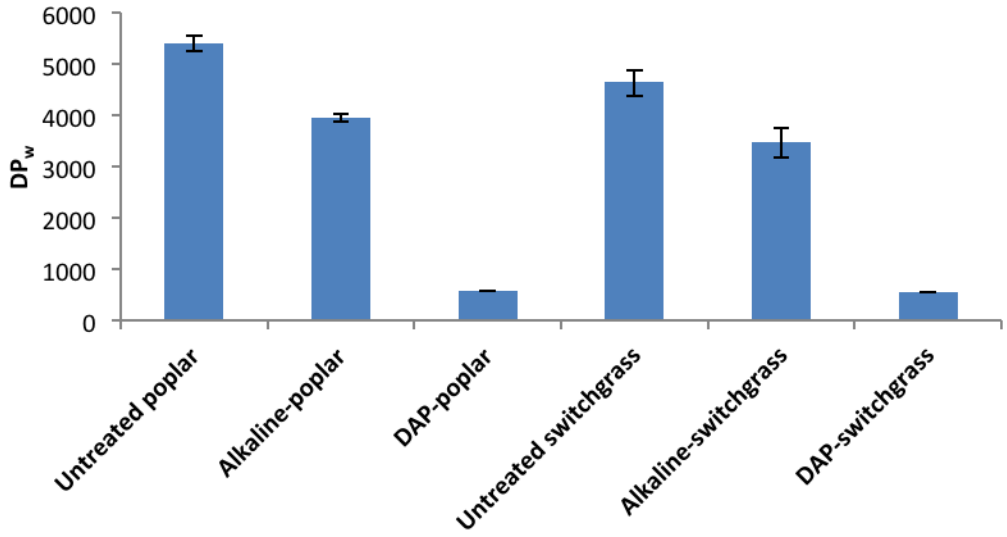

Figure 7.5 Weight average degree of polymerization of cellulose isolated from untreated, DAP, and alkaline pretreated poplar and switchgrass.

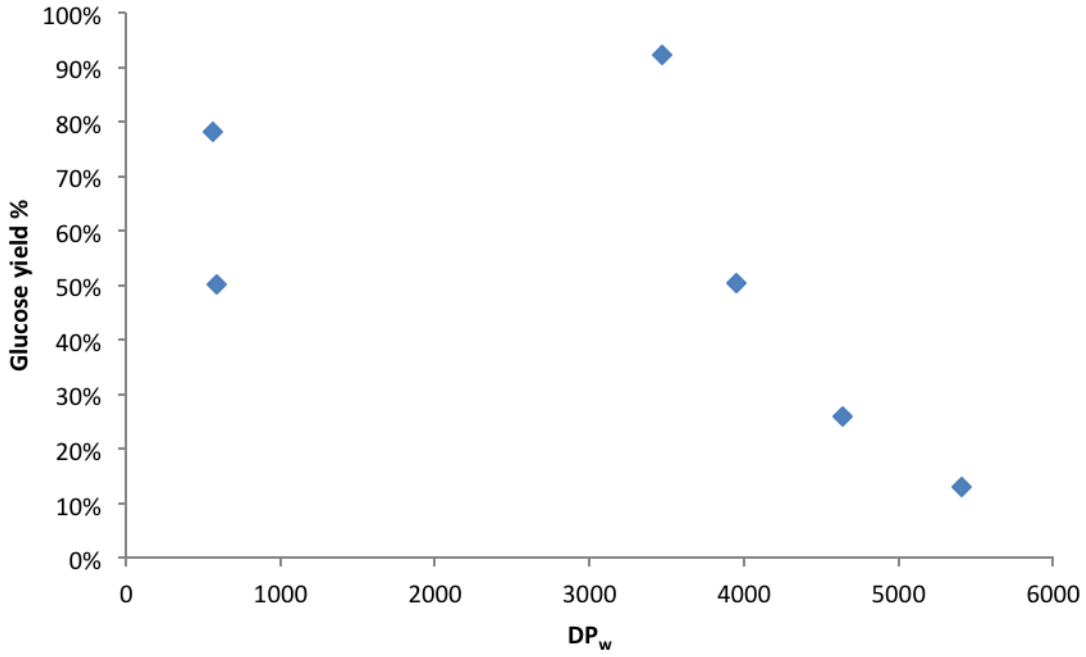

Figure 7.6 Effect of DP_w on digestibility of various untreated, DAP, and alkaline pretreated poplar and switchgrass.

The change of cellulose degree of polymerization (DP_w) upon enzymatic hydrolysis for untreated and pretreated poplar and switchgrass is shown in Figure 7.7 and 7.8. Obviously, the DP_w of cellulose decreased after enzymatic hydrolysis. For example, the DP_w of cellulose decreased from 3950 to 2124 and from 3467 to 1341 after enzymatic hydrolysis for alkaline pretreated poplar and switchgrass, respectively. It is also noted that the most significant DP_w variation occurred at the very beginning of the enzymatic hydrolysis (0 to 4 h), after this initial period, the DP_w begin to decrease at a significantly slower rate (4 to 12 h), and then remained approximately constant (12 to 72 h). For example, ~42% reduction of DP_w of cellulose isolated from alkaline pretreated poplar was observed after the first 4 h enzymatic hydrolysis, while only ~20% of reduction was observed from 4 to 12 h. This could be explained by, first, the existence of the hydrolytic cleavage of internal glucosidic linkages catalyzed by *endo*-glucanase therefore has a much more pronounced effect on the decrease of cellulose DP [233]. The hydrolysis was then probably dominated by a "peeling-off" mechanism of the newly generated chain ends by *exo*-glucanase action therefore resulted in no significant changes in DP [134].

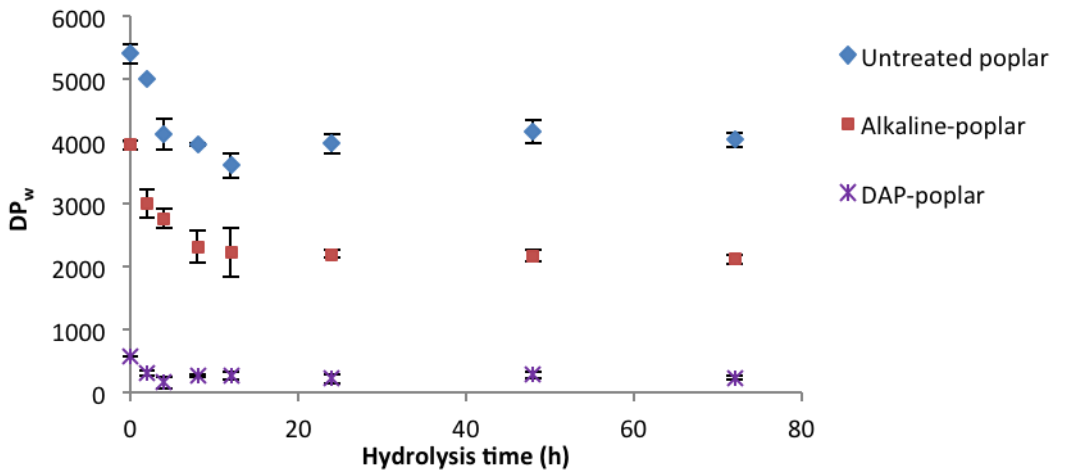

Figure 7.7 Change of cellulose DP_w isolated from untreated and pretreated poplar upon enzymatic hydrolysis.

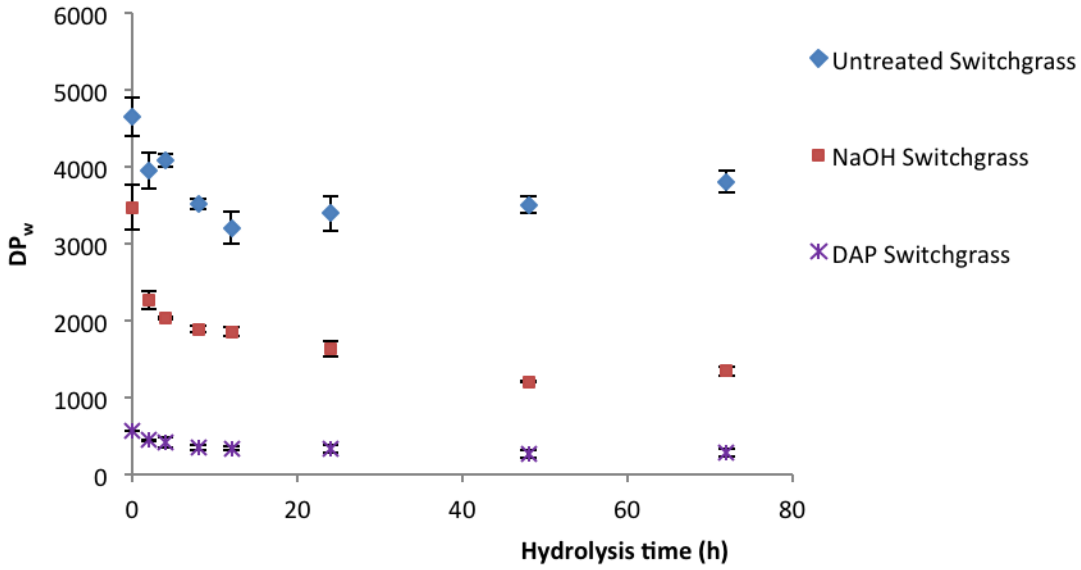

Figure 7.8 Change of cellulose DP_w isolated from untreated and pretreated switchgrass upon enzymatic hydrolysis.

7.3.5 Change of cellulose accessibility upon pretreatment and enzymatic hydrolysis

Cellulose accessibility has been shown to be one of the most important factors affecting substrate digestibility [10,11,119]. However, the effect of cellulase treatment on cellulose structure is still quite limited. Figure 7.9 shows the adsorption of orange dye during Simons' staining (mg dye/g cellulose) of untreated and various pretreated lignocellulosic biomass. Due to the orange dye's approximate molecular size similarity to typical cellulases, the adsorption of orange dye could be used to determine the accessible surface area of cellulose. Results indicated switchgrass always had higher accessible surface area than poplar before and after DAP and alkaline pretreatment. DAP poplar had an orange dye adsorption of 69.5 mg dye/g cellulose while the adsorption for alkaline pretreated poplar was 50.9 mg, indicating DAP of poplar is slightly more effective than alkaline pretreatment in terms of cellulose accessible surface area increase. In contrast, alkaline pretreated switchgrass had much more accessible surface area than DAP switchgrass. Figure 7.10 shows a strong positive linear relationship between cellulose accessibility and substrate digestibility. The removal of hemicellulose specifically xylan (~99%) from poplar after DAP improved cellulose accessibility and glucose yield by about 220% and 37% respectively as compared by untreated poplar. Relatively same amount of xylan could be removed from switchgrass after DAP as well, and the cellulose accessibility and glucose yield was increased by 210% and ~52%. Results indicated that xylan removal had a much more important effect on substrate digestibility of switchgrass than that of poplar. On the other hand, ~15% of lignin from poplar was removed after alkaline pretreatment, causing the cellulose accessibility and the glucose yield increased by 136% and ~37% while 66% of lignin from switchgrass after alkaline pretreatment improved the

cellulose accessibility and glucose yield by about 400% and 66%. At the same level of delignification, e.g. 1% of lignin removal, the increase of accessibility and glucose yield for poplar were actually larger than switchgrass. Therefore, lignin likely plays a more important role in biomass recalcitrance in poplar than switchgrass. Demartini et al. also reported xylan removal from switchgrass resulted in materials that achieved nearly 100% glucose yields at high enzyme loading in subsequent enzymatic hydrolysis, whereas chlorite extractions that reduced the lignin content had the most beneficial effect in poplar [203].

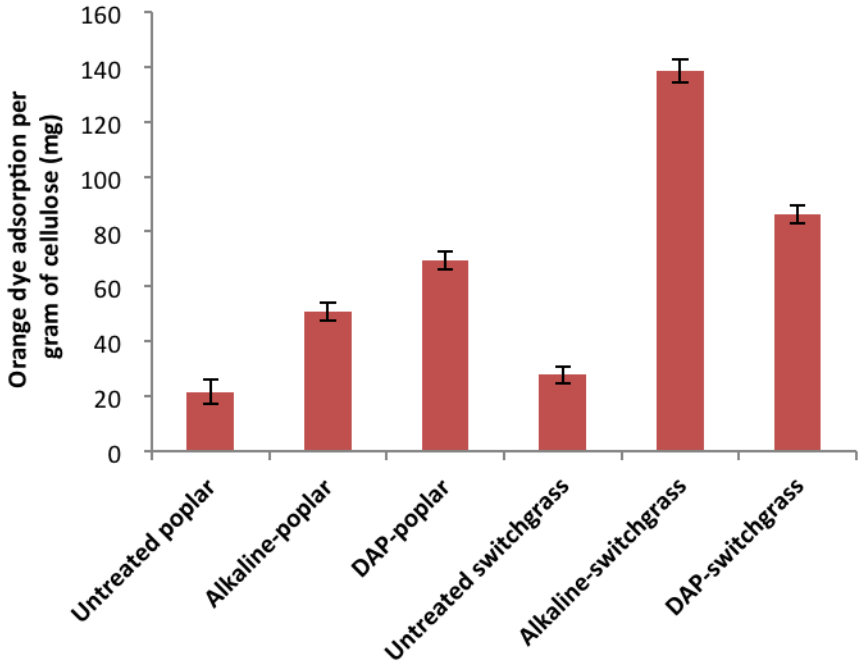

Figure 7.9 The adsorption of orange dye during Simons' staining (mg dye/g cellulose) of untreated and various pretreated lignocellulosic biomass

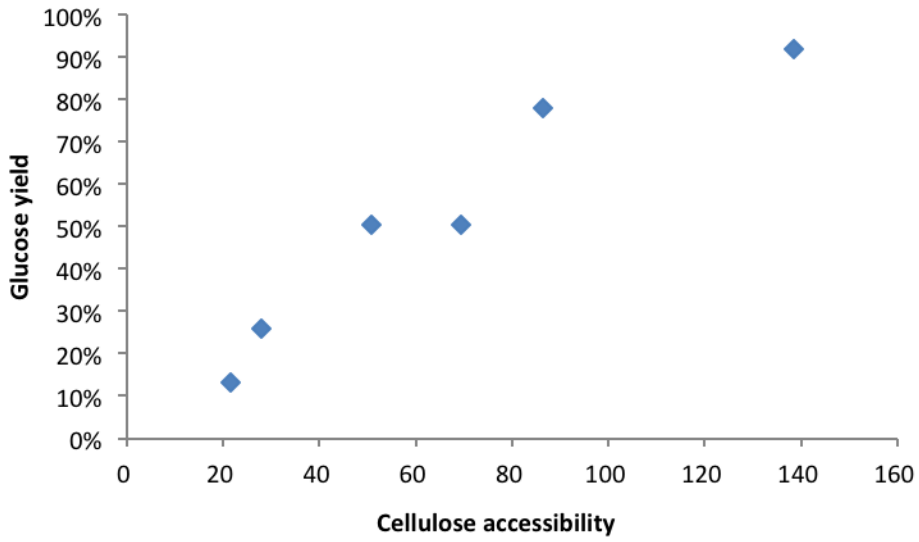

Figure 7.10 Relation between cellulose accessibility measured by Simons' stain (mg dye/g cellulose) and substrate digestibility (mg glucose/g dry biomass) for a series of untreated and pretreated poplar and switchgrass

Hydrolyzed samples were also taken from the enzymatic hydrolysis system at different time intervals, and the change of cellulose accessibility during enzymatic hydrolysis was analyzed by Simons' stain (Figure 7.11). Cellulose accessibility was found to be increased at the beginning of hydrolysis, after reaching a maximum value then starting to decrease until the end of enzymatic hydrolysis. For untreated materials, both poplar and switchgrass increased cellulose accessibility at the first 4 h. DAP poplar increased cellulose accessibility at the first 8 h, while DAP switchgrass increased cellulose accessibility at the first 24 h. ~174% increase of cellulose accessibility was observed at the first 12 h for alkaline pretreated switchgrass, and only 76% increase was noticed at the first 8 h for alkaline pretreated poplar. The increase of cellulose accessibility at the beginning of enzymatic hydrolysis could be due to the increase of porosity as enzyme further opened up the structure. After reaching a maximum value, a drop in cellulose

accessibility could be explained by the successive break-down of pore walls thus again leading to smaller values [222]. Fan et al. showed that the specific surface area drastically increased from 3.9 to 11.6 m^2/g cellulose during the first 6 h of hydrolysis of a hammer-milled sulfite pulp, and a slow increase was observed until 24 h after this period until leveled off at ~12.2 m^2/g cellulose, while the total cellulose surface area increased during the first 6 h of hydrolysis then start to decreased until the end of hydrolysis [234]. An interesting fact is that cellulose accessibility at the end of hydrolysis is actually larger than that at the beginning of hydrolysis, suggesting decreasing of cellulose accessibility is probably not the main reason causing the increase of recalcitrance as hydrolysis proceeds. Cellulose crystallinity could be a potential sensitive substrate indicator relating to the declined enzymatic hydrolysis rate due to the fact that amorphous cellulose was hydrolyzed much faster than crystalline cellulose [85]. As a consequence, the more resistant crystalline cellulose fraction remains and accumulates therefore slows the reaction rate. Other enzyme related features including enzyme inactivation/inhibition, fractal and jamming effects, diffusion constraints, clogging and imperfect processivity might be responsible for the slowdown of reaction rate. Eibinger et al. reported that cellulase showed strongly enhanced adsorption with progressing cellulose conversion, however, the activity of the adsorbed cellulases decreased concomitantly, and the lowering of hydrolytic efficiency of adsorbed cellulases exceeds the potential gain in hydrolysis rate due to enhanced adsorption [226]. To better understand the cause of declining in enzymatic hydrolysis, enzymatic reaction of nearly pure cellulose in Avicel was interrupted by Yang et al. over the course of nearly complete hydrolysis, and fresh cellulase was added to the solids to restart hydrolysis to assess whether substrate

reactivity changes with conversion. Results indicated that cellulose did not lose reactivity as it was converted over time and the surface actually seemed to become more accessible later in the reaction and the slow down of reaction rate was probably due to the action of the enzymes being slowed down by obstacles that interfere with their path or a loss in their activity [235].

(a)

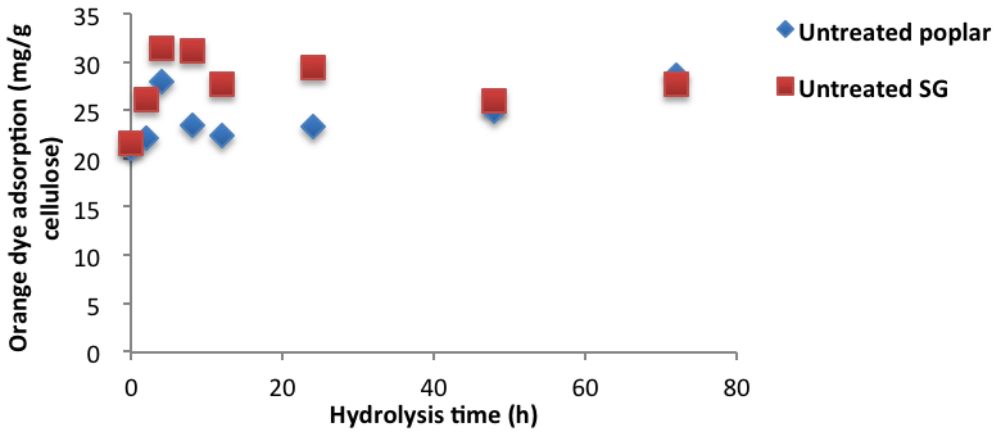

(b)

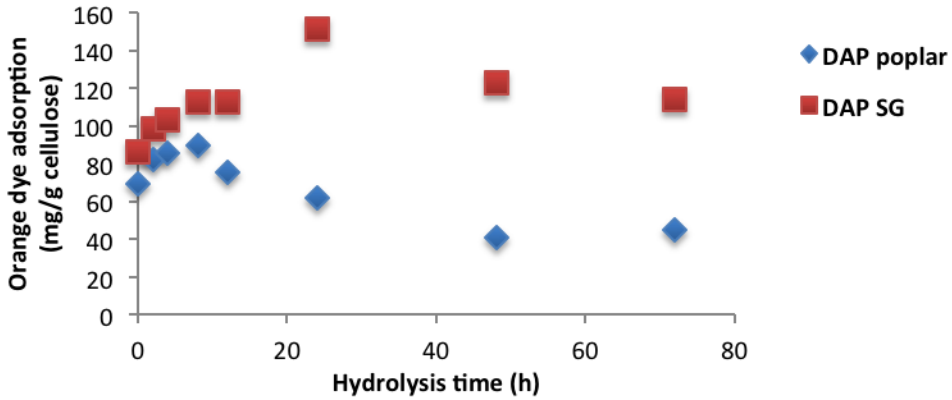

(c)

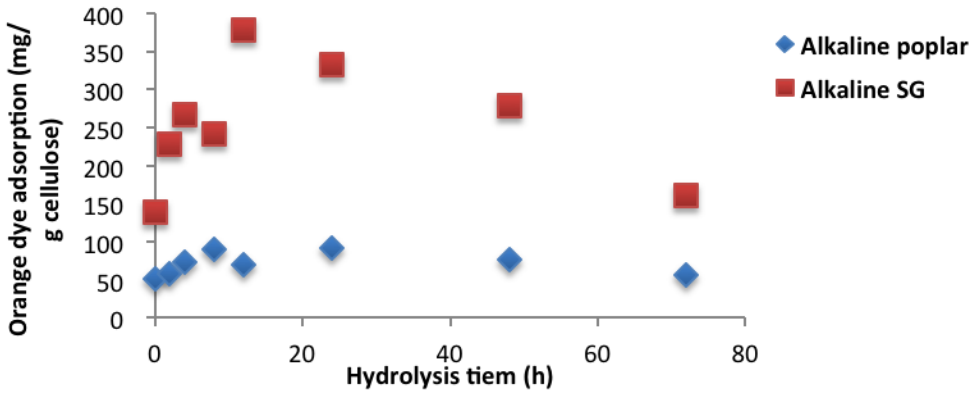

Figure 7.11 The effect of enzymatic hydrolysis on the cellulose accessibility measured by Simons' stain (mg orange dye/g cellulose) of (a) untreated, (b) DAP, and (c) alkaline pretreated poplar and switchgrass.

7.4 Conclusion

The action of cellulase on various characteristics of cellulosic fractions obtained from DAP and alkaline pretreated poplar and switchgrass was investigated. Enzymatic hydrolysis resulted in a rapid decrease in the degree of polymerization of cellulose for both untreated and pretreated poplar and switchgrass. However, the susceptibility of the pretreated substrates to enzymatic hydrolysis could not be easily predicated from the differences in their cellulose DP. Results indicated that it is difficult to relate the increase in recalcitrance of substrates to the structural modifications of cellulose which should occur in the substrate during hydrolysis. Factors associated with the nature of enzyme such as irreversible nonspecific binding of cellulases by lignin or product inhibition could play key role in the decreasing rate of cellulose hydrolysis. However, the determination of cellulose DP and accessibility is helpful in determining the mode of action of the enzymes on untreated and pretreated substrates. DP analysis suggested the existence of a

synergistic action of endo- and exo-glucanases that contribute to the occurrence of a peeling off type mechanism. Tracking the changes in cellulose accessibility during the course of enzymatic hydrolysis showed that limited accessible surface area of cellulose is probably not a major limiting factors that causing the decline of hydrolysis rate in its late stage. Enzyme related factors such as steric hindrance of enzymes might be responsible to the reduction in hydrolysis rate given the large size of cellulase enzymes. In addition, enzymatic hydrolysis of different pretreated poplar and switchgrass strong suggested different strategies should be applied when trying to engineer different plant for reduced recalcitrance.

CHAPTER 8

CONCLUSION

In the US, lignocellulosic biomass, in the form of forest, agricultural residues, and bioenergy crops, have the potential to provide around 500 million dry tons of biomass at $60/ton or less in 2012, and thus replace around 15% of current petroleum based transportation fuels [236]. Therefore, better understanding of the mechanisms contributing to biomass recalcitrance is critical but at the same time also very difficult due to the fact that lignocellulosic biomass is a multi-scale, complex and highly heterogeneous material. Most of researches conducted in an effort to understand and overcome biomass recalcitrance usually fail to take into account the integrated effect of an array of cell wall characteristics, thus the data gathered are sometimes inconclusive. Among all the substrate related factors, cellulose accessibility is particularly important. Most of the current study deals with accessibility measurement especially the surface properties of lignocelluloses have most often applied only one technique and a broader suite of techniques may provide a more definitive analysis. For example, nitrogen adsorption alone only gives the total specific surface area, and the Simons' stain determines the total accessible lignocellulosic surface area. Furthermore, protein adsorption technique involves a cellulose binding module could determine the cellulose accessibility to cellulase that represents only the accessible cellulose surface area. Thus, a combination of these three techniques can provide a better picture of the surface properties of lignocellulosic substrates including information about total specific surface area, total accessible lignocellulosic surface area, and total accessible cellulosic surface

area. The primary goal of this thesis was to study the role of cellulose accessibility in biomass recalcitrance. The prerequisite step is obviously to develop multiple promising analytical techniques that can be directly applied on real lignocellulosic substrates. The first study started with the idea of determining the biomass porosity before and after dilute acid and steam explosion pretreatment. Several analytical techniques including a modified Simons' stain method along with various NMR techniques (e.g., NMR cryoporometry, relaxometry, diffusometry) were developed and applied to characterize surface area/pore size information, thus assess cellulose accessibility on untreated and pretreated biomass. In general, these techniques indicate that pretreated *Populus* has larger pore size distributions and accessible surface area when compared to an untreated sample. Simons' Stain method revealed that acid pretreatment is more effective than steam explosion in terms of the accessible surface area increase, and that dilute acid pretreatment increases cellulose accessibility as a function of pretreatment severity. Relaxometry and diffusion measurements also suggest pore expansion occurs primarily in the first 10 min of acid pretreatment. After revealing the fact that acid based pretreatment increases the cellulose accessibility to some extent by removing the majority of hemicellulose, it is necessary to study the effect of alkaline based pretreatments on cellulose accessibility.

The second part of study try to provide key insights into the reduction of biomass recalcitrance via alkaline pretreatment specifically those associated with cellulose structure and accessibility. Various alkaline pretreatments including sodium hydroxide, calcium hydroxide, and soaking in ammonia solution were applied on milled hybrid

Populus. Cellulose structural features such as degree of polymerization, crystallinity, accessibility were then measured using various analytical tools such as GPC, NMR and Simons' stain. This study reveals the changes in cellulose structure and accessibility upon a variety of low-cost and mild alkaline pretreatments, subsequently identifies important relevant parameters responsible for reduction of biomass recalcitrance via alkaline pretreatment. Generally speaking, lower cellulose DP, crystallinity, and higher cellulose accessibility favors enzymatic hydrolysis. Untreated sample resulted in the lowest glucose yield after enzymatic hydrolysis, due to the highest lignin content, highest cellulose DP, crystallinity, and lowest cellulose accessibility. NaOH pretreatment resulted in highest glucose yield after enzymatic hydrolysis, probably due to the lowest DP and highest cellulose accessibility. Cellulose crystallinity and DP considered as individual isolated factors may not be as significant to recalcitrance as once thought for alkaline pretreatment of *Populus*, while a much better positive relationship between cellulose accessibility and sugar release after enzymatic hydrolysis were clearly obtained. At this point, it is clearly that different pretreatment increase cellulose accessibility through different mechanisms, e.g. acid removes xylan while alkaline mainly removes lignin. However, the relative importance of the removal of one of these two components over the other is still quite limited.

The third part of the thesis provides insights into the effect of hemicellulose and lignin removal on cellulose accessibility increase and the role of cellulose accessibility in biomass recalcitrance. *Populus* (*Populus trichocarpa x deltoids)* was pretreated by dilute acid, hot water and dilute alkaline at different severities, producing substrates differing

substantially in the chemical composition, especially the xylan and lignin content. Simons' stain and mercury porosimetry were used to measure accessible surface area of cellulose and different scales of biomass porosity as related to cellulose accessibility of these different pretreated substrates. Results indicated that accessible surface area of cellulose is an important factor governing the extent of hydrolysis, but the effectiveness of different type of pretreatment cannot be simply judged on this solely common basis. Delignification through alkaline based pretreatment is found less effective than removal of hemicellulose using acid in terms of accessibility increase. Pore size distribution analysis indicated that the most fundamental barrier in terms of biomass porosity scale for efficient enzymatic hydrolysis is the nano-pore space formed between coated microfibrils, despite some of the porous architechture such as cell lumen and pit could be severely destroyed after pretreatment.

The last part of this thesis focuses on understanding the limitations occurring during enzymatic hydrolysis of lignocellulosic substrates that might be responsible for the gradual slowing down of the reaction. *Populus* and switchgrass were pretreated by dilute acid and alkaline and subjected to enzymatic hydrolysis for 72 h. The reducing sugar yield was measured by high performance liquid chromatography at different hydrolysis time points. Hydrolyzed biomass samples were isolated from the hydrolysis system and the cellulose accessible surface area and degree of polymerization were characterized by Simons' stain and GPC. Under same pretreatment conditions, switchgrass proves to be a lower recalcitrant plant compared *Populus*. Alkaline is more effective than acid pretreatment for switchgrass, while acid pretreatment is slightly more effective than

alkaline pretreatment for poplar. Protease treatment is necessary to remove enzyme residue for accurate determination of cellulose accessibility. The accessibility test by Simons' stain suggested that the drop off in reaction rate could not be entirely attributed to limited accessible surface area, other factors such as enzyme activity, the accumulations of crystalline cellulose or lignin content may be responsible. Cellulose DP analysis suggested a synergistic action of endo- and exo-glucanases that contribute to the occurrence of a "peeling-off" type of mechanism.

In conclusion, costs associated with enzymes and pretreatment are the major barriers that hindered the industrial conversion of cellulosic biomass to biofuels. The costs associated with enzyme loadings could be minimized by developing novel cost-effective pretreatments that maximize the cellulose accessibility, while the need for expensive and harsh pretreatments can be reduced by developing genetically modified low recalcitrant energy plants. All these challenges are difficult to overcome by any individual investigator and require broad multi-disciplinary approach in genetics, process chemistry, biotechnology and engineering.

CHAPTER 9

RECOMMENDATIONS FOR FUTURE WORK

Years of research have focused on modifying substrates characteristics and correlating these alterations to biomass recalcitrance. However, when a method is used to alter specific cell wall substrate characteristic, it usually not only targets plant cell wall characteristics of interest, but also changes a variety of other substrate properties. For example, ball milling is usually used to reduce the biomass particle size, but it also has been shown to reduce the cellulose degree of polymerization and crystallinity [97]. Therefore, it is quite challenging to assess the effect of an individual factor on enzymatic hydrolysis and study of the coupling effect of these multi-factors requires future research effect. Moving forward, biomass "reference substrates model" with controlled parameters need to be developed to allow the investigation of individual substrate factors. For example, traditional chemical pulping techniques can be applied on biomass to create a series of substrates with intact lignocellulosic fibers and controlled morphological and chemical properties, in this way, individual effects such as the xylan or lignin content on enzymatic hydrolysis can be investigated.

More surface characterization tools should be developed and used to assess cellulose accessibility, especially imagine techniques. Scanning electron microscopy (SEM) is one of the most versatile and widely used tools of modern science to study the surface morphology of biomass before and after different pretreatments. Atomic force microscopy (AFM) is another powerful scanning probe microscopy surface analyses tool

that can images the topography of the surface at much higher magnification compared SEM. Confocal fluorescence microscopy could be used to visualize lignocellulosic biomass at various stage of pretreatment or enzymatic hydrolysis.

Lignin remains a critical barrier that prevents efficient enzymatic conversion of cellulose to glucose. It has been shown that lignin acts as a barrier can restrict cellulose crystallinity increase and cellulose crystallite growth, and partial delignification instead of complete lignin removal is actually better for enhanced sugar yield [237]. Structure change of lignin during various pretreatments especially acid based pretreatments should be studied. Relationship between lignin substrate related factors such as S/G ratio and enzymatic hydrolysis could be obtained subsequently. It has been shown that pseudo-lignin can be generated from the surface of holocellulose biomass samples, and the effect of pseudo-lignin on cellulose accessibility is still quite limited and can be tested via Simons' stain.

Relationship between cell wall substrate characteristics and biomass recalcitrance is not as simple as first-order linear correlations, and more than likely a change in one characteristic will change the effect of another characteristic has on biomass recalcitrance. Large number of samples containing either natural variants or genetically modified plants could be systematically analyzed to characterize factors such as lignin/xylan content, cellulose DP, crystallinity, accessible surface area, biomass porosity, lignin S/G ratio. A multivariate statistical analysis that allows observation and analysis of more than one

statistical outcome variable at a time could be run based on previously collected data. It is possible to determine the formula of biomass recalcitrance if enough data is collected.

REFERENCES

1. Ragauskas, A.J., Williams, C.K., Davison, B.H., Britovsek, G., Cairney, J., Eckert, C.A., Frederick, W.J., Hallett, J.P., Leak, D.J., Liotta, C.L., Mielenz, J.R., Murphy, R., Templer, R., Tschaplinski, T. 2006. The Path Forward for Biofuels and Biomaterials. *Science*, **311**(5760), 484-489.

2. Naik, S.N., Goud, V.V., Rout, P.K., Dalai, A.K. 2010. Production of first and second generation biofuels: A comprehensive review. *Renewable and Sustainable Energy Reviews*, **14**(2), 578-597.

3. Thompson, P.B. 2012. The Agricultural Ethics of Biofuels: The Food vs. Fuel Debate. *Agriculture*, **2**(4), 339.

4. Zheng, J., Rehmann, L. 2014. Extrusion pretreatment of lignocellulosic biomass: a review. *Int. J. Mol. Sci.*, **15**(10), 18967-18984.

5. Renewable Fuel Standard.
http://www.afdc.energy.gov/laws/RFS.html, accessed 06/29/2015.

6. Zhao, X., Zhang, L., Liu, D. 2012. Biomass recalcitrance. Part I: the chemical compositions and physical structures affecting the enzymatic hydrolysis of lignocellulose. *Biofuels, Bioproducts and Biorefining*, **6**(4), 465-482.

7. Pauly, M., Keegstra, K. 2010. Plant cell wall polymers as precursors for biofuels. *Current Opinion in Plant Biology*, **13**(3), 304-311.

8. Pu, Y., Zhang, D., Singh, P.M., Ragauskas, A.J. 2008. The new forestry biofuels sector. *Biofuels, Bioproducts and Biorefining*, **2**(1), 58-73.

9. Foston, M., Ragauskas, A.J. 2012. Biomass Characterization: Recent Progress in Understanding Biomass Recalcitrance. *Ind. Biotechnol.*, **8**(4), 191-208.

10. Pu, Y., Hu, F., Huang, F., Davison, B., Ragauskas, A.J. 2013. Assessing the molecular structure basis for biomass recalcitrance during dilute acid and hydrothermal pretreatments. *Biotechnology for Biofuels*, **6**(1), 15.

11. Meng, X., Foston, M., Leisen, J., DeMartini, J., Wyman, C.E., Ragauskas, A.J. 2013. Determination of porosity of lignocellulosic biomass before and after pretreatment by using Simons' stain and NMR techniques. *Bioresource Technology*, **144**(0), 467-476.
12. Leu, S.-Y., Zhu, J.Y. 2013. Substrate-Related Factors Affecting Enzymatic Saccharification of Lignocelluloses: Our Recent Understanding. *BioEnergy Research*, **6**(2), 405-415.
13. David, K., Ragauskas, A.J. 2010. Switchgrass as an energy crop for biofuel production: A review of its ligno-cellulosic chemical properties. *Energy & Environmental Science*, **3**(9), 1182-1190.
14. Perlack, R.D., Wright, L.L., Turhollow, A.F., Graham, R.L., Stokes, B.J., Erbach, D.C. 2005. Biomass as feedstock for a bioenergy and bioproducts industry: the technical feasibility of a billion-ton annual supply (U.S. Department of Energy and U.S. Department of Agriculture, April 2005; available at http://feedstockreview.ornl.gov/pdf/billion_ton_vision.pdf Accessed 06/30/2015)
15. Rubin, E.M. 2008. Genomics of cellulosic biofuels. *Nature*, **454**(7206), 841-845.
16. Canilha, L., Chandel, A.K., Suzane dos Santos Milessi, T., Antunes, F.A.F., Luiz da Costa Freitas, W., das Gracas Almeida Felipe, M., da Silva, S.S. 2012. Bioconversion of Sugarcane Biomass into Ethanol: An Overview about Composition, Pretreatment Methods, Detoxification of Hydrolysates, Enzymatic Saccharification, and Ethanol Fermentation. *Journal of Biomedicine and Biotechnology*, **2012**, 1-15.
17. U.S. Department of Energy, Energy Efficiency & Renewable Energy: Office of the Biomass Program. 2011. U.S. Billion-Ton Update: Biomass supply for a bioenergy and bioproducts industry. (http://www.energy.gov/sites/prod/files/2015/01/f19/billion_ton_update_0.pdf, accessed 06/30/2015)
18. Vassilev, S.V., Baxter, D., Andersen, L.K., Vassileva, C.G. 2010. An overview of the chemical composition of biomass. *Fuel*, **89**(5), 913-933.
19. Huang, F. 2014. What is biomass. *Mater. Energy*, **4**(Materials for Biofuels), 1-26.

20. Ding, S., Himmel, M.E. 2006. The Maize Primary Cell Wall Microfibril: A New Model Derived from Direct Visualization. *Journal of Agricultural and Food Chemistry*, **54**(3), 597-606.
21. Chabannes, M., Ruel, K., Yoshinaga, A., Chabbert, B., Jauneau, A., Joseleau, J.-P., Boudet, A.-M. 2001. In situ analysis of lignins in transgenic tobacco reveals a differential impact of individual transformations on the spatial patterns of lignin deposition at the cellular and subcellular levels. *The Plant Journal*, **28**(3), 271-282.
22. Li, H., Pattathil, S., Foston, M., Ding, S.-Y., Kumar, R., Gao, X., Mittal, A., Yarbrough, J., Himmel, M., Ragauskas, A., Hahn, M., Wyman, C. 2014. Agave proves to be a low recalcitrant lignocellulosic feedstock for biofuels production on semi-arid lands. *Biotechnology for Biofuels*, **7**(1), 50.
23. Walker, G.M. 2010. Bioethanol: Science and technology of fuel alcohol. *Ventus Publishing ApS*: Copenhagen, **2010**.
24. Saha, B. 2003. Hemicellulose bioconversion. *Journal of Industrial Microbiology and Biotechnology*, **30**(5), 279-291.
25. Silverstein, R.A., Chen, Y., Sharma-Shivappa, R.R., Boyette, M.D., Osborne, J. 2007. A comparison of chemical pretreatment methods for improving saccharification of cotton stalks. *Bioresource Technology*, **98**(16), 3000-3011.
26. Kim, S.J., Kim, M.Y., Jeong, S.J., Jang, M.S., Chung, I.M. 2012. Analysis of the biomass content of various Miscanthus genotypes for biofuel production in Korea. *Industrial Crops and Products*, **38**(0), 46-49.
27. Hamelinck, C.N., Hooijdonk, G.v., Faaij, A.P.C. 2005. Ethanol from lignocellulosic biomass: techno-economic performance in short-, middle- and long-term. *Biomass and Bioenergy*, **28**(4), 384-410.
28. Sun, J.X., Mao, F.C., Sun, X.F., Sun, R. 2004. Comparative study of hemicelluloses isolated with alkaline peroxide from lignocellulosic materials. *J. Wood Chem. Technol.*, **24**(3), 239-262.
29. Galbe, M., Zacchi, G. 2007. Pretreatment of Lignocellulosic Materials for Efficient Bioethanol Production. in: *Biofuels*, (Ed.) L. Olsson, Vol. 108, Springer Berlin Heidelberg, pp. 41-65.

30. Silva, G.G.D., Xavier, R.S.G. 2011. Successive centrifugal grinding and sieving of wheat straw. *Powder Technology*, **208**(2), 266-270.
31. Sannigrahi, P., Ragauskas, A.J., Tuskan, G.A. 2010. Poplar as a feedstock for biofuels: A review of compositional characteristics. *Biofuels, Bioproducts and Biorefining*, **4**(2), 209-226.
32. Park, S., Baker, J., Himmel, M., Parilla, P., Johnson, D. 2010. Cellulose crystallinity index: measurement techniques and their impact on interpreting cellulase performance. *Biotechnology for Biofuels*, **3**(1), 10
33. Atalla, R.H., Vanderhart, D.L. 1984. Native Cellulose: A Composite of Two Distinct Crystalline Forms. *Science*, **223**(4633), 283-285
34. Nishiyama, Y., Langan, P., Chanzy, H. 2002. Crystal Structure and Hydrogen-Bonding System in Cellulose Iβ from Synchrotron X-ray and Neutron Fiber Diffraction. *Journal of the American Chemical Society*, **124**(31), 9074-9082
35. Stephens, C.H., Whitmore, P.M., Morris, H.R., Bier, M.E. 2008. Hydrolysis of the Amorphous Cellulose in Cotton-Based Paper. *Biomacromolecules*, **9**(4), 1093-1099
36. Wickholm, K., Hult, E.-L., Larsson, P., Iversen, T., Lennholm, H. 2001. Quantification of cellulose forms in complex cellulose materials: a chemometric model. *Cellulose*, **8**(2), 139-148.
37. Terzopoulou, Z., Kyzas, G., Bikiaris, D. 2015. Recent Advances in Nanocomposite Materials of Graphene Derivatives with Polysaccharides. *Materials*, **8**(2), 652
38. Chunilall, V., Bush, T., Larsson, P.T. 2013. Supra-molecular structure and chemical reactivity of cellulose I studied using CP/MAS 13C-NMR. InTech. pp. 69-90.
39. Zhao, X.-B., Wang, L., Liu, D.-H. 2008. Peracetic acid pretreatment of sugarcane bagasse for enzymatic hydrolysis: a continued work. *Journal of Chemical Technology & Biotechnology*, **83**(6), 950-956.
40. Terinte, N., Ibbett, R., Schuster, K.C. 2011. Overview on native cellulose and microcrystalline cellular I structure studied by x-ray diffraction (WAXD): comparison between measurement techniques. *Lenzinger Ber* **89**, 118-131.

41. Foston, M., Ragauskas, A.J. 2010. Changes in lignocellulosic supramolecular and ultrastructure during dilute acid pretreatment of Populus and switchgrass. *Biomass and Bioenergy*, **34**(12), 1885-1895
42. Hallac, B.B., Sannigrahi, P., Pu, Y., Ray, M., Murphy, R.J., Ragauskas, A.J. 2009. Biomass Characterization of Buddleja davidii: A Potential Feedstock for Biofuel Production. *Journal of Agricultural and Food Chemistry*, **57**(4), 1275-1281.
43. Foston, M., Hubbell, C., Davis, M., Ragauskas, A. 2009. Variations in Cellulosic Ultrastructure of Poplar. *BioEnergy Research*, **2**(4), 193-197.
44. Samuel, R., Pu, Y., Foston, M., Ragauskas, A.J. 2010. Solid-state NMR characterization of switchgrass cellulose after dilute acid pretreatment. *Biofuels*, **1**(1), 85-90.
45. Hallac, B.B., Ragauskas, A.J. 2011. Analyzing cellulose degree of polymerization and its relevancy to cellulosic ethanol. *Biofuels, Bioproducts and Biorefining*, **5**(2), 215-225.
46. Hubbell, C.A., Ragauskas, A.J. 2010. Effect of acid-chlorite delignification on cellulose degree of polymerization. *Bioresource Technology*, **101**(19), 7410-7415.
47. Kumar, R., Mago, G., Balan, V., Wyman, C.E. 2009. Physical and chemical characterizations of corn stover and poplar solids resulting from leading pretreatment technologies. *Bioresource Technology*, **100**(17), 3948-3962
48. Kumar, R., Hu, F., Hubbell, C.A., Ragauskas, A.J., Wyman, C.E. 2013. Comparison of laboratory delignification methods, their selectivity, and impacts on physiochemical characteristics of cellulosic biomass. *Bioresource Technology*, **130**(0), 372-381.
49. Gupta, R., Lee, Y.Y. 2009. Mechanism of cellulase reaction on pure cellulosic substrates. *Biotechnology and Bioengineering*, **102**(6), 1570-1581
50. Girio, F.M., Fonseca, C., Carvalheiro, F., Duarte, L.C., Marques, S., Bogel-Lukasik, R. 2010. Hemicelluloses for fuel ethanol: A review. *Bioresour. Technol.*, **101**(13), 4775-4800.
51. Barakat, A., Winter, H., Rondeau-Mouro, C., Saake, B., Chabbert, B., Cathala, B. 2007. Studies of xylan interactions and cross-linking to synthetic lignins formed by bulk

and end-wise polymerization: a model study of lignin carbohydrate complex formation. *Planta*, **226**(1), 267-281.
52. Cao, S., Pu, Y., Studer, M., Wyman, C., Ragauskas, A.J. 2012. Chemical transformations of Populus trichocarpa during dilute acid pretreatment. *RSC Advances,* **2** (29), 10925-10936.
53. El Hage, R., Brosse, N., Chrusciel, L., Sanchez, C., Sannigrahi, P., Ragauskas, A.J. 2009. Characterization of milled wood lignin and ethanol organosolv lignin from miscanthus. *Polymer Degradation and Stability***, 94** (10), 1632-1638.
54. Kanitskaya, L.V., Rokhin, A.V., Kushnarev, D.F., Kalabin, G.A. 1998. Chemical structure of wheat dioxane lignin: 1H and 13C NMR study. *Vysokomol. Soedin., Ser. A Ser. B*, **40**(5), 800-805.
55. Buranov, A. U., Mazza, G. 2008. Lignin in straw of herbaceous crops. *Industrial Crops and Products***, 28** (3), 237-259.
56. Fox, S.C., McDonald, A.G. 2010. Chemical and thermal characterization of three industrial lignins and their corresponding lignin esters. *Bioresources***, 5** (2), 990-1009.
57. Glasser, W.G., Glasser, H.R. 1981. Evaluation of lignin's chemical structure by experimental and computer simulation techniques. *Pap. Puu*, **63**(2), 71-4, 77-80, 82-3.
58. Erickson, M., Larsson, S., Miksche, G.E. 1973. Gas-chromatographic analysis of lignin oxidation products. Structure of the spruce lignins. *Acta Chem. Scand.*, **27**(3), 903-14.
59. Choi, J.W., Faix, O., Meier, D. 2001. Characterization of residual lignins from chemical pulps of spruce (Picea abies L.) and beech (Fagus sylvatica L.) by analytical pyrolysis-gas chromatography/mass spectrometry. *Holzforschung*, **55**(2), 185-192.
60. Ralph, J., Lundquist, K., Brunow, G., Lu, F., Kim, H., Schatz, P.F., Marita, J.M., Hatfield, R.D., Ralph, S.A., Christensen, J.H., Boerjan, W. 2004. Lignins: Natural polymers from oxidative coupling of 4-hydroxyphenylpropanoids. *Phytochem. Rev.*, **3**(1-2), 29-60.
61. Koshijima, T., Yaku, F., Tanaka, R. 1976. Fractionation of Bjorkman LCC from Pinus densiflora. *Appl. Polym. Symp.*, **28**(Proc. Cellul. Conf., 8th, 1975, Vol. 3), 1025-39.

62. Balakshin, M., Capanema, E., Gracz, H., Chang, H.M., Jameel, H. 2011. Quantification of lignin-carbohydrate linkages with high-resolution NMR spectroscopy. *Planta*, **233** (6), 1097-1110

63. Iversen, T. 1985. Lignin-carbohydrate bonds in a lignin-carbohydrate complex isolated from spruce. *Wood Science and Technology*, **19**(3), 243-251.

64. Achyuthan, K.E., Achyuthan, A.M., Adams, P.D., Dirk, S.M., Harper, J.C., Simmons, B.A., Singh, A.K. 2010. Supramolecular self-assembled chaos: polyphenolic lignin's barrier to cost-effective lignocellulosic biofuels. *Molecules*, **15**(12), 8641-88.

65. Azuma, J., Tetsuo, K. 1988. Lignin-carbohydrate complexes from various sources. *Methods Enzymol.*, **161**(Biomass, Pt. B), 12-18.

66. Azuma, J., Takahashi, N., Koshijima, T. 1981. Isolation and characterization of lignin-carbohydrate complexes from the milled-wood lignin fraction of Pinus densiflora Sieb. et Zucc. *Carbohydr. Res.*, **93**(1), 91-104.

67. Tanaka, K., Nakatsubo, F., Higuchi, T. 1976. Reactions of guaiacylglycerol-β-guaiacyl ether with several sugars. I. Reaction of quinonemethide with D-glucuronic acid. *Mokuzai Gakkaishi*, **22**(10), 589-90.

68. Himmel, M.E., Ding, S.-Y., Johnson, D.K., Adney, W.S., Nimlos, M.R., Brady, J.W., Foust, T.D. 2007. Biomass Recalcitrance: Engineering Plants and Enzymes for Biofuels Production. *Science (Washington, DC, U. S.)*, **315**(5813), 804-807.

69. Chang, V., Holtzapple, M. 2000. Fundamental factors affecting biomass enzymatic reactivity. *Applied Biochemistry and Biotechnology*, **84-86**(1-9), 5-3.

70. Zhao, X., Zhang, L., Liu, D. 2008. Comparative study on chemical pretreatment methods for improving enzymatic digestibility of crofton weed stem. *Bioresource Technology*, **99**(9), 3729-3736.

71. Mooney, C.A., Mansfield, S.D., Touhy, M.G., Saddler, J.N. 1998. The effect of initial pore volume and lignin content on the enzymatic hydrolysis of softwoods. *Bioresource Technology*, **64**(2), 113-119.

72. Eriksson, T., Borjesson, J., Tjerneld, F. 2002. Mechanism of surfactant effect in enzymatic hydrolysis of lignocellulose. *Enzyme Microb. Technol.*, **31**(3), 353-364.

73. Voelker, S.L., Lachenbruch, B., Meinzer, F.C., Jourdes, M., Ki, C., Patten, A.M., Davin, L.B., Lewis, N.G., Tuskan, G.A., Gunter, L., Decker, S.R., Selig, M.J., Sykes, R., Himmel, M.E., Kitin, P., Shevchenko, O., Strauss, S.H. 2010. Antisense down-regulation of 4CL expression alters lignification, tree growth, and saccharification potential of field-grown poplar. *Plant Physiol.*, **154**(2), 874-886.
74. Yu, Z., Jameel, H., Chang, H.-m., Park, S. 2011. The effect of delignification of forest biomass on enzymatic hydrolysis. *Bioresource Technology*, **102**(19), 9083-9089.
75. Studer, M.H., DeMartini, J.D., Davis, M.F., Sykes, R.W., Davison, B., Keller, M., Tuskan, G.A., Wyman, C.E. 2011. Lignin content in natural Populus variants affects sugar release. *Proc. Natl. Acad. Sci. U. S. A.*, **108**(15), 6300-6305, S6300/1-S6300/6.
76. Stewart, J.J., Akiyama, T., Chapple, C., Ralph, J., Mansfield, S.D. 2009. The effects on lignin structure of overexpression of ferulate 5-hydroxylase in hybrid poplar. *Plant Physiol.*, **150**(2), 621-635.
77. Kishimoto, T., Chiba, W., Saito, K., Fukushima, K., Uraki, Y., Ubukata, M. 2010. Influence of Syringyl to Guaiacyl Ratio on the Structure of Natural and Synthetic Lignins. *J. Agric. Food Chem.*, **58**(2), 895-901.
78. Ramos, L., Breuil, C., Saddler, J. 1992. Comparison of steam pretreatment of eucalyptus, aspen, and spruce wood chips and their enzymatic hydrolysis. *Appl. Biochem. Biotechnol.* **34** (1), 37-48.
79. Grohmann, K., Mitchell, D.J., Himmel, M.E., Dale, B.E., Schroeder, H.A. 1989. The role of ester groups in resistance of plant cell wall polysaccharides to enzymic hydrolysis. *Appl. Biochem. Biotechnol.*, **20-21**, 45-61.
80. Pan, X., Gilkes, N., Saddler, J.N. 2006. Effect of acetyl groups on enzymatic hydrolysis of cellulosic substrates. *Holzforschung*, **60**(4), 398-401.
81. d'Errico, C., Jørgensen, J.O., Krogh, K.B.R.M., Spodsberg, N., Madsen, R., Monrad, R.N. 2015. Enzymatic degradation of lignin-carbohydrate complexes (LCCs): Model studies using a fungal glucuronoyl esterase from Cerrena unicolor. *Biotechnology and Bioengineering*, **112**(5), 914-922.

82. Zhang, Y.-H.P., Lynd, L.R. 2004. Toward an aggregated understanding of enzymatic hydrolysis of cellulose: Noncomplexed cellulase systems. *Biotechnology and Bioengineering*, **88**(7), 797-824.
83. Lynd, L.R., Weimer, P.J., van Zyl, W.H., Pretorius, I.S. 2002. Microbial cellulose utilization: Fundamentals and biotechnology. *Microbiol. Mol. Biol. Rev.*, **66**(3), 506-577.
84. Mansfield, S.D., Mooney, C., Saddler, J.N. 1999. Substrate and Enzyme Characteristics that Limit Cellulose Hydrolysis. *Biotechnology Progress*, **15**(5), 804-816.
85. Hall, M., Bansal, P., Lee, J.H., Realff, M.J., Bommarius, A.S. 2010. Cellulose crystallinity – a key predictor of the enzymatic hydrolysis rate. *FEBS Journal*, **277**(6), 1571-1582.
86. Lee, S.B., Shin, H.S., Ryu, D.D.Y., Mandels, M. 1982. Adsorption of cellulase on cellulose: Effect of physicochemical properties of cellulose on adsorption and rate of hydrolysis. *Biotechnology and Bioengineering*, **24**(10), 2137-2153.
87. Nazhad, M.M., Ramos, L.P., Paszner, L., Saddler, J.N. 1995. Structural constraints affecting the initial enzymic hydrolysis of recycled paper. *Enzyme Microb. Technol.*, **17**(1), 68-74.
88. Sadhu, S., Maiti, T.K. 2013. Cellulase production by bacteria: a review. *Br. Microbiol. Res. J.*, **3**(3), 235-258.
89. Sun, Q. 2014. Enzymatic deconstruction of lignocellulose to fermentable sugars. *Mater. Energy*, **4**(Materials for Biofuels), 127-153.
90. Cowling, E.B., Kirk, T.K. 1976. Properties of cellulose and lignocellulosic materials as substrates for enzymatic conversion processes. *Biotechnol Bioeng Symp*, **6**, 95-123.
91. Arantes, V., Saddler J.N. 2010. Access to cellulose limits the efficiency of enzymatic hydrolysis: the role of amorphogenesis. *Biotechnol. Biofuels*, **3**, 4.
92. Wang, Q.Q., He, Z., Zhu, Z., Zhang, Y.H.P., Ni, Y., Luo, X.L., Zhu, J.Y. 2012. Evaluations of cellulose accessibilities of lignocelluloses by solute exclusion and protein adsorption techniques. *Biotechnol. Bioeng.*, **109**(2), 381-389.
93. Arantes, V., Saddler, J.N. 2011. Cellulose accessibility limits the effectiveness of minimum cellulase loading on the efficient hydrolysis of pretreated lignocellulosic substrates. *Biotechnol. Biofuels*, **4**, 3.

94. Ju, X., Grego, C., Zhang, X. 2013. Specific effects of fiber size and fiber swelling on biomass substrate surface area and enzymatic digestibility. *Bioresour. Technol.* **144**, 232-239.
95. Zhang, Q., Zhang, P., Pei, Z.J., Wang. D. 2013. Relationships between cellulosic biomass particle size and enzymatic hydrolysis sugar yield: Analysis of inconsistent reports in the literature. *Renewable Energy*, **60**, 127-136.
96. Sinitsyn, A.P., Gusakov, A.V., Vlasenko, E.Y. 1991. Effect of structural and physico-chemical features of cellulosic substrates on the efficiency of enzymatic hydrolysis. *Applied Biochemistry and Biotechnology*, **30**, 43-59.
97. Yeh, A-I., Huang, Y-C., Chen, S.H. 2010. Effect of particle size on the rate of enzymatic hydrolysis of cellulose. *Carbohydrate Polymers*, **79**, 192-199.
98. Peters, L.E., Walker, L.P., Wilson, D.B., Irwin, D.C. 1991. The impact of initial particle size on the fragmentation of cellulose by cellulases of Thermomonosporafusca. *Bioresour. Technol.*, **35**, 313-319.
99. Dasari, R.K., Berson, R.E. 2007. The effect of particle size on hydrolysis reaction rates and rheological properties in cellulosic slurries. *Appl. Biochem. Biotechnol.*, **137-140**, 289-299.
100. Monavari, S., Galbe, M., Zacchi, G. 2009. Impact of impregnation time and chip size on sugar yield in pretreatment of softwood for ethanol production. *Bioresour. Technol.*, **100**, 6312-6316.
101. Pedersen, M., Meyer, A.S. 2009. Influence of substrate particle size and wet oxidation on physical surface structures and enzymatic hydrolysis of wheat straw. *Biotechnol.Prog.*, **25**, 399-408.
102. Lamsal, B., Madl. R., Tsakpunidis, K. 2011. Comparison of Feedstock Pretreatment Performance and Its Effect on Soluble Sugar Availability. *BioEnergy Research*, **4**, 193-200.
103. Theerarattananoon, K., Xu, F., Wilson, J., Staggenborg, S., McKinney, L., Vadlani, P., Pei, Z., Wang, D. 2012. Effects of the pelleting conditions on chemical composition and sugar yield of corn stover, big bluestem, wheat straw, and sorghum stalk pellets. *Bioprocess Biosyst. Eng.*, **35**, 615-623.

104. Zhang, M., Song, X., Deines, T.W., Pei, Z.J., Wang, D. 2012. Biofuel Manufacturing from Woody Biomass: Effects of Sieve Size Used in Biomass Size Reduction. *Journal of Biomedicine and Biotechnology*, **2012**, 9.
105. Davison, B.H., Parks, J., Davis, M.F., Donohoe, B.S. 2013. Plant Cell Walls: Basics of Structure, Chemistry, Accessibility and the Influence on Conversion. in: *Aqueous Pretreatment of Plant Biomass for Biological and Chemical Conversion to Fuels and Chemicals*, John Wiley & Sons, Ltd, pp. 23-38.
106. Carpita, N., Sabularse, D., Montezinos, D., Delmer, D.P. 1979. Determination of the pore size of cell walls of living plant cells. *Science (Washington, D. C.)*, **205**, 1144-1147.
107. Huang, R., Su, R., Qi, W., He, Z. 2010. Understanding the key factors for enzymatic conversion of pretreated lignocellulose by partial least square analysis. *Biotechnol.Prog.*, **26**, 384-392.
108. Luo, X., Zhu, J. 2010. Effects of drying-induced fiber hornification on enzymatic saccharification of lignocelluloses. *Enzyme Microb. Technol.*, 48, 92-99.
109. Meng, X., Wells, T., Sun, Q., Huang, F., Ragauskas, A. 2015. Insights into the effect of dilute acid, hot water or alkaline pretreatment on the cellulose accessible surface area and the overall porosity of Populus. *Green Chemistry. Accepted, Ahead-of-Print.*
110. Grethlein, H.E. 1985. The effect of pore size distribution on the rate of enzymic hydrolysis of cellulosic substrates. *Bio/Technology*, **3**, 155-160.
111. Viamajala, S., Donohoe, B., Decker, S., Vinzant, T., Selig, M., Himmel, M., Tucker, M. 2010. Heat and Mass Transport in Processing of Lignocellulosic Biomass for Fuels and Chemicals. in: *Sustainable Biotechnology*, (Eds.) O.V. Singh, S.P. Harvey, Springer Netherlands, pp. 1-18.
112. Chen, W-H., Tu, Y-J., Sheen, H-K. 2011. Disruption of sugarcane bagasse lignocellulosic structure by means of dilute sulfuric acid pretreatment with microwave-assisted heating. *Appl. Energy*, **88**, 2726-2734.
113. Park, S., Venditti, R.A., Jameel, H., Pawlak, J.J. 2006. Changes in pore size distribution during the drying of cellulose fibers as measured by differential scanning calorimetry. *Carbohydr.Polym.*, **66**, 97-103.

114. Chandra, R., Ewanick, S., Hsieh, C., Saddler, J.N. 2008. The characterization of pretreated lignocellulosic substrates prior to enzymatic hydrolysis, Part 1: a modified Simons' staining technique. *Biotechnol.Prog.*, **24**, 1178-1185.

115. Ostlund, A., Kohnke, T., Nordstierna, L., Nyden, M. 2010. NMR cryoporometry to study the fiber wall structure and the effect of drying. *Cellulose (Dordrecht, Neth.),* **17**, 321-328.

116. Felby, C., Thygesen, L.G., Kristensen, J.B., Jorgensen, H., Elder, T. 2008. **Cellulose-water interactions during enzymatic hydrolysis as studied by time domain NMR**. *Cellulose (Dordrecht, Neth.)*, **15**, 703-710.

117. Foston, M., Ragauskas, A.J. 2010. Changes in the Structure of the Cellulose Fiber Wall during Dilute Acid Pretreatment in Populus Studied by 1H and 2H NMR. *Energy & Fuels*, **24**, 5677-5685.

118. Suurnakki, A., Li, T.Q., Buchert, J., Tenkanen, M., Viikari, L., Vuorinen, T, Odberg, L. 1997. Effects of enzymic removal of xylan and glucomannan on the pore size distribution of kraft fibers. *Holzforschung*, **51**, 27-33.

119. Meng, X., Ragauskas, A.J. 2014. Recent advances in understanding the role of cellulose accessibility in enzymatic hydrolysis of lignocellulosic substrates. *Curr. Opin. Biotechnol.*, **27**, 150-158.

120. Li, C., Cheng, G., Balan, V., Kent, M.S., Ong, M., Chundawat, S.P.S., Sousa, L.d., Melnichenko, Y.B., Dale, B.E., Simmons, B.A. et al. 2011. Influence of physico-chemical changes on enzymatic digestibility of ionic liquid and AFEX pretreated corn stover. *Bioresource Technology*, **102**, 6928-6936.

121. Wiman, M., Dienes, D., Hansen, M.A.T., van der Meulen, T., Zacchi, G., Lidén, G. 2012. Cellulose accessibility determines the rate of enzymatic hydrolysis of steam-pretreated spruce. *Bioresource Technology*, **126**(0), 208-215.

122. Rouquerol, J., Baron, G., Denoyel, R., Giesche, H., Groen, J., Klobes, P., Levitz, P., Neimark, A.V., Rigby, S., Skudas, R. et al. 2012. Liquid intrusion and alternative methods for the characterization of macroporous materials (IUPAC technical report). *Pure Appl. Chem.*, **84**, 107-136.

123. Giesche, H. 2006. Mercury Porosimetry: A General (Practical) Overview. *Particle & Particle Systems Characterization,* **23**, 9-19.
124. Thompson, D.N., Chen, H.-C., Grethlein, H.E. 1992. Comparison of pretreatment methods on the basis of available surface area. *Bioresource Technology*, **39**, 155-163.
125. Keshwani, D.R., Cheng, J.J. 2010. Microwave-based alkali pretreatment of switchgrass and coastal bermudagrass for bioethanol production. *Biotechnol.Prog.,* **26**, 644-652.
126. Hu, J., Arantes, V., Saddler, J. 2011. The enhancement of enzymatic hydrolysis of lignocellulosic substrates by the addition of accessory enzymes such as xylanase: is it an additive or synergistic effect? *Biotechnology for Biofuels*, **4**(1), 36.
127. Kumar, R., Wyman, C. 2009. Cellulase adsorption and relationship to features of corn stover solids produced by leading pretreatments. *Biotechnol Bioeng*, **103**(2), 252 – 267.
128. Selig, M., Vinzant, T., Himmel, M., Decker, S. 2009. The effect of lignin removal by alkaline peroxide pretreatment on the susceptibility of corn stover to purified cellulolytic and xylanolytic enzymes. *Appl Biochem Biotechnol*, **155**(1-3), 397 – 406.
129. Beeson, W.T., Phillips, C.M., Cate, J.H.D., Marletta, M.A. 2012. Oxidative Cleavage of Cellulose by Fungal Copper-Dependent Polysaccharide Monooxygenases. *J. Am. Chem. Soc.*, **134**(2), 890-892.
130. Hu, F., Ragauskas, A.J. 2012. Pretreatment and Lignocellulosic Chemistry. *BioEnergy Research,* **5**, 1043-1066.
131. Hu, Z., Ragauskas, A.J. 2001. Hydrothermal pretreatment of switchgrass. *Ind. Eng. Chem. Res.,* **50**, 4225-4230.
132. Kang, Y., Bansal, P., Realff, M.J., Bommarius, A.S. 2013. SO2-catalyzed steam explosion: the effects of different severity on digestibility, accessibility, and crystallinity of lignocellulosic biomass. *Biotechnol.Prog.,* **29**, 909-916.
133. Sannigrahi, P., Ragauskas, A.J. 2013. Fundamentals of biomass pretreatment by fractionation. John Wiley & Sons Ltd., 201-222.

134. Cateto, C., Hu, G., Ragauskas, A.J. 2011. Enzymatic hydrolysis of organosolv Kanlow switchgrass and its impact on cellulose crystallinity and degree of polymerization. *Energy Environ. Sci.*, **4**, 1516-1521.
135. Yang, B., Wyman, C.E. 2006. BSA treatment to enhance enzymatic hydrolysis of cellulose in lignin containing substrates. *Biotechnol. Bioeng.*, **94**, 611-617.
136. Kumar, L., Arantes, V., Chandra, R,, Saddler, J. 2012. The lignin present in steam pretreated softwood binds enzymes and limits cellulose accessibility. *Bioresour. Technol.*, **103**, 201-208.
137. Kumar, L., Chandra, R., Saddler, J. 2011. Influence of steam pretreatment severity on post-treatments used to enhance the enzymatic hydrolysis of pretreated softwoods at low enzyme loadings. *Biotechnol. Bioeng.*, **108**, 2300-2311.
138. Ishizawa, C., Jeoh, T., Adney, W., Himmel, M,, Johnson, D., Davis, M. 2009. Can delignification decrease cellulose digestibility in acid pretreated corn stover? *Cellulose*, **16**, 677-686.
139. Chundawat, S.P.S., Donohoe, B.S., Sousa, L.d.C., Elder, T., Agarwal, U.P., Lu, F., Ralph, J., Himmel, M.E., Balan, V., Dale, B.E. 2011. Multi-scale visualization and characterization of lignocellulosic plant cell wall deconstruction during thermochemical pretreatment. *Energy Environ. Sci.*, **4**, 973-984.
140. Chen, Y., Stevens, M.A., Zhu, Y., Holmes, J., Xu, H. 2013. Understanding of alkaline pretreatment parameters for corn stover enzymatic saccharification. *Biotechnol. Biofuels*, **6**, 8.
141. Yoon, L.W., Ang, T.N., Ngoh, G.C., Chua, A.S.M. 2012. Regression analysis on ionic liquid pretreatment of sugarcane bagasse and assessment of structural changes. *Biomass and Bioenergy*, **36**, 160-169.
142. Goshadrou, A., Karimi, K., Lefsrud, M. 2013. Characterization of ionic liquid pretreated aspen wood using semi-quantitative methods for ethanol production. *Carbohydrate Polymers*, **96**, 440-449.
143. Zhao, X., Zhang, L., Liu, D. 2012. Biomass recalcitrance. Part II: Fundamentals of different pre-treatments to increase the enzymatic digestibility of lignocellulose. *Biofuels, Bioprod. Biorefin.*, **6,** 561-579.

144. Vancov, T., McIntosh, S. 2011. Alkali Pretreatment of Cereal Crop Residues for Second-Generation Biofuels. *Energy & Fuels*,25, 2754-2763.
145. Singh, S., Varanasi, P., Singh, P., Adams, P.D., Auer, M., Simmons, B.A. 2013. Understanding the impact of ionic liquid pretreatment on cellulose and lignin via thermochemical analysis. *Biomass Bioenergy*, **54**, 276-283.
146. Agbor, V.B., Cicek, N., Sparling, R., Berlin, A., Levin, D.B. 2011. Biomass pretreatment: Fundamentals toward application. *Biotechnology Advances*, **29**, 675-685.
147. Klein-Marcuschamer, D., Simmons, B.A., Blanch, H.W. 2011. Techno-economic analysis of a lignocellulosic ethanol biorefinery with ionic liquid pre-treatment. *Biofuels, Bioproducts and Biorefining*, **5**, 562-569.
148. Sanchez, O.J., Cardona, C.A. 2008. Trends in biotechnological production of fuel ethanol from different feedstocks. *Bioresour. Technol.*, **99**(13), 5270-5295.
149. Fu, C., Mielenz, J.R., Xiao, X., Ge, Y., Hamilton, C.Y., Rodriguez, M., Chen, F., Foston, M., Ragauskas, A.J., Bouton, J. et al. 2011. Genetic manipulation of lignin reduces recalcitrance and improves ethanol production from switchgrass. *Proceedings of the National Academy of Sciences*, **108**, 3803-3808.
150. Fu, C., Xiao, X., Xi, Y., Ge, Y., Chen, F., Bouton, J., Dixon, R., Wang, Z-Y. 2011. Downregulation of Cinnamyl Alcohol Dehydrogenase (CAD) Leads to Improved Saccharification Efficiency in Switchgrass. *BioEnergy Research*, **4**, 153-164.
151. Shen, H., Poovaiah, C., Ziebell, A., Tschaplinski, T., Pattathil, S., Gjersing, E., Engle, N., Katahira, R., Pu, Y., Sykes, R. et al. 2013. Enhanced characteristics of genetically modified switchgrass (Panicum virgatum L.) for high biofuel production. *Biotechnology for Biofuels*, **6**, 71.
152. Lee, C., Teng, Q., Huang, W., Zhong, R., Ye, Z-H. 2009. The F8H Glycosyltransferase is a Functional Paralog of FRA8 Involved in Glucuronoxylan Biosynthesis in Arabidopsis. *Plant Cell Physiol.*, **50**, 812-827.
153. Simons, F.L., 1950. A stain for use in the microscopy of beaten fibers. Tappi J. **33**, 312-314
154. Yu, X., Atalla, R.H., 1998. A staining technique for evaluating the pore structure variations of microcrystalline cellulose powders. Powder Technol., **98**, 135-138.

155. Esteghlalian, A.R., Bilodeau, M., Mansfield, S.D., Saddler, J.N., 2001. Do enzymic hydrolyzability and Simons' stain reflect the changes in the accessibility of lignocellulosic substrates to cellulase enzymes? Biotechnol. Prog., **17**, 1049-1054.
156. Hu, F., Jung, S., Ragauskas, A.J. 2012. Pseudo-lignin formation and its impact on enzymatic hydrolysis. *Bioresour Technol,* **117**, 7-12
157. Ghose, T. K. 1987. Measurement of cellulase activities. *Pure and Applied Chemistry***, 59** (2), 257-268
158. Jahnert, S., Vaca Chavez, F., Schaumann, G.E., Schreiber, A., Schonhoff, M., Findenegg, G.H. 2008. Melting and freezing of water in cylindrical silica nanopores. *Physical Chemistry Chemical Physics* **10**, 6039-6051.
159. Um, B.-H., Karim, M.N., Henk, L. 2003. Effect of sulfuric and phosphoric acid pretreatments on enzymatic hydrolysis of corn stover. *Applied Biochemistry and Biotechnology*, **105**(1-3), 115-125.
160. Jensen, J.R., Morinelly, J.E., Gossen, K.R., Brodeur-Campbell, M.J., Shonnard, D.R. 2010. Effects of dilute acid pretreatment conditions on enzymatic hydrolysis monomer and oligomer sugar yields for aspen, balsam, and switchgrass. *Bioresour. Technol.*, **101**(7), 2317-2325.
161. Tian, S., Zhu, W., Gleisner, R., Pan, X.J., Zhu, J.Y. 2011. Comparisons of SPORL and dilute acid pretreatments for sugar and ethanol productions from aspen. *Biotechnol. Prog.*, **27**(2), 419-427.
162. Sun, Y., Cheng, J. 2002. Hydrolysis of lignocellulosic materials for ethanol production: a review. *Bioresour. Technol.*, **83**(1), 1-11.
163. Tanaka, M., Ikesaka, M., Matsuno, R., Converse, A.O. 1988. Effect of pore size in substrate and diffusion of enzyme on hydrolysis of cellulosic materials with cellulases. *Biotechnol. Bioeng.*, **32**, 698-706
164. White, A.R., Brown, R.M. 1981. Enzymatic hydrolysis of cellulose: Visual characterization of the process. *Proc. Natl Acad. Sci. USA*, **78**, 1047-51.
165. Chen, Y., Wang, Y., Wan, J., Ma, Y. 2010. Crystal and pore structure of wheat straw cellulose fiber during recycling. *Cellulose (Dordrecht, Neth.)*, **17**, 329-338.

166. Simitzis, J., Sfyrakis, J., Faliagas, A. 1995. Characterization of pore structure by porosimetry and sorption on adsorbent produced from novolac-biomass. *Mater. Chem. Phys.*, **41**(4), 245-250.
167. Choudhary, R., Umagiliyage, A.L., Liang, Y., Siddaramu, T., Haddock, J., Markevicius, G. 2012. Microwave pretreatment for enzymatic saccharification of sweet sorghum bagasse. *Biomass Bioenergy*, **39**, 218-226
168. Inglesby, M.K., Zeronian, S.H. 2002. Direct dyes as molecular sensors to characterize cellulose substrates. *Cellulose (Dordrecht, Neth.)*, **9**, 19-29.
169. Hsu, T.-C., Guo, G.-L., Chen, W.-H., Hwang, W.-S. 2010. Effect of dilute acid pretreatment of rice straw on structural properties and enzymatic hydrolysis. *Bioresour. Technol.*, **101**(13), 4907-4913.
170. Strange, J.H., Rahman, M., Smith, E.G. 1993. Characterization of porous solids by NMR. *Phys. Rev. Lett.*, **71**, 3589-91.
171. Menon, R.S., MacKay, A.L., Hailey, J.R.T., Bloom, M., Burgess, A.E., Swanson, J.S. 1987. An NMR determination of the physiological water distribution in wood during drying. *J. Appl. Polym. Sci.*, **33**, 1141-55.
172. Araujo, C.D., Mackay, A.L., Whittall, K.P., Hailey, J.R.T. 1993. A Diffusion Model for Spin-Spin Relaxation of Compartmentalized Water in Wood. *Journal of Magnetic Resonance, Series B*, **101**, 248-261.
173. Haggkvist, M., Li, T.-Q., Odberg, L. 1998. Effects of drying and pressing on the pore structure in the cellulose fiber wall studied by proton and deuteron NMR relaxation. *Cellulose (London)*, 5, 33-49.
174. Li, T.Q., Henriksson, U., Oedberg, L. 1993. Determination of pore sizes in wood cellulose fibers by deuterium and proton NMR. *Nord. Pulp Pap. Res. J.*, **8**, 326-30.
175. Tanner, J.E., Stejskal, E.O. 1968. Restricted self-diffusion of protons in colloidal systems by the pulsed-gradient, spin-echo method. *J. Chem. Phys.*, **49**, 1768-77
176. Topgaard, D., Soederman, O. 2001. Diffusion of water absorbed in cellulose fibers studied with proton NMR. *Langmuir*, **17**, 2694-2702

177. Li, T.Q., Haeggkvist, M., Oedberg, L. 1997. Porous Structure of Cellulose Fibers Studied by Q-Space NMR Imaging. *Langmuir*, **13**, 3570-3574.
178. Stilbs, P. 1987. Fourier transform pulsed-gradient spin-echo studies of molecular diffusion. P*rog. Nucl. Magn. Reson. Spectrosc.*, **19**, 1-45.
179. Wyman, C.E. 2008. Cellulosic Ethanol: A Unique Sustainable Liquid Transportation Fuel. *MRS Bulletin*, **33**(04), 381-383.
180. Gasparatos, A., Stromberg, P., Takeuchi, K. 2013. Sustainability impacts of first-generation biofuels. *Animal Frontiers*, **3**(2), 12-26.
181. Somerville, C., Youngs, H., Taylor, C., Davis, S.C., Long, S.P. 2010. Feedstocks for lignocellulosic biofuels. *Science*, **329**(5993), 790-2.
182. Kumar, P., Barrett, D.M., Delwiche, M.J., Stroeve, P. 2009. Methods for Pretreatment of Lignocellulosic Biomass for Efficient Hydrolysis and Biofuel Production. *Industrial & Engineering Chemistry Research*, **48**(8), 3713-3729.
183. Wyman, C.E., Decker, S.R., Himmel, M.E., Brady, J.W., Skopec, C.E., Viikari, L. 2005. Hydrolysis of cellulose and hemicellulose. *Polysaccharides: Structural Diversity and Functional Versatility*, **1**, 1023-1062.
184. Ioelovich, M. 2009. Accessibility and crystallinity of cellulose. *BioResources*, **4**(3), 1168-1177.
185. Puri, V.P. 1984. Effect of crystallinity and degree of polymerization of cellulose on enzymatic saccharification. *Biotechnol Bioeng*, **26**(10), 1219-22.
186. Jeoh, T., Ishizawa, C.I., Davis, M.F., Himmel, M.E., Adney, W.S., Johnson, D.K. 2007. Cellulase digestibility of pretreated biomass is limited by cellulose accessibility. *Biotechnology and Bioengineering*, **98**(1), 112-122.
187. Rollin, J.A., Zhu, Z., Sathitsuksanoh, N., Zhang, Y.H.P. 2010. Increasing cellulose accessibility is more important than removing lignin: A comparison of cellulose solvent-based lignocellulose fractionation and soaking in aqueous ammonia. *Biotechnol. Bioeng.*, **108**(1), 22-30.
188. Mosier, N., Wyman, C., Dale, B., Elander, R., Lee, Y.Y., Holtzapple, M., Ladisch, M. 2005. Features of promising technologies for pretreatment of lignocellulosic biomass. *Bioresource Technology*, **96**(6), 673-686.

189. Brodeur, G., Yau, E., Badal, K., Collier, J., Ramachandran, K.B., Ramakrishnan, S. 2011. Chemical and Physicochemical Pretreatment of Lignocellulosic Biomass: A Review. *Enzyme Research*, **2011**, 17.
190. Gupta, R., Lee, Y.Y. 2010. Investigation of biomass degradation mechanism in pretreatment of switchgrass by aqueous ammonia and sodium hydroxide. *Bioresource Technology*, **101**(21), 8185-8191.
191. Kim, T.H., Gupta, R., Lee, Y.Y. 2009. Pretreatment of biomass by aqueous ammonia for bioethanol production. *Methods Mol Biol*, **581**, 79-91.
192. Kaar, W.E., Holtzapple, M.T. 2000. Using lime pretreatment to facilitate the enzymic hydrolysis of corn stover. *Biomass and Bioenergy*, **18**(3), 189-199.
193. Bjerre, A.B., Olesen, A.B., Fernqvist, T., Plöger, A., Schmidt, A.S. 1996. Pretreatment of wheat straw using combined wet oxidation and alkaline hydrolysis resulting in convertible cellulose and hemicellulose. *Biotechnology and Bioengineering*, **49**(5), 568-577.
194. Xu, J., Cheng, J.J., Sharma-Shivappa, R.R., Burns, J.C. 2010. Sodium Hydroxide Pretreatment of Switchgrass for Ethanol Production. *Energy & Fuels*, **24**(3), 2113-2119.
195. Sierra, R., Holtzapple, M.T., Granda, C.B. 2011. Long-term lime pretreatment of poplar wood. *AIChE Journal*, **57**(5), 1320-1328.
196. Kang, K.E., Jeong, G.-T., Sunwoo, C., Park, D.-H. 2012. Pretreatment of rapeseed straw by soaking in aqueous ammonia. *Bioprocess and Biosystems Engineering*, **35**(1-2), 77-84.
197. Ucar, G. 1990. Pretreatment of poplar by acid and alkali for enzymatic hydrolysis. *Wood Science and Technology*, **24**(2), 171-180.
198. Newman, R.H. 1999. Estimation of the lateral dimensions of cellulose crystallites using 13C NMR signal strengths. *Solid State Nuclear Magnetic Resonance*, **15**(1), 21-29.
199. Mittal, A., Katahira, R., Himmel, M.E., Johnson, D.K. 2011. Effects of alkaline or liquid-ammonia treatment on crystalline cellulose: changes in crystalline structure and effects on enzymatic digestibility. *Biotechnol. Biofuels*, **4**, 41.

200. Sun, Q., Foston, M., Sawada, D., Pingali, S., O'Neill, H., Li, H., Wyman, C., Langan, P., Pu, Y., Ragauskas, A. 2014. Comparison of changes in cellulose ultrastructure during different pretreatments of poplar. *Cellulose,* **21**(4), 2419-243.
201. Langan, P., Petridis, L., O'Neill, H.M., Pingali, S.V., Foston, M., Nishiyama, Y., Schulz, R., Lindner, B., Hanson, B.L., Harton, S., Heller, W.T., Urban, V., Evans, B.R., Gnanakaran, S., Ragauskas, A.J., Smith, J.C., Davison, B.H. 2014. Common processes drive the thermochemical pretreatment of lignocellulosic biomass. *Green Chemistry*, **16**(1), 63-68.
202. Chandra, R., Bura, R., Mabee, W., Berlin, A., Pan, X., Saddler, J. 2007. Substrate pretreatment: the key to effective enzymatic hydrolysis of lignocellulosics? *Biofuels*, **108**, 67 – 93.
203. DeMartini, J.D., Pattathil, S., Miller, J.S., Li, H., Hahn, M.G., Wyman, C.E. 2013. Investigating plant cell wall components that affect biomass recalcitrance in poplar and switchgrass. *Energy Environ. Sci.*, **6**(3), 898-909.
204. Jungnikl, K., Paris, O., Fratzl, P., Burgert, I. 2008. The implication of chemical extraction treatments on the cell wall nanostructure of softwood. *Cellulose*, **15**(3), 407-418.
205. Wang, Z., Keshwani, D.R., Redding, A.P., Cheng, J.J. 2010. Sodium hydroxide pretreatment and enzymatic hydrolysis of coastal Bermuda grass. *Bioresour. Technol.*, **101**(10), 3583-3585.
206. Cheng, G., Zhang, X., Simmons, B., Singh, S. 2015. Theory, practice and prospects of X-ray and neutron scattering for lignocellulosic biomass characterization: towards understanding biomass pretreatment. *Energy & Environmental Science*, **8**(2), 436-455.
207. Kumar, R., Wyman, C.E. 2009. Access of cellulase to cellulose and lignin for poplar solids produced by leading pretreatment technologies. *Biotechnol. Prog.*, **25**(3), 807-819.
208. Zheng, Y., Zhang, S., Miao, S., Su, Z., Wang, P. 2013. Temperature sensitivity of cellulase adsorption on lignin and its impact on enzymatic hydrolysis of lignocellulosic biomass. *J. Biotechnol.*, **166**(3), 135-143.
209. Nonaka, H., Kobayashi, A., Funaoka, M. 2013. Behavior of lignin-binding cellulase in the presence of fresh cellulosic substrate. *Bioresour. Technol.*, **135**, 53-57.

210. Plötze, M., Niemz, P. 2011. Porosity and pore size distribution of different wood types as determined by mercury intrusion porosimetry. *European Journal of Wood and Wood Products*, **69**(4), 649-657.
211. Thygesen, L.G., Engelund, E.T., Hoffmeyer, P. 2010. Water sorption in wood and modified wood at high values of relative humidity. Part I: results for untreated, acetylated, and furfurylated Norway spruce. *Holzforschung*, **64**(3), 315-323.
212. Zauer, M., Pfriem, A., Wagenführ, A. 2013. Toward improved understanding of the cell-wall density and porosity of wood determined by gas pycnometry. *Wood Science and Technology*, **47**(6), 1197-1211.
213. Fan, X., Cheng, G., Zhang, H., Li, M., Wang, S., Yuan, Q. 2014. Effects of acid impregnated steam explosion process on xylose recovery and enzymatic conversion of cellulose in corncob. *Carbohydr. Polym.*, **114**, 21-26.
214. Zhao, J., Chen, H. 2013. Correlation of porous structure, mass transfer and enzymatic hydrolysis of steam exploded corn stover. *Chem. Eng. Sci.*, **104**, 1036-1044.
215. Xu, F., Shi, Y.-C., Wang, D. 2013. Towards understanding structural changes of photoperiod-sensitive sorghum biomass during sulfuric acid pretreatment. *Bioresour. Technol.*, **135**, 704-709.
216. Yang, D., Moran-Mirabal, J.M., Parlange, J.-Y., Walker, L.P. 2013. Investigation of the porous structure of cellulosic substrates through confocal laser scanning microscopy. *Biotechnol. Bioeng.*, **110**(11), 2836-2845.
217. Hu, J., Arantes, V., Pribowo, A., Gourlay, K., Saddler, J.N. 2014. Substrate factors that influence the synergistic interaction of AA9 and cellulases during the enzymatic hydrolysis of biomass. *Energy Environ. Sci.*, **7**(7), 2308-2315.
218. Luterbacher, J.S., Parlange, J.-Y., Walker, L.P. 2014. A pore-hindered diffusion and reaction model can help explain the importance of pore size distribution in enzymatic hydrolysis of biomass [Erratum to document cited in CA159:195400]. *Biotechnol. Bioeng.*, **111**(12), 2587-2588.
219. Yang, B., Dai, Z., Ding, S.-Y., Wyman, C.E. 2011. Enzymatic hydrolysis of cellulosic biomass. *Biofuels*, **2**(4), 421-450.

220. Cao, Y., Tan, H. 2002. Effects of cellulase on the modification of cellulose. *Carbohydrate Research*, **337**(14), 1291-1296.
221. Li, C., Ladisch, C.M., Ladisch, M.R. 2001. Pore characterization of cellulase enzyme treated cotton fabric. *Text. Res. J.*, **71**(5), 407-414.
222. Buschle-Diller, G., Fanter, C., Loth, F. 1999. Structural changes in hemp fibers as a result of enzymic hydrolysis with mixed enzyme systems. *Text. Res. J.*, **69**(4), 244-251.
223. Lee, S.B., Kim, I.H., Ryu, D.D.Y., Taguchi, H. 1983. Structural properties of cellulose and cellulase reaction mechanism. *Biotechnol. Bioeng.*, **25**(1), 33-51.
224. Santa-Maria, M., Jeoh, T. 2010. Molecular-Scale Investigations of Cellulose Microstructure during Enzymatic Hydrolysis. *Biomacromolecules*, **11**(8), 2000-2007.
225. Ramos, L.P., Nazhad, M.M., Saddler, J.N. 1993. Effect of enzymic hydrolysis on the morphology and fine structure of pretreated cellulosic residues. *Enzyme Microb. Technol.*, **15**(10), 821-31.
226. Eibinger, M., Bubner, P., Ganner, T., Plank, H., Nidetzky, B. 2014. Surface structural dynamics of enzymatic cellulose degradation, revealed by combined kinetic and atomic force microscopy studies. *FEBS J.*, **281**(1), 275-290.
227. Wang, W., Zhuang, X., Yuan, Z., Yu, Q., Qi, W., Wang, Q., Tan, X. 2012. Effect of structural changes on enzymatic hydrolysis of eucalyptus, sweet sorghum bagasse and sugarcane bagasse after liquid hot water pretreatment. *BioResources*, **7**(2), 2469-2482.
228. Sun, X.F., Xu, F., Sun, R.C., Fowler, P., Baird, M.S. 2005. Characteristics of degraded cellulose obtained from steam-exploded wheat straw. *Carbohydrate Research*, **340**(1), 97-106.
229. Li, C., Knierim, B., Manisseri, C., Arora, R., Scheller, H.V., Auer, M., Vogel, K.P., Simmons, B.A., Singh, S. 2010. Comparison of dilute acid and ionic liquid pretreatment of switchgrass: Biomass recalcitrance, delignification and enzymatic saccharification. *Bioresource Technology*, **101**(13), 4900-4906.
230. Corredor, D.Y., Salazar, J.M., Hohn, K.L., Bean, S., Bean, B., Wang, D. 2009. Evaluation and Characterization of Forage Sorghum as Feedstock for Fermentable Sugar Production. *Applied Biochemistry and Biotechnology*, **158**(1), 164-179.

231. Kobayashi, N., Okada, N., Hirakawa, A., Sato, T., Kobayashi, J., Hatano, S., Itaya, Y., Mori, S. 2009. Characteristics of Solid Residues Obtained from Hot-Compressed-Water Treatment of Woody Biomass. *Industrial & Engineering Chemistry Research*, **48**(1), 373-379.
232. Tian, X.-F., Fang, Z., Jiang, D., Sun, X.-Y. 2011. Pretreatment of microcrystalline cellulose in organic electrolyte solutions for enzymatic hydrolysis. *Biotechnol. Biofuels*, **4**, 53.
233. Marx-Figini, M., Blanco, S., Ellenrieder, G.v. 1990. Action of the cellulase multienzyme complex on the degree of polymerization of high-molecular-weight cellulose. *Die Makromolekulare Chemie*, **191**(7), 1649-1656.
234. Fan, L.T., Lee, Y.-H., Beardmore, D.H. 1980. Mechanism of the enzymatic hydrolysis of cellulose: Effects of major structural features of cellulose on enzymatic hydrolysis. *Biotechnology and Bioengineering*, **22**(1), 177-199.
235. Yang, B., Willies, D.M., Wyman, C.E. 2006. Changes in the enzymatic hydrolysis rate of Avicel cellulose with conversion. *Biotechnology and Bioengineering*, **94**(6), 1122-1128.
236. Blanch, H.W. 2012. Bioprocessing for biofuels. *Curr. Opin. Biotechnol.*, **23**, 390-395.
237. Sun, Q., Foston, M., Meng, X., Sawada, D., Pingali, S.V., O'Neill, H.M., Li, H., Wyman, C.E., Langan, P., Ragauskas, A.J., Kumar, R. 2014. Effect of lignin content on changes occurring in poplar cellulose ultrastructure during dilute acid pretreatment. *Biotechnol. Biofuels*, **7**, 150/1-150/14.